FLOW INVESTIGATION IN A CHANNEL REACTOR USING CHEMICALLY
REACTING BOUNDARY LAYER EQUATIONS

A THESIS SUBMITTED TO
THE GRADUATE SCHOOL OF NATURAL AND APPLIED SCIENCES
OF
MIDDLE EAST TECHNICAL UNIVERSITY

BY

DOĞU HAZAR KENAR

IN PARTIAL FULFILLMENT OF THE REQUIREMENTS
FOR
THE DEGREE OF MASTER OF SCIENCE
IN
AEROSPACE ENGINEERING

JANUARY 2023

Approval of the thesis:

**FLOW INVESTIGATION IN A CHANNEL REACTOR USING
CHEMICALLY REACTING BOUNDARY LAYER EQUATIONS**

submitted by **DOĞU HAZAR KENAR** in partial fulfillment of the requirements for the degree of **Master of Science** in **Aerospace Engineering, Middle East Technical University** by,

Prof. Dr. Halil Kalıpçılar
Dean, Graduate School of **Natural and Applied Sciences**   _____

Prof. Dr. Serkan Özgen
Head of the Department, **Aerospace Engineering**   _____

Prof. Dr. Yusuf Özyörük
Supervisor, **Aerospace Engineering, METU**   _____

Examining Committee Members:

Prof. Dr. Serkan Özgen
Aerospace Engineering, METU   _____

Prof. Dr. Yusuf Özyörük
Aerospace Engineering, METU   _____

Prof. Dr. Oğuz Uzol
Aerospace Engineering, METU   _____

Prof. Dr. Sinan Eyi
Aerospace Engineering, METU   _____

Assist. Prof. Dr. Onur Baş
Mechanical Engineering, TED   _____

Date: 13.01.2023

I hereby declare that all information in this document has been obtained and presented in accordance with academic rules and ethical conduct. I also declare that, as required by these rules and conduct, I have fully cited and referenced all material and results that are not original to this work.

Name Last name : Doğu Hazar Kenar

Signature :

ABSTRACT

FLOW INVESTIGATION IN A CHANNEL REACTOR USING CHEMICALLY REACTING BOUNDARY LAYER EQUATIONS

Kenar, Doğu Hazar
Master of Science, Aerospace Engineering
Supervisor: Prof. Dr. Yusuf Özyörük

January 2023, 114 pages

In this study, an algorithm for the solution of chemically reacting flows in a channel reactor is developed by using boundary layer equations. The governing flow equations are simplified under certain assumptions with the application of similarity transformation. As a consequence of simplification, the characteristics of flow equations are changed to parabolic partial differential equations (PDE). Parabolic PDEs can be solved by numerical techniques initially designed for ordinary differential equations (ODE), such as a method of lines. The spatial terms of the equation set are discretized by the finite difference method. The resulting set of boundary layer equations is written in differential algebraic form. The set of equations is solved as a marching problem in the 2D domain with given initial and boundary conditions using MATLAB ode15i solver. The developed algorithm is used to investigate the formation of a flame in a reacting channel flow and the parameters affecting flame development.

Keywords: Boundary Layer Equations, Flame Formation, Channel Combustion

ÖZ

KANAL YAPISINDA KİMYASAL REAKSİYONLU AKIŞIN SINIR TABAKASI DENKLEMLERİYLE İNCELENMESİ

Kenar, Doğu Hazar
Yüksek Lisans, Havacılık ve Uzay Mühendisliği
Tez Yöneticisi: Prof. Dr. Yusuf Özyörük

Ocak 2023, 114 sayfa

Bu çalışmada, bir kanal reaktörde reaksiyona giren akışların çözümü için sınır tabakası denklemleri kullanılarak bir algoritma geliştirilmiştir. Ana akış denklemleri, benzerlik dönüşümünün uygulanmasıyla belirli varsayımlar altında basitleştirilmiştir. Sadeleştirmenin bir sonucu olarak, akış denklemlerinin özellikleri parabolik kısmi diferansiyel denklemlere dönüştürülmüştür. Parabolik kısmi diferansiyel denklemlere, başlangıçta çizgi yöntemi gibi adi diferansiyel denklemler için tasarlanmış sayısal tekniklerle çözülebilir. Denklem setindeki uzamsal terimler sonlu farklar yöntemiyle ayrıklaştırmaktadır. Ortaya çıkan sınır tabakası denklemleri seti, diferansiyel cebirsel denklemler şeklinde yazılır ve MATLAB ode15i çözücü kullanılarak verilen başlangıç ve sınır koşulları ile 2 boyutlu alanda ilerleyen bir problem olarak çözülür. Geliştirilen algoritma kullanılarak, tepkimeye giren bir kanal akışında alev oluşumu ve alev gelişimine etki eden parametreler incelenmiştir.

Anahtar Kelimeler: Sınır Katmanı Denklemleri, Alev Oluşumu, Kanal Yanması

To my family,

ACKNOWLEDGMENTS

TABLE OF CONTENTS

LIST OF TABLES

LIST OF FIGURES

FIGURES

CHAPTER 1

INTRODUCTION

1.1   Background and Early Studies

Chemically reacting flows in a duct or channel are highly encountered problems in industrial cases. Thus, investigating this engineering problem and its solution is still an exciting topic in the industry and academia. It is necessary to understand the related reacting flow problem to analyze catalytic channel problem physics [1] [2]. The catalytic channels are used in the solid-oxide fuel cells as monoliths. In addition, in automobiles, the catalytic converters take part [3]. Moreover, catalytic monoliths can be used as tubular reactors, in which chemical processes are involved. The chemical vapor deposition process is a common example of a chemical process in a channel, where film deposition or growth on the channel wall occurs in addition to reactions in the flow [4]. The gas-phase reactions in a channel are also widely observed in chemically reacting flows. The catalytic tubes are commonly used in household type of boilers. In addition, gas-phase chemistry is still being investigated in laboratory-scale reactors.

Boundary layer equations can be used in the simulation of reacting flows developing in a channel or duct. With the help of the boundary layer approximation, diffusive transport in flow direction can be neglected with respect to convective diffusion [5]. This simplification provides a way for the solution of the flow equations coupled with species and energy equations.

There are numerous examples of the numerical modeling of reacting channel flows in literature. The most common method of application is the decomposition process. Coltrin et al. have studied chemical vapor deposition and provided a mathematical model by using boundary layer equations coupled with species equations [4] [6]. They described a general boundary layer method for axisymmetric and planar

coordinates. They examined the deposition of silicon in a reactor due to the thermal decomposition of silane. They modeled boundary layer equations with chemical rate equations to produce a coupled system of PDEs in parabolic characteristics and solved those equations using numerical methods. The methodology of deriving boundary layer equations, making necessary transformations and introducing correct boundary conditions for reacting surface is explained in detail. The fields of temperature, velocity and species concentration were predicted for the given problem using the developed model [4]. Moreover, this study shows the effects of thermal diffusion and the multicomponent transport properties on resulting fields of temperature, velocity and species concentration [6]. The calculated results of decomposition rates were compared with the experimental results. The results show to well agree with the experimental results. In addition, they reported the effects of gas phase chemical kinetics and the temperature level on silane decomposition, indicating that thermal diffusion significantly affects the distribution of chemical species concentrations.

Moreover, the characteristics of the surface reactions in reacting channel flows have been an interesting topic for researchers through the years. Andrae et al. have conducted a series of studies to investigate the effects of different fuels on wall quenching and to observe extinction characteristics of flames [5], [7], [8]. The authors started by investigating near-wall chemistry for hydrogen-air combustion in a planar duct at lean conditions where the equivalence ratios are 0.5 and 0.1. Numerical computation of flow in a 1 cm long 1 cm high planar channel is performed to observe the effect of wall temperature and the equivalence ratio on surface chemistry for the catalytic and inert walls. The gas-phase hydrogen-air combustion and the surface reactions of hydrogen oxidation on platinum were considered and the mechanisms were introduced in their study. After the ignition, they investigated the interactions of flame and wall in the wall boundary layer. The interactions of flame and wall after ignition showed that the development of velocity and thermal boundary layers was significantly affected by different wall temperatures. Finally, a propane air unburnt mixture is introduced on regions close to the wall. A burnt

mixture is introduced at other regions, taking a lower wall temperature to see its effect on flame quenching for ranging inlet conditions. The consumption of unburnt fuels was considerably affected by the change in fuel-air stoichiometry and wall temperature.

Another typical example of reacting channel flows is the catalytic monoliths. Researchers have used these devices in many numerical studies of channel flow applications to investigate the characteristics of reacting flows under various conditions. Raja et al. have evaluated the solutions of Navier Stokes equations, boundary layer equations and plug flow models to analyze reacting flow in catalytic monoliths [1]. They modeled a steady state and reacting flow in a honeycomb channel to simulate the catalytic combustion of natural gas. The Navier-Stokes equations were solved using common and commercially available software, which implements a finite-volume discretization method. The boundary layer equations and plug-flow models were solved in Chemkin using DASSL software [9]. They used a single cylindrical channel geometry with a 2 mm dimeter and 100 mm length in the axial direction, with a methane-air mixture for their studies. The walls were held at constant temperature and covered with platinum. The flow conditions were selected to simulate the combustor conditions of a gas turbine. The validity and comparison studies for each model were conducted. They concluded that the results of Navier Stokes and boundary layer equations were in good agreement. In addition, Dogwiller et al. have numerically investigated the catalytically stabilized combustion of methane-air mixtures in lean conditions [10]. The primary target of the study was to study the coupling between homogenous and heterogeneous reactions under technically applicable operating conditions. The geometry was planar and parallel plates with a 2 mm distance between them and 50 mm length in the axial direction. The model consisted of 2D elliptic flow equations with gaseous and surface reactions and a molecular transport model including thermal diffusion. The radiative heat transfer from the catalytic walls and the conduction in solid plates of the wall were included in the model. The analyses were conducted for including both surface and gaseous reactions and for only surface reactions. They concluded that the effects of

adsorption and desorption of species were limited on ignition. In addition, they observed that homogenous combustion was dominant and directly affected radial production. Finally, they reported that the surface coverage was significantly changed in the flow direction; however, platinum and oxygen stayed as major surface species.

Elliptic equations can be used for modeling reacting channel flow problems. Deutschmann et al. have numerically studied the partial oxidation of methane in the monoliths, of which walls were coated with a noble metal, to investigate short contact time reactor modeling [11]. The reactor was modeled using 2D elliptic flow equations. The flow was kept in a laminar regime and the temperature and composition-dependent transport properties were used in the model. The elementary surface reactions were included in the model to calculate the mass fluxes of species on the surface. In addition to surface reactions, the gas-phase reactions were also considered in the analyses. The simulations of the model were conducted by using commonly used commercial software. The dependence of species conversion on the surface on flow velocity, diameter, pressure, catalyst material and the fuel-air ratio was investigated. A single tube was selected to model the monolith structure. The tube diameter varied between 0.25 mm and 1.0 mm and the length was 1 cm. The flow in the channel was kept in a laminar regime by considering the Reynolds number. They observed that rapid variations of temperature, velocity and transport coefficients have occurred in the catalyst entrance of the channel. They concluded that the larger diameter of the channel caused a decrease in methane conversion. In addition, methane conversion was decreased with the flow velocity. They observed that gas-phase reactions could be neglected at atmospheric pressures.

The parametric analyses of detailed chemistry mechanisms of fuels have been investigated with the simulations of reacting channel flows in the monolith structures. Hwang et al. have studied the characteristics of a hybrid catalytic combustor using boundary layer equations with detailed chemistry [12]. The hybrid catalytic combustor consisted of a thermal combustor section and catalytic bed. The numerical analyses were validated with the experimental data given in the literature

for the platinum-coated monolith. A parametric study for different flow properties, such as temperature, equivalence ratio, inlet pressure, velocity and channel entrance diameter, was conducted to study the effects of those parameters on catalytic combustion. A cylindrical and symmetric single-channel structure with a 0.15 cm diameter and 8.0 cm length was modeled for the analyses. A premixed methane-air mixture was introduced into the channel at atmospheric pressure. A Chemkin solver was used for the numerical calculations. They concluded that homogeneous and heterogeneous chemistry must be used for chemical reactions in the catalyst bed.

In addition to numerical studies, experiments on reacting channel flows have been conducted by researchers. Di Stazio et al. have experimentally studied the combustion of methane-air mixtures in a microchannel over a range of equivalence ratios and flow velocities to obtain detailed insight into flame behavior [13]. They developed new experimental devices to examine premixed air and methane combustion in narrow channels. The experiments were conducted at atmospheric pressure. Hydrogen-oxygen flames heated the channel downstream of the tube to satisfy uniform heating inside the channel. The inlet flow rate was varied between 0.03 m/s and 1.3 m/s in a channel with a 2.15 mm diameter to compare the results with previous studies. The experiments were conducted using a tube with a 1.85 mm diameter. In addition, the equivalence ratio varied between 0.5 and 1.5 in the experiments. The resulting stabilization position of flame for different conditions was presented as a function of inlet velocity, equivalence ratio and wall temperature. In addition, instability analyses for the flame for varying conditions were conducted and the results were reported. Moreover, the effect of flow velocity, heat source and equivalence ratio on flame shape were analyzed and the results were reported with their comparison by previous studies. They validated their new test setup using previous studies and provided a detailed frequency analysis for flames.

Another study of reacting channel flows with the wall temperature variation has been conducted using numerical and experimental methods. Maruta et al. have experimentally, numerically and analytically investigated premixed combustion in a heated channel [14]. The diameter of the channels was selected to be smaller than

the quenching distance of the fuel-oxidizer mixture. A cylindrical tube with a 2 mm inner diameter was used in the analyses to model the channel. In addition, the tube was heated on the downstream part by an external heat source to create a temperature gradient in the middle of the tube in the axial direction. In this channel, premixed flames were stabilized depending on the temperature gradient. The methane-air and propane-air mixtures with varying flow rates and fuel-air ratios were introduced into the channel using a controller in the experiments. The stationary flat premixed flames, pulsating flames and oscillating flames with high frequency were observed in the tube. In addition to the experiments, a stability analysis was conducted with detailed mechanisms using a 1D laminar model. They concluded that different flame modes were observed for intermediate mixture velocities in the experiments. In addition, they reported that experimental results and numerical results for stability analysis were in good agreement.

The transient process of catalytic combustion is another field of research for reacting channel flows. Schwiedernoch et al. have experimentally and numerically studied the catalytic ignition of methane in a cylindrical monolith, of which walls were coated with platinum, to investigate transient processes of catalytic combustion in monoliths [15]. In the experimental part of the study, the mixture of methane-oxygen-argon was introduced into a honeycomb monolith with platinum walls placed in a furnace. At the exit of the monolith, the temperature and species concentration were measured and analyzed. The study's numerical part investigated the temperature distribution around the solid structure and the flow field inside a single channel. The boundary layer equations were used for the modeling of the numerical problem. In addition, multistep surface reactions were included in the model. The heat transfer for the solid structure was coupled with the flow equations. The ignition temperatures, the exit temperature and species concentrations were numerically calculated and experimentally measured. For numerical calculations of the boundary layer equations, the DETCHEM code was used [16]. Data obtained by the two methods were compared for varying ratios of methane and oxygen in the mixture. The analyses were conducted under atmospheric pressure conditions. They

concluded that the simulation and experiment data were in excellent agreement. An increasing percentage of methane in the mixture increased the formation of hydroxide. For those cases, gas-phase reactions had to be included in the model. Moreover, they reported that the ignition was first started at the rear end of the outmost channels. At that time, the inner channels were cooled down by incoming flow. After the entire structure was heated, inner channels were ignited, beginning at the rear end.

Finally, the simulations of reacting channel flows can be used as a validation tool for the chemistry mechanisms of various fuels. Weedle et al. have developed a boundary layer model to investigate chemically reacting flow in a Chen nozzle, an experimental device to create a high-speed choked flow. The channel had a diameter of 1 mm and a reactor length of 32 mm. The walls of the reactor were held at a constant high temperature. For numerical evaluation, a boundary layer model for steady, axisymmetric channel flow was used. MATLAB ode15i function was used to assess a coupled parabolic set of equations. The slip boundary conditions were applied to the model. The premixed mixture of acetaldehyde and air was introduced into the channel for the analyses. The developed model was used to evaluate measured data. As a result, a model was proposed to be used to develop reaction mechanisms. They concluded that measured species concentrations by experiment could be predicted and evaluated by the model.

Most studies conducted for numerical model development for reacting flow in a channel include catalytic or decomposition surface reactions. However, sensitivity analyses and the effects of flow parameters on flame development for inert walls are limited in the literature. Also, developing an in-house code for reacting channel flow can be used to validate internally developed experiment setups. In this study, a code for chemically reacting flows in a channel reactor is formed by using boundary layer equations. Similarity transformation rules are applied to the governing flow equations under certain assumptions. Due to the simplification, the characteristics of governing flow equations are changed to parabolic PDEs. Parabolic PDEs are solved numerical techniques initially designed for ODEs using a method of lines. The

spatial terms are discretized by the finite difference method. The resulting set of boundary layer equations is written in differential algebraic equations. It is solved as a marching problem in the 2D domain with given initial and boundary conditions by using MATLAB ode15i solver. The flame position in a reacting channel flow and the parameters affecting flame development are investigated using the developed algorithm.

In this study, the channel flow reactors are first introduced as practical devices. Previous studies on numerical and experimental studies for modeling reacting channel flow are reviewed. Secondly, the theory of flow equations and boundary layer equations are discussed in detail. In addition, the theory of reacting boundary layer equations and their derivation for the numerical model is explained in detail. Furthermore, the numerical approach to model reacting channel flow is described. The solver and chemical library used by the developed code are presented. Finally, case problems for validation of generated code are introduced. In addition, parametric analyses of flow parameters to investigate their effect on flame development are conducted. Discussions of the results are presented.

CHAPTER 2

THEORY

In this section, the fundamental equations for boundary layer equations are discussed. Similarity arguments as a simplification method and their well-known examples are presented. Later, boundary layer equations for chemically reacting flows are derived and discretized to be integrated numerically.

2.1   Definitions of Fundamental Equations

Many problems in fluid dynamics can be explained by the action of the particles in a finite space. The analyses of fluid particles depend on fundamental principles of physics, which are the conservation of mass, conservation of momentum and the laws of thermodynamics [17].

2.1.1   Conservation of Mass

The conservation of mass states that the amount of mass coming in and out of a closed system should be equal [17].

$$
\left\{ \begin{array}{c} \text{Rate of Change} \\ \text{of Mass} \\ \text{of System} \end{array} \right\} = \left\{ \begin{array}{c} \text{Rate of Change} \\ \text{of Mass in} \\ \text{Control Volume} \end{array} \right\} + \left\{ \begin{array}{c} \text{Rate of Mass Flow} \\ \text{Through} \\ \text{Control Surface} \end{array} \right\}
$$

Therefore, the continuity equation can be defined in differential form as follows

$$
\frac{\partial \rho}{\partial t} + \nabla \cdot (\rho \vec{V}) = 0 \tag{2.1}
$$

2.1.2 Conservation of Momentum

Conservation of momentum is based on Newton's second law of motion, which states that the rate of change of momentum of a body equals the total forces applied to it [17].

$$
\left\{ \begin{array}{c} \text{Rate of Change} \\ \text{of Linear} \\ \text{Momentum} \\ \text{of System} \end{array} \right\} = \left\{ \begin{array}{c} \text{Rate of Change} \\ \text{of Linear} \\ \text{Momentum in} \\ \text{Control Volume} \end{array} \right\} + \left\{ \begin{array}{c} \text{Rate of Momentum} \\ \text{Flow Through} \\ \text{Control Surface} \end{array} \right\}
$$

$$
\frac{d}{dt}\left(m\vec{V}\right) = \frac{d}{dt}\left(\int_{CV} \vec{V}\rho dV\right) + \int_{CS} \vec{V}\rho(\vec{V}\cdot\hat{n})dA \tag{2.2}
$$

The conservation of momentum can be defined for an infinitesimally small fluid element by using differential-form expression as follows [19].

$$
\frac{d}{dt}\left(\rho\vec{V}\right) + \vec{V}\cdot\left(\nabla\rho\vec{V}\right) = \left(\rho\vec{f} - \nabla p + \nabla\sigma_{ij}\right) \tag{2.3}
$$

The stresses are modeled as a linear variation of deformation rates for each direction for viscous flows[18]:

$$
\sigma_{ij} = 2\mu\frac{\partial v_i}{\partial x_i}
$$

$$
\tau_{ij} = \mu\left(\frac{\partial v_i}{\partial x_j} + \frac{\partial v_j}{\partial x_i}\right) \tag{2.4}
$$

The Navier-Stokes equations are obtained by combining viscous flow representation of stress terms into an equation of motion. The Navier-Stokes equations are basic motion equations used to describe the flow of Newtonian fluid and are named in honor of Claude-Louis Navier and George Stokes [17].

$$\frac{\partial \rho u}{\partial t} + u\frac{\partial}{\partial x}(\rho u) + v\frac{\partial}{\partial y}(\rho u) + w\frac{\partial}{\partial z}(\rho u)$$

$$= -\frac{\partial p}{\partial x} + \mu\left(\frac{\partial^2 u}{\partial x^2} + \frac{\partial^2 u}{\partial y^2} + \frac{\partial^2 u}{\partial z^2}\right) + \rho g_x$$

$$\frac{\partial \rho v}{\partial t} + u\frac{\partial}{\partial x}(\rho v) + v\frac{\partial}{\partial y}(\rho v) + w\frac{\partial}{\partial z}(\rho v)$$

$$= -\frac{\partial p}{\partial y} + \mu\left(\frac{\partial^2 v}{\partial x^2} + \frac{\partial^2 v}{\partial y^2} + \frac{\partial^2 v}{\partial z^2}\right) + \rho g_y \tag{2.5}$$

$$\frac{\partial \rho w}{\partial t} + u\frac{\partial}{\partial x}(\rho w) + v\frac{\partial}{\partial y}(\rho w) + w\frac{\partial}{\partial z}(\rho w)$$

$$= -\frac{\partial p}{\partial z} + \mu\left(\frac{\partial^2 w}{\partial x^2} + \frac{\partial^2 w}{\partial y^2} + \frac{\partial^2 w}{\partial z^2}\right) + \rho g_z$$

2.1.3   Energy Equation

The energy equation is based on the first law of thermodynamics. It is stated that energy cannot be created or destroyed [20]. The first law of thermodynamics is written for a system as [17]:

$$\left\{\begin{matrix} Rate\ of\ Change \\ of\ Stored\ Energy \\ of\ System \end{matrix}\right\} = \left\{\begin{matrix} Rate\ of\ Energy \\ Addition\ by\ Heat \\ Transfer\ to\ System \end{matrix}\right\} + \left\{\begin{matrix} Rate\ of\ Energy \\ Addition\ by\ Work \\ to\ System \end{matrix}\right\}$$

$$\frac{D}{Dt}\int_{sys} e\rho dV = \dot{Q}_{net} + \dot{W}_{net} \tag{2.6}$$

The stored energy is the sum of internal energy, kinetic energy and potential energy per unit mass:

$$e = u + \frac{V^2}{2} + gz \tag{2.7}$$

The net heat flux is the sum of heat conduction and heat transfer due to species mass flux across the control surface [21]. Fourier's law defines heat flux in a system:

$$\vec{q} = -\lambda \nabla T \tag{2.8}$$

The work done on the system can also be written for a differential element after detailed tensor calculations as follows [21]:

$$\frac{dW}{dt} = \nabla \cdot (\vec{V} \cdot T) \delta V \tag{2.9}$$

The energy equation can be expressed in terms of temperature by combining these equations for an ideal gas as follows [21]:

$$\rho c_p \frac{DT}{Dt} = \frac{Dp}{Dt} + \nabla \cdot \lambda \nabla T - \sum_{k=1}^{K} c_{pk}(\vec{j}_k \cdot \nabla T) - \sum_{k=1}^{K} h_k \dot{\omega}_k W_k + \Phi \tag{2.10}$$

A chemical reaction term is found in the temperature form of the energy equation since a change in potential energy on the chemical bonds of species to thermal energy affects the temperature changes[21].

2.1.4 Conservation of Species

Conservation of species should be taken into account when computing chemically reacting flows. The fluid is generally a mixture of fuel, oxidizer and inert species for reacting flows. For that reason, it is necessary to define the relation between mass flux and species concentration [21].

Mass fraction is the most elementary quantity for species conservation and can be expressed with the given conditions:

$$Y_k = \frac{\rho_k}{\rho}$$

$$\sum_k^K \rho_k = \rho_{total} \quad \sum_k^K Y_k = 1 \tag{2.11}$$

When the flow is non-homogenous for species concentrations, species transportation inside the flow is occurred by molecular diffusion due to concentration differences in flow regions. This tendency is modeled by Fick's law, which states that the species concentration gradient is proportional negatively to a diffusive mass flux of that species [21][22]. Diffusive mass flux can be expressed as follows using Fick's Law:

$$\vec{j} = \rho Y_k \vec{V_k} \tag{2.12}$$

$\vec{V_k}$ is diffusion velocity vector for species k and it can be defined as follows

$$\vec{V_k} = -\frac{1}{X_k} D'_{km} \nabla X_k \tag{2.13}$$

where D'_{km} is mixture averaged diffusion coefficient term for species k with respect to the mixture and X_k is the molar fraction for species k.

The species mass flux is written by combining these relations:

$$\vec{j} = -\rho \frac{Y_k}{X_k} D'_{km} \nabla X_k \tag{2.14}$$

With these expressions, the species conservation equation can be written in integral form as follows [21]:

$$\left(\frac{dm_k}{dt}\right)_{sys} = -\int_{CS} \vec{j} \cdot \hat{n} dA + \int_{CV} \dot{\omega}_k W_k dV \tag{2.15}$$

13

The species conservation equation can be written for a differential element Using divergence theory [22]:

$$\rho \frac{DY_k}{Dt} = -\nabla \cdot \vec{j} + \dot{\omega}_k W_k \tag{2.16}$$

2.2 Classifications of Differential Equations

The conservation equations defining the fluid flow are a coupled nonlinear partial differential equations system. The Navier-Stokes equations contain second derivatives of velocity and temperature with respect to an independent spatial variable. Therefore, they can be labeled as second-order partial differential equations. The solution of second-order partial differential equations is highly dependent on their types, which are namely elliptic, parabolic and hyperbolic.

In order to start the classification of second-order partial differential equations, the following general form for partial equations can be considered [23], where independent variables are x and y, the dependent variables are "ϕ", and the coefficient of the terms are respectively A, B, C, D, E, F and G.

$$A\frac{\partial^2\phi}{\partial x^2} + B\frac{\partial^2\phi}{\partial x\partial y} + C\frac{\partial^2\phi}{\partial y^2} + D\frac{\partial\phi}{\partial x} + E\frac{\partial\phi}{\partial y} + F\phi + G = 0 \tag{2.17}$$

The terms not containing second-order derivatives can be summed on the right-hand side and the general form can be written as follows [2].

$$H = -\left(D\frac{\partial\phi}{\partial x} + E\frac{\partial\phi}{\partial y} + F\phi + G\right)$$

$$A\frac{\partial^2\phi}{\partial x^2} + B\frac{\partial^2\phi}{\partial x\partial y} + C\frac{\partial^2\phi}{\partial y^2} = H \tag{2.18}$$

For the second-order derivatives to exist and to be calculated, the first-order derivatives must be existing and continuous functions of independent variables of x and y [2]. As such, the first-order derivatives of "ϕ" can be written to represent the change of the characteristics between two locations of (x,y) and (x+dx,y+dy)

$$d\left(\frac{\partial\phi}{\partial x}\right) = \frac{\partial}{\partial x}\left(\frac{\partial\phi}{\partial x}\right)dx + \frac{\partial}{\partial y}\left(\frac{\partial\phi}{\partial x}\right)dy$$

$$d\left(\frac{\partial\phi}{\partial y}\right) = \frac{\partial}{\partial x}\left(\frac{\partial\phi}{\partial y}\right)dx + \frac{\partial}{\partial y}\left(\frac{\partial\phi}{\partial y}\right)dy$$

(2.19)

The resulting equations can be written in matrix form [2]. In this form of the equation, Cramer's rule can be applied to solve the second-order derivatives of the dependent variable ϕ.

$$\begin{bmatrix} A & B & C \\ dx & dy & 0 \\ 0 & dx & dy \end{bmatrix}\begin{bmatrix} \partial^2\phi/\partial x^2 \\ \partial^2\phi/\partial x\partial y \\ \partial^2\phi/\partial y^2 \end{bmatrix} = \begin{bmatrix} H \\ d(\partial\phi/\partial x) \\ d(y) \end{bmatrix}$$

(2.20)

The unique solutions of "ϕ" can be obtained by the result of this method unless discontinuities arise in the determinant of the coefficient matrix. The characteristic equation of the general form of a second-order partial differential equation can be obtained by setting the determinant of the coefficient matrix to zero.

$$A(dy)^2 - B(dx)(dy) + C\,(dx)^2 = 0$$

(2.21)

The solution of the characteristic equation represents the characteristic curves of the second-order partial differential equation [2].

$$\frac{dy}{dx} = \frac{B \pm \sqrt{B^2 - 4AC}}{2A}$$

(2.22)

The characteristic values are determined according to the sign of the discriminant of the characteristic curve representation formula. The value of the discriminant can be positive, zero, or negative so that the characteristic curves can be real and distinct,

real and repeated and complex, respectively. The classification of partial differential equations depends on this value, as represented in Table 2.1[2].

Table 2.1 Classification of Partial Differential Equations [23]

B^2-4AC	Characteristic Curves	Classification
Positive	Real and Distinct	Hyperbolic
Zero	Real and Repeated	Parabolic
Negative	Complex	Elliptic

When the value of the discriminant of characteristic lines representation is zero, there exists one real and repeated characteristic line and the partial differential equation is classified as parabolic. The viscosity diffusion equation and one-dimensional unsteady heat transfer equations are examples of parabolic PDEs. In order to define the problem and obtain a solution for parabolic PDEs, the initial condition for dependent variables and boundary conditions for two boundaries are required. The solution of parabolic PDEs is obtained by marching the initial conditions through the domain by satisfying boundary conditions [2][3].

The following figure shows the solution domains for the different classifications of partial differential equations [3].
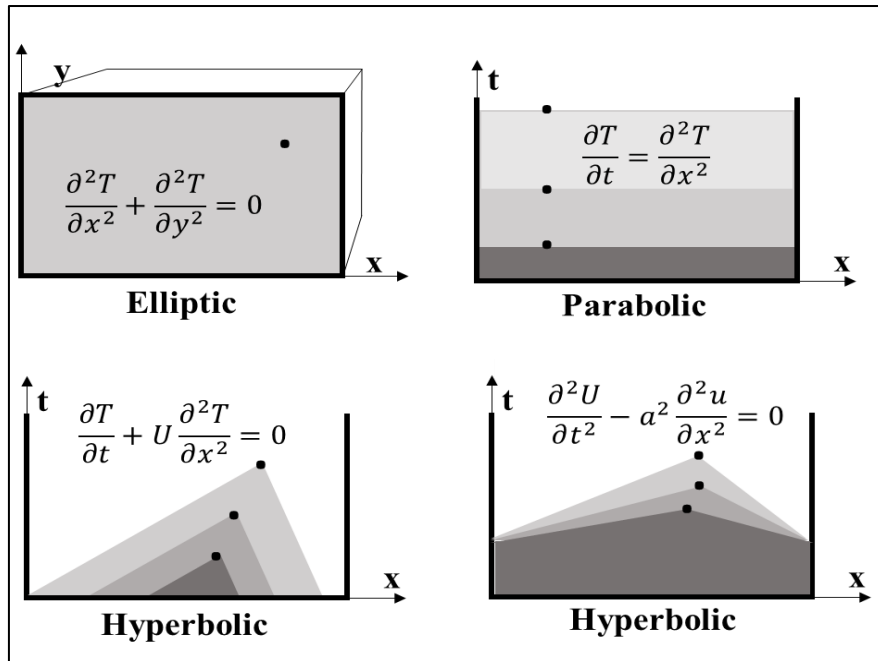
Figure 2.1 2D Domains For Different Partial Differential Equations [21]

The problem can be either unsteady or steady. The dependent variables are presented in the (t,x) domain in unsteady problems. The initial conditions are prescribed at initial time t0 and are marched forward in the time domain to get the complete solution in the domain of (t,x). In steady problems, the dependent variables are defined in the (x,y) domain, where both independent variables are spatial. The initial conditions are described at the initial location y0 and are marched forward in the space of y-direction. The characteristic of time in unsteady problems and spatial direction in steady problems are identical, so the direction of marching in steady problems is called time-like direction.

2.3   Similarity Theory

The Navier Stoke equations are non-linear and second-order partial differential equations defining the motion of the fluids. Due to the complexity of Navier Stokes equations, the exact mathematical solution is not commonly introduced except for a

few examples. Therefore, approximations are required to make the problems less complex and solvable by fluid equations under certain situations. One of the most important steps before the solution of flow equations is to analyze the relative effects of terms in the solution. The terms in the flow equations can be related with suitable chosen reference values to obtain dimensionless independent and dependent variables in flow equations [19]. With the help of the similarity method, the relative effects of the dimensionless terms on each other can be achieved by comparing their coefficients to simplify the equations. As a result of these simplifications, the characteristics of equations are changed to parabolic, which can be efficiently solved.

The dimensionless quantities can be considered as follows with respect to reference length, reference velocity, reference density, and reference time [19]:

$$\hat{x} = \frac{x}{l}$$
$$\hat{u} = \frac{v}{U}$$
$$\hat{\rho} = \frac{\rho}{\rho_R}$$
$$\hat{t} = \frac{t\,U}{l}$$

(2.23)

The continuity equation and momentum equation are written as follows using reference arguments:

$$\frac{D\hat{\rho}}{D\hat{t}} = -\hat{\rho}\,\widehat{div}\,\vec{v}$$
$$\hat{\rho}\,\frac{D\,\vec{\hat{v}}}{D\hat{t}} = -\widehat{grad}\,\hat{p} + \frac{1}{Re}\,\widehat{Div}\left[\hat{\mu}\left(2\hat{\varepsilon} - \frac{2}{3}\,\delta\,\widehat{div}\,\vec{v}\right)\right]$$

(2.24)

Where Reynolds number is written using reference quantities,

$$Re = \frac{\rho_R U l}{\mu_R}$$

(2.25)

The exact solution of the parabolic Navier Stoke equation can only be obtained under certain assumptions and using similarity parameters. One example of exact solutions

is based on the two-dimensional, steady state, incompressible and parallel flow between one stationary and one moving plate. The flow can be called parallel when one of the velocity components is zero and the other is non-zero. Thus, the particles of fluid can move in the same direction [19]. In addition, velocity cannot be dependent on the independent variable of the flow direction, which can be called x. Thus,

$$\frac{\partial u}{\partial x} + \frac{\partial v}{\partial y} = 0$$

$$\frac{\partial u}{\partial x} = 0 \qquad\qquad (2.26)$$

$$u = u(y); v = 0$$

For Navier Stokes equations, radial velocity vanishes in the radial direction and the resulting equation becomes as follows, which means the pressure is only dependent on axial direction. In the axial direction, the convective derivatives vanish since the velocity only depends on the radial direction.

$$\frac{\partial p}{\partial y} = 0$$

$$\frac{\partial p}{\partial x} = \mu \frac{\partial^2 u}{\partial y^2} \qquad\qquad (2.27)$$

The remaining set of equations, which are linear differential equations having two unknowns, u(y) and p(x), become analytically solvable after defining the corresponding boundary conditions. The terms on both sides can be set to constant value C to obtain the solution.

Boundary conditions are: y = 0 u = 0 , y = H, u = U

$$\frac{\partial p}{\partial x} = \mu \frac{\partial^2 u}{\partial y^2} = C \qquad\qquad (2.28)$$
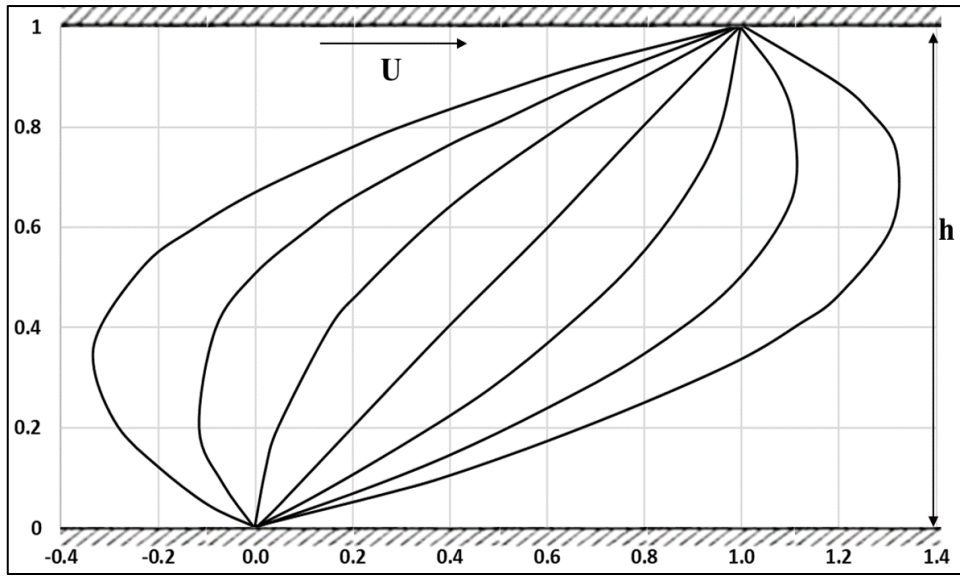
Figure 2.2. Dimensionless Velocity Profiles [19]

The solution of the flow field can be found as follows after applying boundary conditions.

$$u = \frac{C_1}{\mu}y^2 + \frac{C_2}{\mu}y + C_3$$

$$u = \frac{y}{H}U - \frac{H^2}{2\mu}\frac{dp}{dx}\frac{y}{H}\left(1 - \frac{y}{H}\right)$$

(2.29)

The resulting flow field is called Coutte-Poiseuille flow [19] and the value of the velocity field is determined according to the value of the pressure gradient in the axial direction.

Another example of exact solutions is based on the assumptions of the two-dimensional, incompressible and plane flow with very low viscosity passing a slender geometry [19].

20
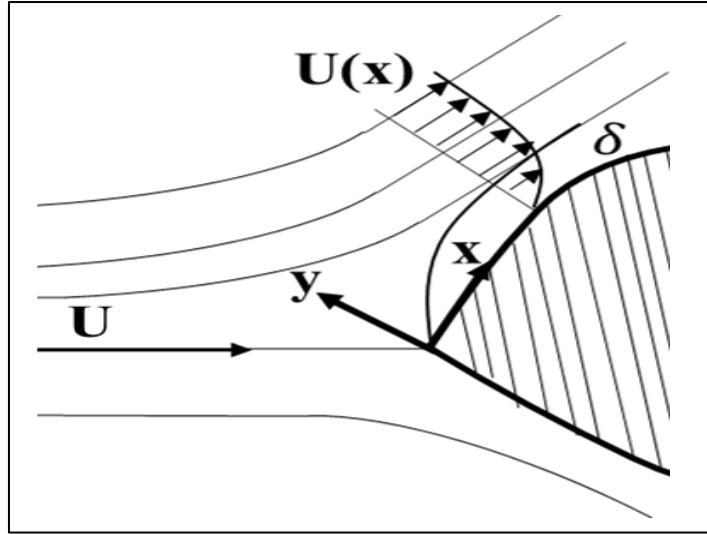
Figure 2.3. Velocity profile on slender geometry [19]

It can be easily assumed that the thickness of boundary layer δ, which is proportional to the square-root of kinematic viscosity [19], is very small compared to the length of the geometry l, which is δ ≪ l. Thus, the relation becomes as

$$\frac{\delta}{l} \sim \frac{1}{\sqrt{Re}}$$

(2.30)

The order of the terms in the dimensionless form of the Navier-Stokes equation takes the following magnitudes

$$\frac{1}{Re}\frac{\partial^2 \hat{u}}{\partial \hat{x}^2} \sim \delta^2$$

$$\hat{v} \sim \delta \quad , \quad \hat{y} \sim \delta$$

(2.31)

Since the value of dimensionless velocity in the radial direction term and spatial term of radial direction becomes too small, while the thickness of the boundary layer goes to zero, it is more appropriate to define new variables $\bar{v}$ and $\bar{y}$ as

$$\bar{v} \sim \hat{v}/\delta \quad , \quad \bar{y} \sim \hat{y}/\delta$$

(2.32)

Finally, Prandtl boundary layer equations can be obtained by simplifying negligibly small terms when the value of the Reynolds number goes to infinity.

$$\frac{\partial \hat{u}}{\partial \hat{x}} + \frac{\partial \bar{v}}{\partial \bar{y}} = 0$$

$$\frac{\partial \hat{u}}{\partial \hat{t}} + \hat{u}\frac{\partial \hat{u}}{\partial \hat{x}} + \bar{v}\frac{\partial \hat{u}}{\partial \hat{y}} = -\frac{\partial \hat{p}}{\partial \hat{x}} + \frac{\partial^2 \hat{u}}{\partial \bar{y}^2} \qquad (2.33)$$

$$0 = -\frac{\partial \hat{p}}{\partial \bar{y}}$$

Moreover, the pressure gradient term can be eliminated from equations by equating velocity distribution inside the boundary layer to outer velocity distribution at the outer edge limit of the boundary layer. For given outer flow velocity distribution U(x,t), the boundary layer equations for incompressible plane flows can be solved with appropriate boundary conditions and the velocity distribution inside the boundary layer can be calculated.

The final example of the exact solution is called the Hagen Poiseulle flow. The solution of the fully developed axisymmetric flow through a pipe in circular coordinates can be written using the similarity solutions of Navier-Stokes equations. The previously introduced boundary layer equations can be used to solve steady pipe flow in a circular coordinate system[24]. Thus, the resulting momentum equation in the axial direction can be written as follows.

$$\frac{dp}{dx} = \mu\left(\frac{\partial^2 u}{\partial r^2} + \frac{1}{r}\frac{du}{dr}\right) \qquad (2.34)$$

With the no-slip boundary conditions on the wall, the solution of the velocity field in the pipe becomes as follows [19].

$$u(r) = u_{max}\left(1 - \frac{r^2}{R^2}\right) \qquad (2.35)$$

$$u_{max} = 2u_{mean} = \frac{R^2}{4\mu}\left(-\frac{dp}{dx}\right)$$ (2.36)

These relations can be used as the analytical solution for the flow in a pipe and shows excellent agreement with the experimental measurements, while the Reynolds number for the corresponding flow is below 2300, which is the critical Reynolds number [19].

The usage of similarity arguments in the solution of flow problems is summarized with examples of the exact solution of the Navier-Stokes equations. In this study, similarity variables are also used in simplifying flow equations. In addition, the boundary layer equations are non-dimensionalized by using similarity arguments. After the simulations are completed, the similarity analyses of the parameters of reacting channel flow are conducted and the similitude parameters are defined.

2.4   Simplification of Flow Equations using Scaling Arguments

The fundamental flow equations and similarity theory with its examples are discussed in the previous chapter in detail. The generation of boundary layer equations using scaling arguments is one of the solutions to Navier Stoke's equations. The boundary layer equations can also be used to solve reacting flows in channels.

The derivation of boundary layer equations can be started by defining the conversation of mass, momentum and species and energy equations, respectively, for cylindrical coordinates of an ideal-gas mixture [21]:

$$\frac{\partial\rho}{\partial t} + \frac{\partial(\rho u)}{\partial z} + \frac{1}{r}\frac{\partial(r\rho v)}{\partial r} = 0$$ (2.37)

$$\rho \left(\frac{\partial u}{\partial t} + u \frac{\partial u}{\partial z} + v \frac{\partial u}{\partial r} \right)$$

$$= -\frac{\partial p}{\partial z} + \frac{\partial}{\partial z} \left[2\mu \frac{\partial u}{\partial z} + \kappa \nabla \cdot \boldsymbol{V} \right] + \frac{1}{r} \frac{\partial}{\partial r} \left[\mu r \left(\frac{\partial v}{\partial z} + \frac{\partial u}{\partial r} \right) \right] \qquad (2.38)$$

$$+ f_z$$

$$\rho \left(\frac{\partial v}{\partial t} + u \frac{\partial v}{\partial z} + v \frac{\partial v}{\partial r} \right)$$

$$= -\frac{\partial p}{\partial r} + \frac{\partial}{\partial z} \left[\mu \left(\frac{\partial v}{\partial z} + \frac{\partial u}{\partial r} \right) \right] + \frac{\partial}{\partial r} \left[2\mu \frac{\partial v}{\partial r} + \kappa \nabla \cdot \boldsymbol{V} \right] \qquad (2.39)$$

$$+ \frac{2\mu}{r} \left[\frac{\partial v}{\partial r} - \frac{v}{r} \right] + f_r$$

$$\rho \frac{DY_k}{Dt} = \rho \left(\frac{\partial Y_k}{\partial t} + u \frac{\partial Y_k}{\partial z} + v \frac{\partial Y_k}{\partial r} \right) = -\left(\frac{\partial j_{k,z}}{\partial z} + \frac{1}{r} \frac{\partial r j_{k,r}}{\partial r} \right) + \dot{\omega}_k W_k \qquad (2.40)$$

$$\rho c_p \left(\frac{\partial T}{\partial t} + u \frac{\partial T}{\partial z} + v \frac{\partial T}{\partial r} \right)$$

$$= \left(\frac{\partial p}{\partial t} + u \frac{\partial p}{\partial z} + v \frac{\partial p}{\partial r} \right) + \frac{\partial}{\partial z} \left(\lambda \frac{\partial T}{\partial z} \right) + \frac{1}{r} \frac{\partial}{\partial r} \left(r\lambda \frac{\partial T}{\partial r} \right)$$

$$- \sum_{k=1}^{K} c_{pk} \left(j_{k,z} \frac{\partial T}{\partial z} + j_{k,r} \frac{\partial T}{\partial r} \right) - \sum_{k=1}^{K} h_k \dot{\omega}_k W_k + \Phi \qquad (2.41)$$

The reacting boundary layer equations are derived assuming steady, axisymmetric flow at low-speed with no body force satisfying Stokes hypothesis. [25].

For axisymmetric cylindrical coordinates, the divergence of the flow field is written as follows:

$$\nabla \cdot \vec{V} = \frac{\partial u}{\partial z} + \frac{\partial v}{\partial r} + \frac{v}{r} \qquad (2.42)$$

Moreover, Stokes theorem is used to relate two terms of viscosities given as follows:

$$\kappa = -\frac{2}{3}\mu \tag{2.43}$$

Using these relations, the conservation of mass and momentum equations are simplified for cylindrical coordinates. The scaling arguments can be applied to simplified equations to observe the scale relations between terms to obtain boundary layer equations.

$$\frac{\partial(\rho u)}{\partial z} + \frac{1}{r}\frac{\partial(r\rho v)}{\partial r} = 0 \tag{2.44}$$

$$\rho u \frac{\partial u}{\partial z} + \rho v \frac{\partial u}{\partial r}$$
$$= -\frac{\partial p}{\partial z} + \frac{\partial}{\partial z}\left[\frac{4}{3}\mu\frac{\partial u}{\partial z} - \frac{2}{3}\frac{1}{r}\frac{\partial(rv)}{\partial r}\right] \tag{2.45}$$
$$+ \frac{1}{r}\frac{\partial}{\partial r}\left[\mu r\left(\frac{\partial v}{\partial z} + \frac{\partial u}{\partial r}\right)\right]$$

$$\rho u \frac{\partial v}{\partial z} + \rho v \frac{\partial v}{\partial r} = -\frac{\partial p}{\partial r} + \frac{\partial}{\partial z}\left[\mu\left(\frac{\partial v}{\partial z} + \frac{\partial u}{\partial r}\right)\right]$$
$$+ \frac{\partial}{\partial r}\left[\frac{4}{3}\mu\frac{\partial v}{\partial r} - \frac{2}{3}\mu\left(\frac{\partial u}{\partial z} + \frac{v}{r}\right)\right] + \frac{2\mu}{r}\left[\frac{\partial v}{\partial r} - \frac{v}{r}\right] \tag{2.46}$$

The boundary layer approach scales the arguments in Navier Stokes equations to reduce negligible terms under certain conditions. The derivation starts with non-dimensionalizing the equations by using reference scaling arguments to make all dependent and independent variables order one. Then, the magnitudes of terms are relatively compared and the negligible terms are sought.

$$\hat{z} = \frac{z}{z_s} \ , \qquad \hat{r} = \frac{r}{r_s} \ , \qquad \hat{u} = \frac{u}{u_0} \ , \qquad \hat{v} = \frac{v}{v_s} \ , \qquad \hat{\rho} = \frac{\rho}{\rho_0}$$

$$\hat{\mu} = \frac{\mu}{\mu_0} \ , \qquad \hat{p} = \frac{p}{\rho_0 u_0^2}$$

(2.47)

The reference scales are, respectively z_s is for axial coordinate, r_s is for radial coordinate, u_0 is for axial velocity, ρ_0 and μ_0 are for density and viscosity and v_s is for radial velocity. The reference scales for coordinates are arbitrary at the beginning of the derivation. The axial velocity reference scale is a uniform inlet velocity, and density and viscosity scales are their values in the inlet, respectively. Finally, the radial velocity reference scale is unknown.

Conservation of mass equation is expressed in terms of reference scales and flow properties as follows:

$$\left(\frac{\rho_0 u_0}{z_s}\right)\frac{\partial(\hat{\rho}\hat{u})}{\partial \hat{z}} + \left(\frac{\rho_0 v_s}{r_s}\right)\frac{1}{\hat{r}}\frac{\partial(\hat{r}\hat{\rho}\hat{v})}{\partial \hat{r}} = 0$$

(2.48)

The two terms of the continuity equation must be retained for the two-dimensional boundary layer equation as order one-terms. Thus, the axial and radial velocity scales must be related to each other.

$$\frac{\rho_0 u_0}{z_s} = \frac{\rho_0 v_s}{r_s}$$

$$v_s = \frac{u_0 r_s}{z_s}$$

(2.49)

The mass conservation equation is simplified to the following form using the introduced relations.

$$\frac{\partial(\hat{\rho}\hat{u})}{\partial \hat{z}} + \frac{1}{\hat{r}}\frac{\partial(\hat{r}\hat{\rho}\hat{v})}{\partial \hat{r}} = 0$$

(2.50)

Conservation of the momentum equation in the axial direction is presented below, considering the previous scale relation in the non-dimensional form:

$$
\left(\frac{\rho_0 u_0{}^2}{z_s}\right)\hat{\rho}\hat{u}\frac{\partial \hat{u}}{\partial \hat{z}} + \left(\frac{\rho_0 u_0}{r_s}\left(\frac{u_0 r_s}{z_s}\right)\right)\hat{\rho}\hat{v}\frac{\partial \hat{u}}{\partial \hat{r}}
$$

$$
= -\left(\frac{\rho_0 u_0{}^2}{z_s}\right)\frac{\partial \hat{p}}{\partial \hat{z}} + \left(\frac{\rho_0 u_0}{z_s{}^2}\right)\frac{\partial}{\partial \hat{z}}\left[\frac{4}{3}\hat{\mu}\frac{\partial \hat{u}}{\partial \hat{z}} - \frac{2}{3}\hat{\mu}\frac{1}{\hat{r}}\frac{\partial(\hat{r}\hat{v})}{\partial \hat{r}}\right] \quad (2.51)
$$

$$
+ \left(\frac{\mu_0}{r_s z_s}\left(\frac{u_0 r_s}{z_s}\right)\right)\frac{1}{\hat{r}}\frac{\partial}{\partial \hat{r}}\left(\hat{\mu}\hat{r}\frac{\partial \hat{v}}{\partial \hat{z}}\right) + \left(\frac{\mu_0 u_0}{r_s{}^2}\right)\frac{1}{\hat{r}}\frac{\partial}{\partial \hat{r}}\left(\hat{\mu}\hat{r}\frac{\partial \hat{u}}{\partial \hat{r}}\right)
$$

Reynolds number can be defined with respect to the channel radius as $\mathrm{Re}_r = \frac{\rho_0 u_0 r_s}{\mu_0}$ and all terms can be multiplied with $\frac{z_s}{\rho_0 u_0^2}$ to simplify and get the axial momentum equation in the following form.

$$
\hat{\rho}\hat{u}\frac{\partial \hat{u}}{\partial \hat{z}} + \hat{\rho}\hat{v}\frac{\partial \hat{u}}{\partial \hat{r}}
$$

$$
= -\frac{\partial \hat{p}}{\partial \hat{z}}
$$

$$
+ \left(\frac{r_s}{z_s}\frac{1}{\mathrm{Re}_r}\right)\left\{\frac{\partial}{\partial \hat{z}}\left[\frac{4}{3}\hat{\mu}\frac{\partial \hat{u}}{\partial \hat{z}} - \frac{2}{3}\hat{\mu}\frac{1}{\hat{r}}\frac{\partial(\hat{r}\hat{v})}{\partial \hat{r}}\right]\right. \quad (2.52)
$$

$$
\left. + \frac{1}{\hat{r}}\frac{\partial}{\partial \hat{r}}\left(\hat{\mu}\hat{r}\frac{\partial \hat{v}}{\partial \hat{z}}\right)\right\} + \left(\frac{z_s}{r_s}\frac{1}{\mathrm{Re}_r}\right)\frac{1}{\hat{r}}\frac{\partial}{\partial \hat{r}}\left(\hat{\mu}\hat{r}\frac{\partial \hat{u}}{\partial \hat{r}}\right)
$$

After expressing the momentum equation in the axial direction, the application of reference scales in the radial direction can be given below using the same scaling relations.

$$\left(\frac{\rho_0 u_0}{z_s}\left(\frac{u_0 r_s}{z_s}\right)\right)\hat{\rho}\hat{u}\frac{\partial \hat{v}}{\partial \hat{z}} + \left(\frac{\rho_0 u_0}{r_s}\left(\frac{u_0 r_s}{z_s}\right)^2\right)\hat{\rho}\hat{v}\frac{\partial \hat{v}}{\partial \hat{r}}$$

$$= -\left(\frac{\rho_0 u_0^2}{r_s}\right)\frac{\partial \hat{p}}{\partial \hat{r}} + \left(\frac{\mu_0}{r_s^2}\left(\frac{u_0 r_s}{z_s}\right)\right)\frac{\partial}{\partial \hat{r}}\left(\frac{4}{3}\hat{\mu}\frac{\partial \hat{v}}{\partial \hat{z}} - \frac{2}{3}\hat{\mu}\frac{\hat{v}}{\hat{r}}\right)$$

$$- \left(\frac{\mu_0 u_0}{r_s z_s}\right)\frac{\partial}{\partial \hat{r}}\left(\frac{2}{3}\hat{\mu}\frac{\partial \hat{u}}{\partial \hat{z}}\right) + \left(\frac{\mu_0}{r_s^2}\left(\frac{u_0 r_s}{z_s}\right)\right)\frac{2\hat{\mu}}{\hat{r}}\left[\frac{\partial \hat{v}}{\partial \hat{r}} - \frac{\hat{v}}{\hat{r}}\right]$$

$$+ \left(\frac{\mu_0}{z_s^2}\left(\frac{u_0 r_s}{z_s}\right)\right)\frac{\partial}{\partial \hat{z}}\left(\hat{\mu}\frac{\partial \hat{v}}{\partial \hat{z}}\right) + \left(\frac{\mu_0 u_0}{r_s z_s}\right)\frac{\partial}{\partial \hat{z}}\left(\hat{\mu}\frac{\partial \hat{u}}{\partial \hat{r}}\right) \qquad (2.53)$$

Hence, it takes the following form after the coefficients of terms are simplified.

$$\left(\frac{r_s^2}{z_s^2}\right)\hat{\rho}\hat{u}\frac{\partial \hat{v}}{\partial \hat{z}} + \left(\frac{r_s^2}{z_s^2}\right)\hat{\rho}\hat{v}\frac{\partial \hat{v}}{\partial \hat{r}}$$

$$= -\frac{\partial \hat{p}}{\partial \hat{r}} + \left(\frac{1}{Re_r}\frac{r_s^3}{z_s^3}\right)\frac{\partial}{\partial \hat{z}}\left(\hat{\mu}\frac{\partial \hat{v}}{\partial \hat{z}}\right)$$

$$+ \left(\frac{1}{Re_r}\frac{r_s}{z_s}\right)\left\{\frac{\partial}{\partial \hat{z}}\left(\hat{\mu}\frac{\partial \hat{u}}{\partial \hat{r}}\right) + \frac{\partial}{\partial \hat{r}}\left(\frac{4}{3}\hat{\mu}\frac{\partial \hat{v}}{\partial \hat{z}} - \frac{2}{3}\hat{\mu}\left(\frac{\partial \hat{u}}{\partial \hat{z}} + \frac{\hat{v}}{\hat{r}}\right)\right) \qquad (2.54)$$

$$+ \frac{2\hat{\mu}}{\hat{r}}\left[\frac{\partial \hat{v}}{\partial \hat{r}} - \frac{\hat{v}}{\hat{r}}\right]\right\}$$

In channel flows, the height of the channel is narrow compared to its length, the reason that it can be considered as $z_s \gg r_s$. In addition, after considering the Reynolds number as $Re_r > 1$, it is observed that the only term order one is the pressure gradient term. Therefore, the momentum equation in the radial direction is reduced to the following form for boundary layer approximation.

$$\frac{\partial p}{\partial r} = 0 \qquad (2.55)$$

For the momentum equation in the axial direction, considering $z_s \gg r_s$ and $\mathrm{Re}_r > 1$, comparison of the coefficients of two terms shows that the radial diffusion term is always much more dominant than other diffusion terms.

$$\left(\frac{z_s}{r_s} \frac{1}{\mathrm{Re}_r}\right) \gg \left(\frac{r_s}{z_s} \frac{1}{\mathrm{Re}_r}\right) \tag{2.56}$$

In addition, the coefficient of radial diffusion can be considered to order one as the most relevant assumption for diffusion term notation [21].

$$\left(\frac{z_s}{r_s} \frac{1}{\mathrm{Re}_r}\right) \sim 1 \tag{2.57}$$

The axial length scale is defined as a characteristic radial length scale by taking the channel radius as r_0.

$$z_s \sim r_0 \mathrm{Re}_r \tag{2.58}$$

Once a flow with any inlet velocity profile is introduced at the inlet, the fully developed flow is reached after a distance in the channel. In that developing range, the vortices and instabilities in the flow can be generated close to the wall so that the boundary layer equation cannot resolve the flow [19]. However, after a distance in the channel, the flow development is completed and a profile of the Hagen-Poiseuille flow is reached. In that case, pressure gradient and radial diffusion terms become dominant concerning convective terms.

Furthermore, the energy equation and conservation of species equation are simplified using reference scales. For a steady and 2D flow, where circumferential variations are neglected, the equations are written for axisymmetric cylindrical coordinates [21].

$$\rho u \frac{\partial Y_k}{\partial z} + \rho v \frac{\partial Y_k}{\partial r} = \left(\frac{\partial j_{k,z}}{\partial z} + \frac{1}{r} \frac{\partial (r j_{k,r})}{\partial r} \right) + \dot{\omega}_k W_k \qquad (2.59)$$

$$\rho c_p u \frac{\partial T}{\partial z} + \rho c_p v \frac{\partial T}{\partial r}$$

$$= u \frac{\partial p}{\partial z} + \frac{\partial}{\partial z} \left(\lambda \frac{\partial T}{\partial z} \right) + \frac{1}{r} \frac{\partial}{\partial r} \left(r \lambda \frac{\partial T}{\partial r} \right) \qquad (2.60)$$

$$- \sum_{k=1}^{K} c_{pk} \left(j_{k,z} \frac{\partial T}{\partial z} + j_{k,r} \frac{\partial T}{\partial r} \right) - \sum_{k=1}^{K} h_k \dot{\omega}_k W_k$$

Using mixture-averaged diffusion coefficient for species k as expressed in section 2.1.4, the diffusive mass flux term can be written in a non-dimensional form as follows:

$$\vec{J_k} = \rho Y_k \vec{V_k} = -\rho \frac{W_k}{\overline{W}} D_{km} \nabla X_k \qquad (2.61)$$

$D_{k,0}$ is defined as a reference diffusion coefficient term. Therefore, diffusive mass flux is written using reference scales in both radial and axial directions.

$$j_{k,z} = -\frac{\rho_0 D_{k,0}}{z_s} \hat{\rho} \frac{W_k}{\overline{W}} \widehat{D}_{km} \frac{\partial X_k}{\partial \hat{z}} \qquad (2.62)$$

$$j_{k,z} = -\frac{\rho_0 D_{k,0}}{z_s} \hat{\rho} \frac{W_k}{\overline{W}} \widehat{D}_{km} \frac{\partial X_k}{\partial \hat{z}} \qquad (2.63)$$

Secondly, a non-dimensional temperature can be defined using reference temperature scales, which T_0 is the inlet flow temperature and T_w is the wall temperature.

$$\hat{T} = \frac{T - T_0}{T_w - T_0} = \frac{T - T_0}{\Delta T} \qquad (2.64)$$

With these reference arguments, a non-dimensional form of the conservation of species and energy equations is written as follows:

$$\hat{\rho}\hat{u}\frac{\partial Y_k}{\partial \hat{z}} + \hat{\rho}\hat{v}\frac{\partial Y_k}{\partial r}$$

$$= -\left(\frac{r_s}{z_s}\frac{\mu_0}{\rho_0 u_0 r_s}\frac{\mu}{\rho D_k}\right)\frac{\partial \hat{j}_{k,z}}{\partial \hat{z}} \qquad (2.65)$$

$$- \left(\frac{z_s}{r_s}\frac{\mu_0}{\rho_0 u_0 r_s}\frac{\mu}{\rho D_k}\right)\frac{1}{\hat{r}}\frac{\partial(\hat{r}\hat{j}_{k,r})}{\partial \hat{r}} + \frac{z_s}{\rho_0 u_0}\dot{\omega}_k W_k$$

$$\hat{\rho}\hat{u}\hat{c}_p\frac{\partial \hat{T}}{\partial \hat{z}} + \hat{\rho}\hat{v}\hat{c}_p\frac{\partial \hat{T}}{\partial \hat{r}}$$

$$= \frac{u_0^2}{c_{p,0}}\hat{u}\frac{\partial \hat{p}}{\partial \hat{z}} + \left(\frac{r_s}{z_s}\frac{\mu_0}{\rho_0 u_0 r_s}\frac{\lambda}{\mu c_p}\right)\frac{\partial}{\partial \hat{z}}\left(\hat{\lambda}\frac{\partial \hat{T}}{\partial \hat{z}}\right)$$

$$+ \left(\frac{z_s}{r_s}\frac{\mu_0}{\rho_0 u_0 r_s}\frac{\lambda}{\mu c_p}\right)\frac{1}{\hat{r}}\frac{\partial}{\partial \hat{r}}\left(\hat{r}\hat{\lambda}\frac{\partial \hat{T}}{\partial \hat{r}}\right) \qquad (2.66)$$

$$- \sum_{k=1}^{K}\left[\left(\frac{r_s}{z_s}\frac{\mu_0}{\rho_0 u_0 r_s}\frac{\mu}{\rho D_k}\right)\hat{c}_{pk}\hat{j}_{k,z}\frac{\partial \hat{T}}{\partial \hat{z}}\right.$$

$$\left.+ \left(\frac{z_s}{r_s}\frac{\mu_0}{\rho_0 u_0 r_s}\frac{\mu}{\rho D_k}\right)\hat{c}_{pk}\hat{j}_{k,r}\frac{\partial \hat{T}}{\partial \hat{r}}\right] - \frac{\Delta T z_s}{c_{p,0}\rho_0 u_0}\sum_{k=1}^{K}h_k\dot{\omega}_k W_k$$

In order to assess the weights of equation terms, the order of magnitude of the coefficients of radial and axial diffusion terms are compared:

$$\frac{z_s}{r_s}\frac{\mu_0}{\rho_0 u_0 r_s}\frac{\mu}{\rho D_k} \sim 1$$

$$\frac{z_s}{r_s}\frac{\mu_0}{\rho_0 u_0 r_s}\frac{\lambda}{\mu c_p} \sim 1 \qquad (2.67)$$

These terms are multiplied by $\frac{r_s^2}{z_s^2}$ to make them comparable.

$$\frac{r_s}{z_s}\frac{\mu_0}{\rho_0 u_0 r_s}\frac{\mu}{\rho D_k} \sim \frac{r_s^2}{z_s^2} \qquad (2.68)$$

$$\frac{r_s}{z_s} \frac{\mu_0}{\rho_0 u_0 r_s} \frac{\lambda}{\mu c_p} \sim \frac{r_s{}^2}{z_s{}^2} \tag{2.69}$$

The similarity analysis shows the radial terms in species and energy equations are relatively small compared to axial terms as $\frac{r_s}{z_s} \to 0$. The term $u\frac{\partial p}{\partial z}$ can be neglected in the energy equation since this term becomes relatively small concerning other terms for low-speed flows, where $Ma < 0.3$, in boundary layer approximations.

The flow equations using boundary layer approximation for axisymmetric channel flow can be written as [21]:

$$\frac{\partial(\rho u)}{\partial z} + \frac{1}{r}\frac{\partial(r\rho v)}{\partial r} = 0$$

$$\rho u \frac{\partial u}{\partial z} + \rho v \frac{\partial u}{\partial r} = -\frac{\partial p}{\partial z} + \frac{1}{r}\frac{\partial}{\partial r}\left(\mu r \frac{\partial u}{\partial r}\right)$$

$$\frac{\partial p}{\partial r} = 0$$

$$\rho u \frac{\partial Y_k}{\partial z} + \rho v \frac{\partial Y_k}{\partial r} = -\frac{1}{r}\frac{\partial(rj_{k,r})}{\partial r} + \dot{\omega}_k W_k \tag{2.70}$$

$$\rho c_p u \frac{\partial T}{\partial z} + \rho c_p v \frac{\partial T}{\partial r}$$

$$= \frac{1}{r}\frac{\partial}{\partial r}\left(r\lambda \frac{\partial T}{\partial r}\right) - \sum_{k=1}^{K} c_{pk} j_{k,r} \frac{\partial T}{\partial r} - \sum_{k=1}^{K} h_k \dot{\omega}_k W_k$$

$$\rho = \frac{p}{RT \sum Y_k/W_k}$$

The simplification of flow equations using scaling arguments is given in detail and the boundary layer equations for reaching channel flows are obtained in this section. One of the most significant contributions of scaling arguments is the change of the characteristics of differential equations to parabolic form. Partial differential equations can be solved using numerical methods as ordinary differential equations. One way of solving PDEs is by using the method of lines.

2.5   Method of Lines

The method of lines is a numerical technique especially suited for solving coupled systems of parabolic partially differential equations (PDE) [21]. A wide range of PDEs for the problems of chemical reactions and systems of equations can be successfully solved by using the method of lines [26]. The main idea behind this computational method is to reduce the partial differential equation problem to a less complex differential equation problem by discretizing one of the independent variables [27]. The semi-discrete problem is written in the form of differential-algebraic equations (DAEs) or ordinary differential equations (ODEs) form to be solved numerically. With the usage of the method of lines, the partial differential equations can be converted to DAEs or ODEs, for which many solvers exist to integrate [27].

The boundary layer equations can also be modeled and solved using the line method. The radial terms with the spatial independent variable of the equations system are discretized using the finite-difference method. The axial terms having timelike independent variables are kept in the equations. For the momentum equation, the spatial terms are the diffusive and convective terms. The diffusion terms are discretized using conservative difference approximation at the control-volume faces, where fluxes and transport properties are calculated [21]. The convective terms are evaluated by using the upwind formula. In addition to the momentum equation, the diffusion and the convective terms are considered similarly in the momentum equation.

Although the pressure term is the only function of the timelike independent variable, the gradient of the pressure term is still defined at each spatial mesh point to preserve the banded structure of Jacobian [21]. The pressure is solved by a trivial differential equation. The term pressure gradient is directly used in the momentum equation.

The resulting set of equations is written in DAEs form. In addition, boundary conditions are also adjusted as algebraic constraints, which contain no time

derivatives [21]. The equations in the form of DEAs can be solved with existing and well-established numerical techniques and software packages, such as DASSL [9] and MATLAB ode15i [28]. Since the discretization of spatial terms is only done by forming DAEs, the time discretization, the error control and the solution are managed by solver software.

2.6   Von Mises Transformation

The boundary layer formulations are written in physical coordinates. Alternatively, these equations can be transformed into stream-function coordinates to gain computational advantages. This independent variable changing procedure is called Von Misses Transformation.

The transformation begins with the introduction of stream function ψ as,

$$\rho u r = \frac{\partial \psi}{\partial r}$$
$$\rho v r = - \frac{\partial \psi}{\partial z} \tag{2.71}$$

$$\frac{\partial(\rho u)}{\partial z} + \frac{1}{r}\frac{\partial(r\rho v)}{\partial r} = 0$$
$$\frac{1}{r}\frac{\partial}{\partial z}\left(\frac{\partial \psi}{\partial r}\right) - \frac{1}{r}\frac{\partial}{\partial r}\left(\frac{\partial \psi}{\partial z}\right) = 0 \tag{2.72}$$

As a consequence of the nature of the stream function, these relations satisfy the mass-continuity equation. The independent variable in cross-stream coordinate r is replaced with the streamlines, which are introduced as lines of constant ψ. The transformation of the independent variable can be done by introducing chain rule differentiation.

$$\left(\frac{\partial}{\partial x}\right)_y = \left(\frac{\partial \eta}{\partial x}\right)_y \left(\frac{\partial}{\partial \eta}\right)_\phi + \left(\frac{\partial \phi}{\partial x}\right)_y \left(\frac{\partial}{\partial \phi}\right)_\eta$$

$$\left(\frac{\partial}{\partial y}\right)_x = \left(\frac{\partial \eta}{\partial y}\right)_x \left(\frac{\partial}{\partial \eta}\right)_\phi + \left(\frac{\partial \phi}{\partial y}\right)_x \left(\frac{\partial}{\partial \phi}\right)_\eta$$

(2.73)

The transformation matrix is formed by four coefficient derivatives and can be written as follows:

$$\begin{bmatrix} \left(\dfrac{\partial \eta}{\partial x}\right)_y & \left(\dfrac{\partial \phi}{\partial x}\right)_y \\[3mm] \left(\dfrac{\partial \eta}{\partial y}\right)_x & \left(\dfrac{\partial \phi}{\partial y}\right)_x \end{bmatrix}$$

(2.74)

After the introduction of Von Mises Transformation in general form, the boundary layer form of the transformation can be written for the independent variables (z,ψ). The relation between independent variables is stated below:

$$\left(\frac{\partial z}{\partial z}\right)_r = 1, \quad \left(\frac{\partial \psi}{\partial z}\right)_r = -\rho v r$$

$$\left(\frac{\partial z}{\partial r}\right)_z = 0, \quad \left(\frac{\partial \psi}{\partial r}\right)_z = -\rho u r$$

$$\left(\frac{\partial}{\partial z}\right)_r = \left(\frac{\partial}{\partial z}\right)_\psi - \rho v r \left(\frac{\partial}{\partial \psi}\right)_z$$

$$\left(\frac{\partial}{\partial r}\right)_z = \rho u r \left(\frac{\partial}{\partial \psi}\right)_z$$

(2.75)

The boundary layer equations can be re-written using Von Misses transformation arguments for the independent variables (z,ψ). As a result of a transformation, the continuity equation and the momentum equation in the radial direction, thus the radial velocity term, vanish from the equation set since they are automatically satisfied. The boundary layer equations in stream function form are expressed below [21]:

$$\rho u \frac{\partial u}{\partial z} = -\frac{\partial p}{\partial z} + \mu \rho u \frac{\partial}{\partial \psi}\left(\rho u r^2 \frac{\partial u}{\partial \psi}\right)$$

$$0 = \frac{\partial r^2}{\partial \psi} - \frac{2}{\rho u}$$

$$0 = \frac{\partial p}{\partial \psi} \tag{2.76}$$

$$\rho u \frac{\partial Y_k}{\partial z} + \rho v \left(\rho u r \frac{\partial Y_k}{\partial \psi}\right) = -\rho u \frac{\partial (r j_{k,r})}{\partial \psi} + \dot{\omega}_k W_k$$

$$\rho c_p u \frac{\partial T}{\partial z} = \lambda \rho u \frac{\partial}{\partial \psi}\left(\rho u r^2 \frac{\partial T}{\partial \psi}\right) - \sum_{k=1}^{K} c_{pk} j_{k,r} \rho u r \frac{\partial T}{\partial \psi} - \sum_{k=1}^{K} h_k \dot{\omega}_k W_k$$

The definition of stream function can be specified in terms of radial mesh coordinate, the axial velocity profile, the temperature, and the composition of the flow field, which appears as density in the equation.

$$\psi_j = \int_0^{r_j} (\rho u r) dr \tag{2.77}$$

Since ψ is the independent variable of the equation set, the relation between physical coordinates and stream function coordinates should be modified using the transformed radial momentum equation.

$$r^2 = 2 \int_0^{\psi} \left(\frac{1}{\rho u}\right) d\psi \tag{2.78}$$

After Von Misses transformation is completed, the radial coordinate is no longer an independent variable of the equation set. Moreover, the radial coordinate is explicitly involved in the momentum and energy equation as r^2. Another consequence of the transformation, the radial velocity term vanishes, and a simplification of radial convective terms is obtained. However, the diffusion term arises a computational

36

complication since it is formed by the group of dependent variables $\rho u r^2$, which is called the diffusion coefficient [21].

The range of the independent variable of ψ is from the centerline, which equals zero, to the tube wall, which is defined as a function of inlet flow conditions, u_0 and ρ_0 and R_0, tube wall radius. In addition, the net mass flow rate, which enters the channel, can be calculated as follows for axisymmetric channel flow [25].

$$\psi_0 \ = \ \int_0^{R_0} (\rho_0 u_0 r) dr$$
$$\dot{m} \ = \ 2\pi\psi_0 \qquad\qquad (2.79)$$

The order of the equation system in stream function coordinate is sixth order. The two transport equations, which are the axial momentum and the energy equation and have second derivatives of ψ, are second order. Finally, the radial coordinate and pressure equations are first-order equations [21]. In order to solve the sixth order of equations set, six independent boundary conditions must be introduced.

Boundary conditions are defined as,

$$\text{at the centerline, } \psi \ = \ 0 : \ r \ = \ 0 \,, \ \frac{du}{d\psi} \ = \ 0, \ \frac{dT}{d\psi} \ = \ 0$$
$$\text{at the wall, } \psi \ = \ \psi_0 : \ r \ = \ r_0 \,, \ u \ = \ 0 \,, \ T \ = \ T_w \qquad\qquad (2.80)$$

An implicit boundary condition is defined for pressure since no explicit condition is given for the pressure. As a result, one of the boundary conditions of radial coordinates should be associated with the pressure term [21].

Before completing and finalizing the derivation of boundary layer equations for axisymmetric channel flow, an additional transformation is introduced by converting the stream function coordinate to a normalized stream function [25]. Since the streamline is the constant mass-flux lines, there is no mass transfer across two lines of the value of the constant stream function. In other words, the flow can be modeled

37

by the constant stream function values through the channel without mass transfer from the boundaries. For this reason, the boundaries of the channel become streamlined. In this case, the value of the stream function varies between boundaries from zero to total mass flux. The values on the boundaries are kept constant throughout the channel. However, there can be net mass transfer at the boundaries changing the mass flux of the flow along the flow direction. This follows a change in the value of the stream function in some cases, such as the reacting surface of the wall or the liquid injection from the wall, causing a movement in a coordinate system and complicating the problem. By the normalization of the stream function with the mass flux rate, the independent variable can be fixed for the problem [21]. The normalized stream function is ξ, and M(x) is the local value of the total mass flux. ψ_u represents the upper boundary while ψ_l is the lower boundary of the channel. Both terms are the functions of axial direction only. The net mass transfer at the boundaries is represented by these terms in the equations set along the axial flow direction. The normalized stream function ranges from zero to one by definition.

$$M(x) = \psi_u(x) - \psi_l(x)$$
$$\xi = \frac{\psi - \psi_l}{\psi_u(x) - \psi_l(x)} = \frac{\psi - \psi_l}{M(x)} \tag{2.81}$$

The necessary transformation metrics by chain-rule differentiation to convert physical coordinates to the normalized stream function can be summarized as,

$$\left(\frac{\partial}{\partial x}\right)_y = \left(\frac{\partial x}{\partial x}\right)_y \left(\frac{\partial}{\partial x}\right)_\psi + \left(\frac{\partial \psi}{\partial x}\right)_y \left(\frac{\partial}{\partial \psi}\right)_x$$
$$\left(\frac{\partial}{\partial y}\right)_x = \left(\frac{\partial x}{\partial y}\right)_x \left(\frac{\partial}{\partial x}\right)_\psi + \left(\frac{\partial \psi}{\partial y}\right)_x \left(\frac{\partial}{\partial \psi}\right)_x \tag{2.82}$$

$$\left(\frac{\partial}{\partial x}\right)_y = \left(\frac{\partial}{\partial x}\right)_\psi - \left(\rho vr + \xi\frac{dM}{dx} - \frac{dM_l}{dx}\right)\left(\frac{\partial}{\partial\psi}\right)_x$$

$$\left(\frac{\partial}{\partial y}\right)_x = \rho ur\left(\frac{\partial}{\partial\psi}\right)_x \tag{2.83}$$

$$\left(\frac{\partial}{\partial\psi}\right)_x = \frac{1}{M}\left(\frac{\partial}{\partial\xi}\right)_x$$

$$\left(\frac{\partial}{\partial x}\right)_y = \left(\frac{\partial}{\partial x}\right)_\xi + \frac{1}{M}\left(-\rho vr + \xi\frac{dM}{dx} - \frac{dM_l}{dx}\right)\left(\frac{\partial}{\partial\xi}\right)_x \tag{2.84}$$

The mass flux function M, which shows the effect of net mass transfer along the axial flow direction, is the only function of flow direction and is defined as follows,

$$\frac{dM}{dx} = \frac{dM_l}{dx} + \frac{dM_u}{dx} \tag{2.85}$$

Mass flux at boundaries is calculated using the following relations.

$$\frac{dM_l}{dx} = \rho v|_{r=0}$$

$$\frac{dM_l}{dx} = -\rho vr|_{r=r_{max}} \tag{2.86}$$

After necessary transformations are applied to the equations set, a new set of boundary layer equations in terms of (x,ξ) coordinates are obtained. The momentum, species and energy equations are expressed respectively as follows:

$$\rho u \frac{\partial u}{\partial x} - \frac{\rho u}{M}\left(\xi \frac{dM}{dx} - \frac{dM_l}{dx}\right)\frac{\partial u}{\partial \xi} = -\frac{\partial p}{\partial z} + \frac{\rho u}{M^2}\frac{\partial}{\partial \xi}\left(\rho u \mu r^2 \frac{\partial u}{\partial \xi}\right)$$

$$\rho u \frac{\partial Y_k}{\partial x} - \frac{\rho u}{M}\left(\xi \frac{dM}{dx} - \frac{dM_l}{dx}\right)\frac{\partial Y_k}{\partial \xi} = \dot{\omega}_k W_k - \rho u \frac{\partial}{\partial \psi}\left(\rho r Y_k V_{k,y}\right)$$

$$\rho c_p u \frac{\partial T}{\partial x} - \frac{\rho u c_p}{M}\left(\xi \frac{dM}{dx} - \frac{dM_l}{dx}\right)\frac{\partial T}{\partial \xi}$$

$$\quad\quad = \frac{\rho u}{M^2}\frac{\partial}{\partial \xi}\left(\lambda \rho u r^2 \frac{\partial T}{\partial \xi}\right) - \sum_{k=1}^{K} h_k \dot{\omega}_k W_k$$

$$\quad\quad - \frac{\rho^2 u r}{M}\sum_{k=1}^{K} c_{pk} Y_k V_{k,y} \frac{\partial T}{\partial \xi}$$

(2.87)

The diffusion velocity term can be defined using mixture-average and multicomponent diffusion terms [25]. The equations for diffusion velocity $V_{k,y}$ for multicomponent transport and mixture-averaged transport are given below, respectively.

$$V_{k,y} = \frac{\rho u r}{X_k \overline{W} M}\sum_{j\neq k}^{K_g} W_j D_{kj}\frac{\partial X_k}{\partial \xi} - \frac{D_k^T}{\rho Y_k}\frac{\rho u r}{T M}\frac{\partial T}{\partial \xi}$$

(2.88)

$$V_{k,y} = -\frac{D_{km}\rho u r}{X_k M}\frac{\partial X_k}{\partial \xi} - \frac{D_k^T}{\rho Y_k}\frac{\rho u r}{T M}\frac{\partial T}{\partial \xi}$$

(2.89)

The normalized stream function relation is expressed using a non-dimensional stream function form as follows:

$$r^2 = 2M \int_0^{\xi}\left(\frac{1}{\rho u}\right)d\xi$$

(2.90)

The boundary conditions should be identified at the channel wall and symmetry axis and the inlet of the channel since the parabolic set of equations can easily be solved with the introduction of consistent initial conditions [21][23]. For coupled, nonlinear system of boundary layer equations, the boundary conditions at the channel inlet acts as initial condition as the axial flow direction is a time-like independent variable. On the channel wall, a temperature field or zero gradients of temperature is specified, and zero gradients of temperature are settled on the symmetry axis of the channel. In addition, zero axial flow velocity condition is stated on the channel wall due to the no-slip conditions, while zero velocity gradient is assigned on the symmetry axis. Physical coordinates correspond to zero on the symmetry axis and channel radius at the wall boundary [25].

Zero gradient of species mass fraction is identified on both channel symmetry axis and wall, while there is no mass transfer due to surface reaction on the channel wall. On the other hand, the net production of the surface species should be balanced with the mass fluxes of species in the gas.

$$\rho Y_k \left(V_{k,y} + v \right) = \dot{s}_k W_k \tag{2.91}$$

When the surface reaction occurs on the channel wall, the tangential fluid velocity, which is called Stefan flow velocity, also becomes non-zero and is calculated as follows. However, the values of Stefan velocity and surface chemistry production rates are equal to zero when no surface reaction occurs during channel flow.

$$v = \frac{1}{\rho} \sum_{k=1}^{K_g} \dot{s}_k W_k \tag{2.92}$$

Finally, the summation of all mass fractions on any grid point should be equal to one to satisfy the most fundamental condition of the conservation of species equation.

$$1 = \sum_{k=1}^{K_g} Y_k \tag{2.93}$$

The derivation of boundary layer equations is completed for reacting channel flow problems. The resulting set of equations can be discretized to be solved by numerical techniques, as expressed in section 2.5.

2.7 Discretization of Boundary Layer Equations Set

The discretization of boundary layer equations is required for numerical solutions. The equations are discretization using finite difference approximations [25]. Since the characteristics of the equation set are parabolic, one of the coordinates becomes a time-like independent variable [23]. The axial flow direction acts like time as an independent variable for the coupled boundary layer equations of axisymmetric channel flow. At the same time, the discretization takes place for spatial derivatives on a uniform or non-uniform fixed grid in the normalized stream function.

The second-order derivatives in the momentum, energy, and species equations are approximated using central scheme differentiation, as stated below [25]. In addition, the first-order derivatives are also differentiated using a central scheme, as given in the below equation.

$$\frac{\partial}{\partial \xi}\left(\alpha \frac{\partial f}{\partial \xi}\right) \approx \left(\frac{2}{\xi_{j+1} - \xi_{j-1}}\right)\left[\alpha_{j+1/2}\left(\frac{f_{j+1} - f_j}{\xi_{j+1} - \xi_j}\right) - \alpha_{j-1/2}\left(\frac{f_j - f_{j-1}}{\xi_j - \xi_{j-1}}\right)\right] \tag{2.94}$$

$$\frac{\partial f}{\partial \xi} \approx \frac{f_{j+1} - f_{j-1}}{\xi_{j+1} - \xi_{j-1}} \tag{2.95}$$

Some terms in the set of equations appear with no derivatives. These terms are written directly in the equations as their existing value on the associated grid point. Moreover, the integral equations are represented as first-order differential equations to ease discretization. The first-order ODEs are approximated by using the

trapezoidal rule, as stated below. The selection of differentiation using the trapezoidal rule is related to the Jacobian matrix structure, which remains banded.

$$\frac{1}{M}\left(\frac{r_j^2 - r_{j-1}^2}{\xi_j - \xi_{j-1}}\right) = \frac{2}{\rho_j u_j + \rho_{j-1} u_{j-1}} \tag{2.96}$$

The diffusion term consists of the species flux term as a part of the diffusion velocity component. The equations of diffusion velocities of species k for the multi-component and mixture-averaged diffusion are presented in the previous section. The diffusion coefficient for multi-component and mixture-averaged transport can be written using the mixture-averaged formulation. The most significant advantage of using this form, the numerator and denominator errors are accumulated in the same way in the equation [29].

$$D_{km} = \frac{\sum_{j \neq k}^{K} X_j W_j}{\overline{\overline{W}} \sum_{j \neq k}^{K} X_j / D_{jk}} \tag{2.97}$$

However, the formulation is undefined when the pure species arise in the mixture and create singularities for a computational solution. The small quantity, which is numerically insignificant, is introduced for each species to overcome the computational difficulties as given below.

$$\alpha = 10^{-30}$$

$$X_k = \widehat{X_k} + \alpha$$

$$D_{km} = \frac{\sum_{j \neq k}^{K} X_j D_{kj}(d_j + \alpha)}{\overline{\overline{W}}(d_j + \alpha)} \tag{2.98}$$

CHAPTER 3

NUMERICAL APPROACH

The presentation of the code called as reactFlow, which is generated for the calculations of the reacting boundary layer flow in an axisymmetric channel or planar duct, is explained in this chapter. The algorithm of the code and the functions forming the code reactFlow are investigated in detail in section 3.1. The solver software is reported in section 3.2 and the chemical solver software is expressed in section 0.

3.1 Algorithm of Developed Code

The general algorithm of the code reactFlow is presented in Figure 3.1. The input is introduced into reactFlow in the command prompt of MATLAB and stored in a text file. The input is evaluated to find the solution in reactFlow, which communicates with Cantera and MATLAB ode15i during the process. After the iterations are converged to the solution, the flow field properties, namely temperature, velocity and pressure, and the fractions of specified species throughout the domain are written in a text file. In addition, the graphs of flow field properties are plotted and saved in a file, which is created after starting the code to record the input and output parameters of the current run.

The code reactFlow consists of functions and sub-functions. These functions can be categorized into three groups, namely main functions, auxiliary functions and output functions, as presented in Figure 3.2. The functions and sub-function are generated in .m file format, which can be read and processed by MATLAB. The main functions of reactFlow are reactFlow.m and bodyRF.m. The input text file, which is called inputreactFlow.dat and shown in Figure 3.3, is read by the code when the code is started to run using the MATLAB interface.
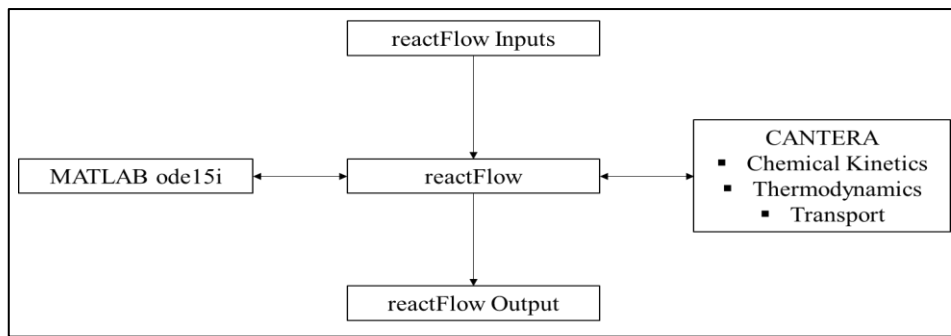
Figure 3.1 Algorithm of code reactFlow

The first command line executed by the run is the Name of the Run. The function of this line is to give a name to run and to create a folder with this name to record the inputs and outputs of the code. Secondly, general case settings are introduced respectively in the input file. The name of the reaction mechanism is submitted by the Working Gas line. After this, the transport property for gas is selected as Mix or Multi. The coordinate system domain is chosen as radial or Cartesian. Finally, the calculation of the thermal diffusion effects and the inlet velocity profile is shown in input lines. After the introduction of general case settings, the settings for calculation dome are presented to reactFlow. The diameter of the channel or height of the planar duct is first written in the unit of meter, then the number of radial nodes and the distribution factor for them are given to the code. Finally, the selection of the axial domain is presented by deciding the minimum and maximum points on the axial domain in units of centimeters and the total number of mesh points in the axial direction.

After the specification of the properties of the calculation domain, the properties of reacting gas and the boundary conditions are introduced to reactFlow. The coefficients of species should be written by considering the stoichiometric condition of fuel and oxidizer. The oxidizer can be either air or oxygen. If any species are not present, it should be given as zero in the input file. Finally, absolute and relative tolerances are given as input to reactFlow to decide the level of convergence of the solver.

46
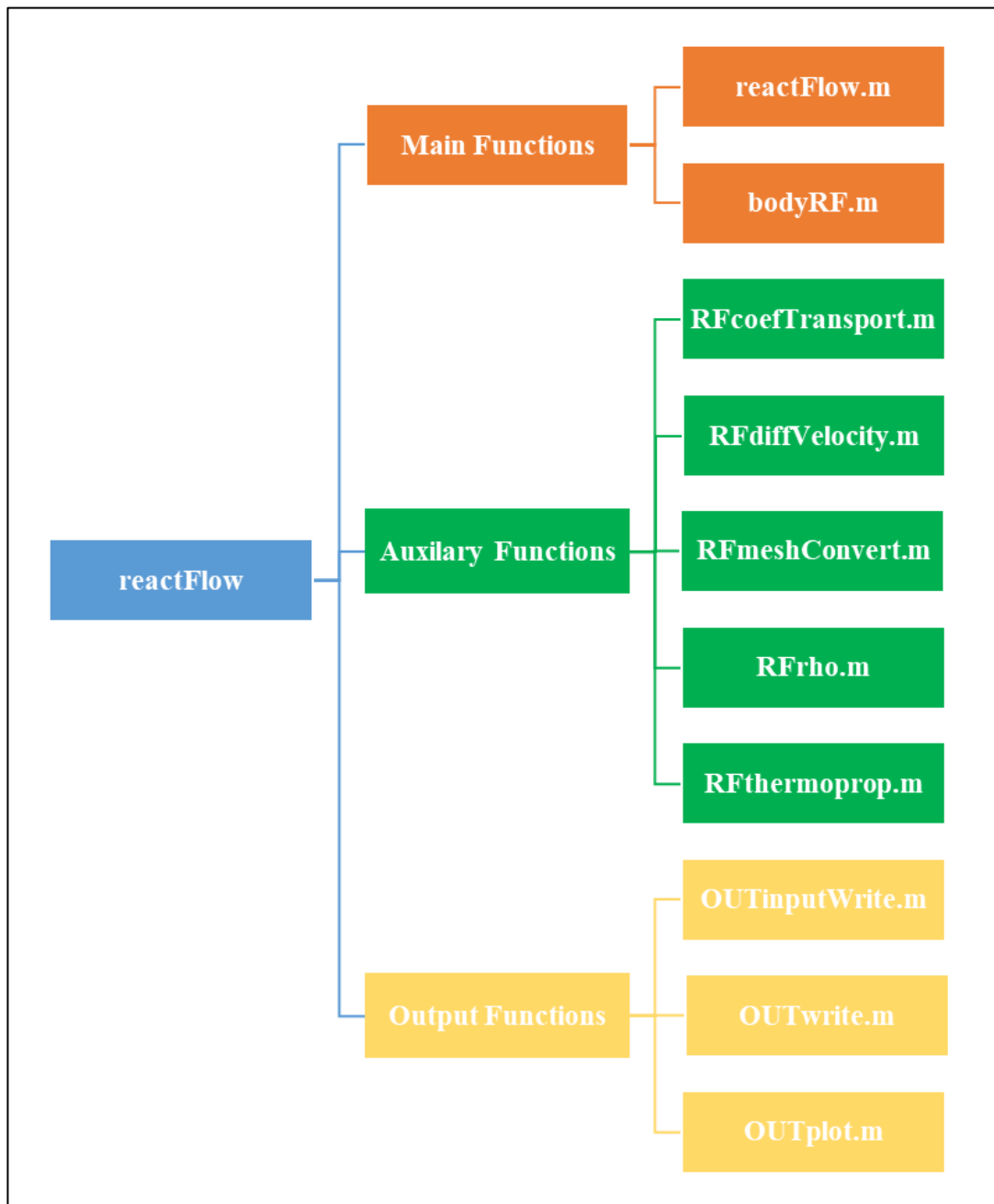
Figure 3.2 The schematic of functions forming reactFlow

```
--------------------------------------------------------
Name of the Run              : Case-1
Working Gas                  : BFER_methane
Transport Property           : Mix
Coordinate System            : radial
Thermal Diffusion            : off
Inlet Velocity Profile       : off
-----
Diameter/Heigth [m]          : 0.010
Radial Node Number           : 21.0
Node Streching Factor        : 1.1
Axial Domain Selection       : User
Min Axial Point [cm]         : 0
Max Axial Point [cm]         : 10.0
Number of Axial Points       : 10000.0
---
Inlet Gas Temperature [K]    : 400.00
Wall Temperature [K]         : 1200.00
Inlet Velocity [m/s]         : 0.5
Wall Velocity [m/s]          : 0.0
Inlet Pressure [Pa]          : 101325.0
O2 Mole Number [-]           : 2.00
N2 Mole Number [-]           : 7.52
CH4 Mole Number [-]          : 1.0
H2 Mole Number [-]           : 0.00
---
Relative Tolerance           : 1e-03
Absolute Tolerance           : 1e-04
--------------------------------------------------------
```

Figure 3.3 The input file for reactFlow

The initiation of the run according to the inputs and the mesh generation for the computation is taken care of at the beginning of reactFlow.m. After this step, the physical mesh coordinates are transformed to stream-function coordinates using the sub-function RFmeshConvert.m. The initial and boundary conditions are combined to form the dependent variable matrix. The values of dependent variables in the radial direction are stored in this matrix since the boundary layer equations are only discretized in the radial direction as a consequence of the method of line solution. The evaluation of ODEs using the MATLAB ode15i function is required an initial condition for both the dependent variables and the derivatives of dependent variables. In order to satisfy this requirement and generate consistent initial conditions, the generated dependent variable matrix is evaluated at the beginning of the axial domain, which corresponds to the value of zero, using the second main

48

function of reactFlow bodyRF.m. All discretized equations are found in bodyRF.m function. With the given dependent variable matrix, the residual vector of DAEs is composed using the sub-functions RFcoefTransport.m, RFdiffVelocity.m and RFthermprop.m, which are formed for the calculation of transport properties such as diffusion coefficients or viscosity value, for calculating diffusion velocities of species in gas and the calculation of thermodynamic properties of gas, respectively. In these calculations, the information on gas properties is exchanged with Cantera for any necessary data. The dependent variable matrix with initial conditions is inputted into BodyRF.m and the vector of residuals of DAEs is outputted from the bodyRF.m. This residual vector is equated to zero, so the derivatives of dependent variables in matrix form for initial conditions at zero axial position are obtained. In addition, the consistent initial condition requirement for ode15i is also satisfied after the generation of the matrix of derivatives using this method. As a result, the set of equations for DAEs and their derivatives are obtained, which are required for MATLAB ode15i solver, as discussed in section 3.2.

The iterations for the solution to the problem can be started by calling ode15i function and supplying the initial conditions for DAEs and their derivatives, the axial domain and the solver settings. When the iterations are converged to a solution, an output is created by ode15i in the form of a vector for each point in the axial domain. The solution vector is evaluated using the output functions of reactFlow to generate figures and output text for discussing the solutions.

3.2   MATLAB Solver

The partial differential equations can be solved with the codes and software that are developed for ordinary differential equations by using the method of lines if their characteristics are parabolic. The boundary layer equations with energy equations used in the simulations of reacting flow in a channel are parabolic PDEs. They can be solved using MATLAB ode15i [21] function after being written as differential-algebraic equations (DAE). MATLAB ode15i is a function that is an implicit,

variable-step and variable-order method implemented using a backward differentiation formula (BDF) to solve ODEs [28][30].

An implicit set of ODEs can be numerically solved with MATLAB ode15i function when they are written in (3.1) on a specified interval with appropriate and consistent initial conditions.

$$F\big(time, y(time), y'(time)\big) = 0 \tag{3.1}$$

BDF can be applied to general DAE as given in (3.2), where α and β are coefficients of the method [30].

$$F\left(t_n, y_n, \frac{1}{\beta h}\sum_{j}^{k} \alpha_j y_{n-j}\right) = 0 \tag{3.2}$$

The details of BDF can also be shown for the backward Euler formula, which is more straightforward and reflects all the properties of the application of BDFs [28].

$$F\left(t_{n+1}, y_{n+1}, \frac{y_{n+1} - y_n}{h}\right) = 0 \tag{3.3}$$

$$y_{n+1} \approx y(t_n + h) \tag{3.4}$$

The set of algebraic equations given in (3.3) is iteratively solved. The relation between the iterations step can be shown in (3.5) so that equation (3.3) can be approximated as a linear system of equations as given in (3.6) [28].

$$y^{s+1}{}_{n+1} = y^s{}_{n+1} + \delta \tag{3.5}$$

$$F\left(t_{n+1}, y^s{}_{n+1}, \frac{y^s{}_{n+1} - y_n}{h}\right) + \left(\frac{1}{h}F_{y'} + F_y\right)\delta = 0 \tag{3.6}$$

The equation (3.6) is solved for δ, which serves as a correction term. As a result, the iteration matrix is presented in the form given in (3.7), where α is called a constant characteristic of the iteration matrix [28].

$$\frac{\alpha}{h}F_{y'} + F_y \tag{3.7}$$

The values of the terms of $F_{y'}$ and F_y are given into the ode15i function as input by the users since the consistent initial conditions are calculated before obtaining the solution of PDE. The PDEs are numerically approximated by ode15i. The PDEs are saved by function ode15i while evaluating backward differentiation functions. When a new iteration matrix is structured due to the change of coefficient given in (3.7), the saved PDEs are used. The storage is increased significantly due to the solution procedure of ode15i; however, consistent initial conditions and integration efficiency are ensured [28].

The derivation of backward differentiation formulations with order k and constant step size h can be approximated with the interpolation representatively given in (3.3) for a polynomial P(t) as follows [28].

$$P'(t_{n+1}) = f(t_{n+1}, P(t_{n+1})) \tag{3.8}$$

The polynomial in (3.8) can be written in Lagrangian form by interpolating values of Y at nodes t for varying order values as follows.

$$R(t) = \sum_{j=0}^{k} Y_{n+1-j} \prod_{i \neq j}^{k} \frac{t - t_{n+1-i}}{t_{n+1-j} - t_{n+1-i}} \tag{3.9}$$

The equations (3.8) and (3.9) can be combined to get backward differentiation formula with step size h and order k as an implicit linear formula presented in (3.10).

51

$$\sum_{j=0}^{k} \alpha_j y^s{}_{n+1} - hf\left(t_{n+1}, y^s{}_{n+1}\right) = 0 \tag{3.10}$$

The absolute and relative error tolerances are specified for ode15i as a positive scalar or vector to decide the convergence of the solution. The value of absolute error tolerance is used as a threshold value for the convergence, while the relative error tolerance is used to control the correct digit number in the solution. If the value of the solution is found to be smaller than the specified absolute error tolerance, the digit number of the solution is not checked by the solver. The success criteria of each iteration step are to successfully satisfy of local error in (3.11) for each solution component [31].

$$|error_i| <= \max(Relative\ Tolerance_i \\ * abs(y_i), Absolute\ Tolerance_i) \tag{3.11}$$

3.3   Calculation of Reactions

Cantera is open-source software used for the calculations of processes with thermodynamics, transport and chemical kinetics [32]. It is widely used in combustion, detonations, batteries and film deposition applications. Cantera can be interfaced with Python, MATLAB, or applications that are written in Fortran 90 and C/C++. The calculations of problems with thermodynamics, transport and chemical kinetics can be efficiently automated by Cantera. The documentation details for the theory and the functions made up of Cantera are presented on their webpage. Any reaction mechanism in the format of CHEMKIN [33] can be converted into Cantera format with the help of the built-in functions of Cantera when the thermodynamic data of species in the reaction mechanism is given in a separate file in NASA format. In addition, the transport properties of these species can also be involved in the conversion depending on the need of the problem.

3.4   Flow Diagrams

The flow diagrams of code reactFlow are presented in this section. The general algorithm of reactFlow from start to end is explained in Figure 3.4. The initial calculations, radial mesh generation, determination of initial derivatives and input of calculations for the whole axial domain are presented in Figure 3.5 using flow diagrams. Finally, the algorithm of main calculations, consisting of boundary layer equations, and convergence check, done by MATLAB in bodyRF.m function, is presented in Figure 3.6.
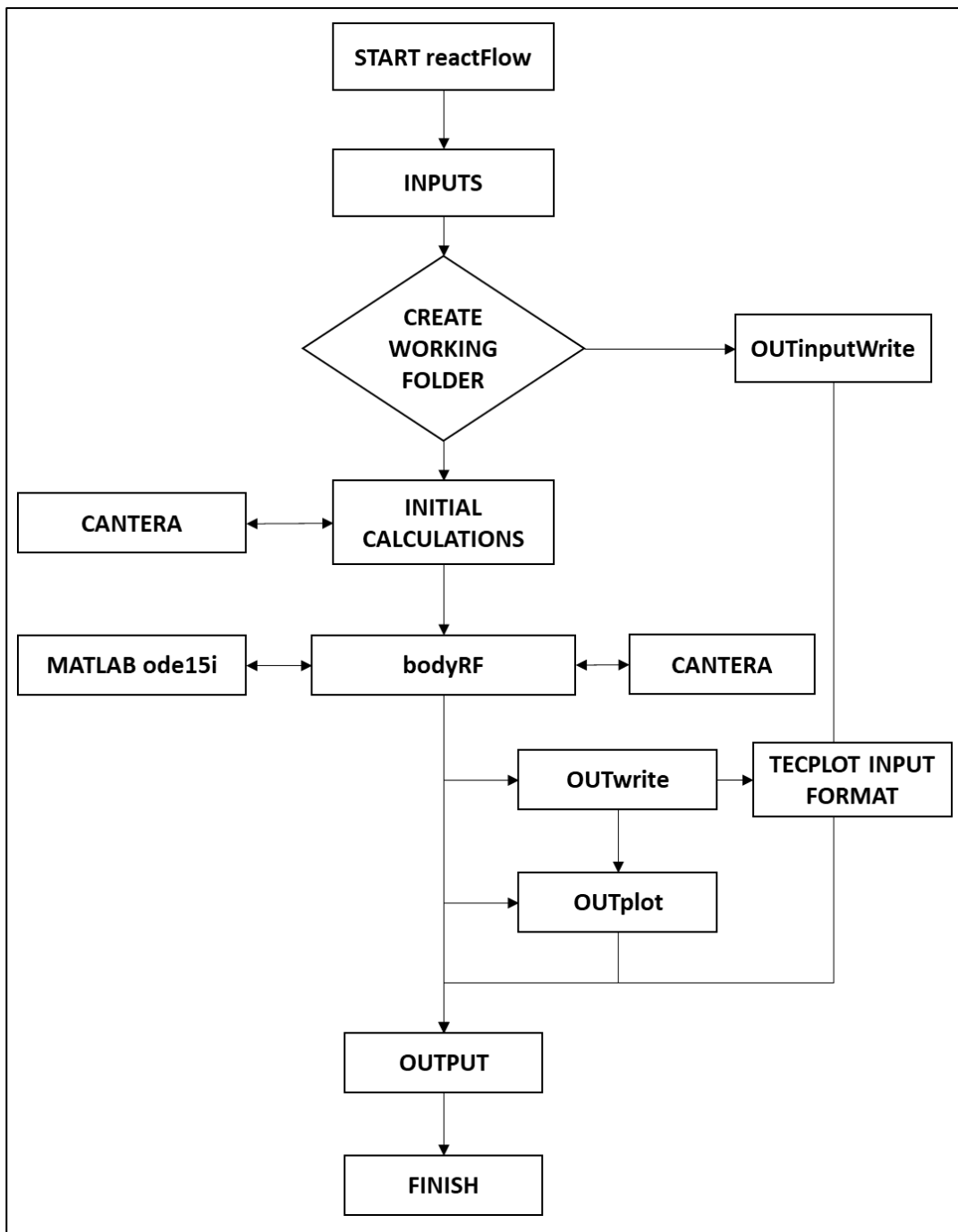
Figure 3.4 Flow Diagram of General Algorithm of reactFlow
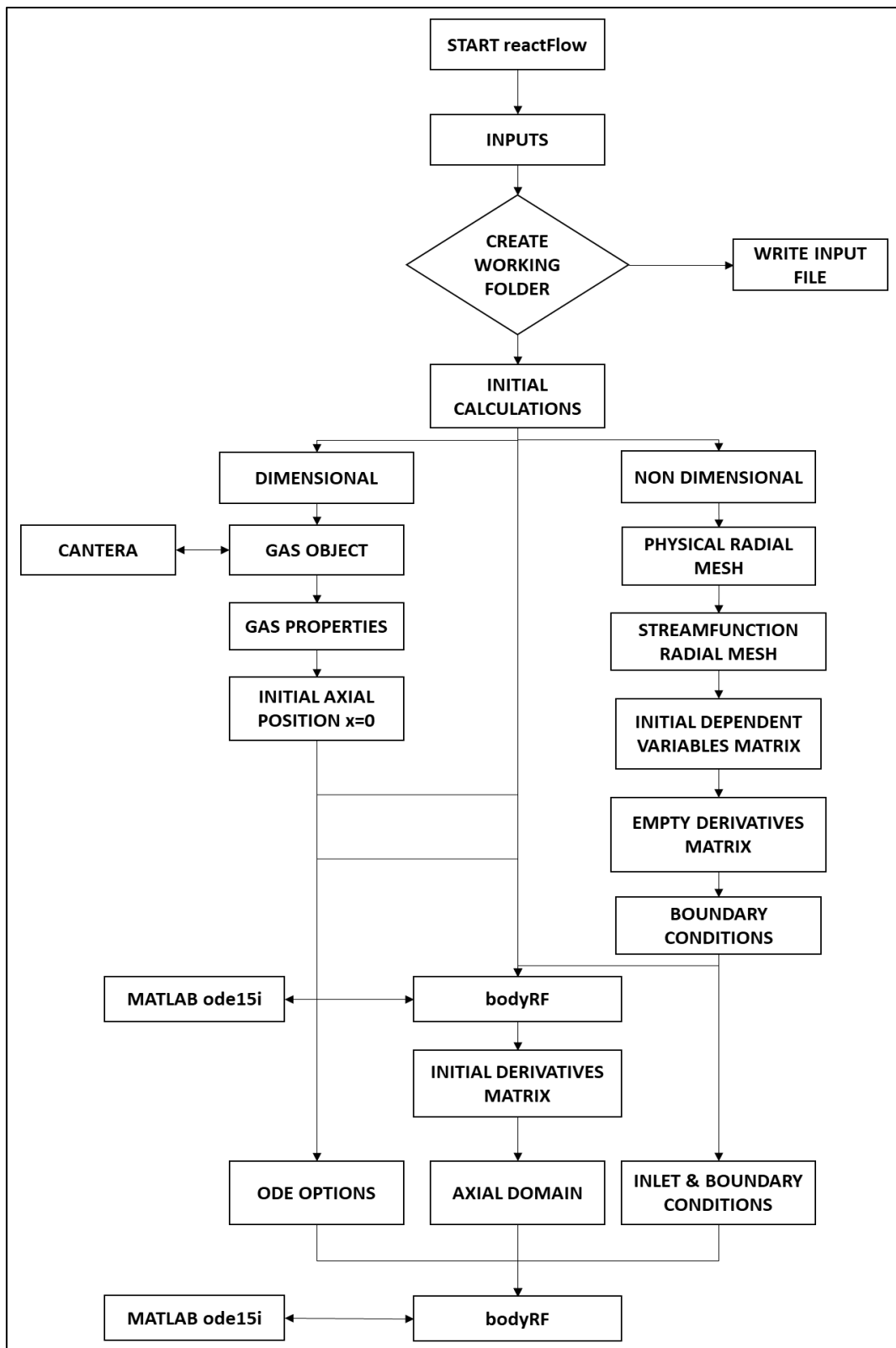
Figure 3.5 Flow Diagram of Initial Calculations of reactFlow
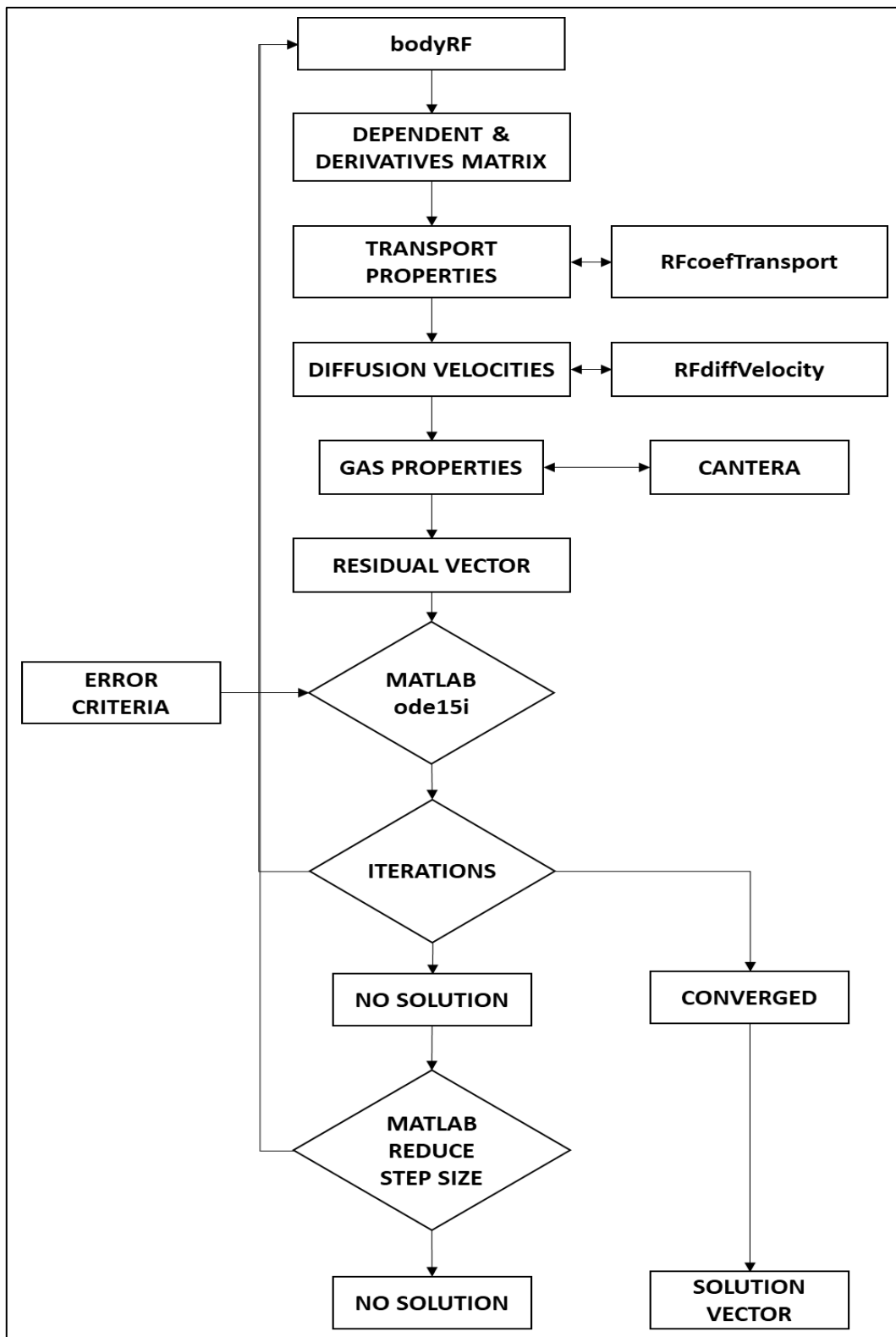
Figure 3.6 Flow Diagram of Main Calculations of reactFlow and Convergence Check

CHAPTER 4

RESULTS & DISCUSSION OF REACTING CHANNEL FLOW
SIMULATIONS

In this chapter, case problems are analyzed by using reactFlow and their results are presented. In section 4.1, the validation of code is discussed by comparing its non-reacting and reacting case results with data from literature and results from Chemkin software. In section 4.2, a study of the sensitivity of flow parameters on flame position is examined and the results are presented.

4.1   Validation Studies

In this chapter, the analyses for the validation of reactFlow are presented for non-reacting and reacting cases.

4.1.1   Non-Reacting Case Validation

A non-reacting channel flow problem with its solutions from literature is applied to code reactFlow to compare its results with the given results from the literature. The validation case is selected from the book of Kee and Coltrin, in which the results are presented as figures for developing flow in a channel [21]. In the problem, a constant temperature of 800K is applied on the channel walls, while the entrance temperature of the flow into the channel is 300K. The viscosity, thermal conductivity and specific heat ratio of the flowing gas are assumed to be constant and equal to their values at the inlet section of the tube. The gas is considered air and modeled using the ideal gas assumption. Thus, the density of the gas through the channel is calculated by using this assumption. No other properties of the domain or the gas are given in the problem. However, it is stated that the Reynolds number at the inlet is taken as 1000,

while the Prandtl number at the same section is 0.7. The remaining properties are calculated by using Reynolds and Prandtl numbers in the inlet section. In addition, it is given in the problem that a non-uniform radial mesh with 51 mesh points is used for the radial domain; however, a value of the non-uniformity parameter, called a stretch factor, is not clarified in the problem. The value of boundary conditions and the mesh properties are specified to code reactFlow as presented in Table 4.1.

Table 4.1 The Boundary Conditions and Mesh Setup for Validation Case

Name of Parameter	Unit	Value
Reynolds Number	-	1000
Prandtl Number	-	0.7
Channel Diameter	m	0.016
Inlet Velocity	m/s	1.0
Inlet Temperature	K	300
Wall Temperature	K	800
Inlet Pressure	Pa	100000
Number of Nodes	-	51
Stretch Factor	-	1.1
Absolute Error Tolerance	-	10^{-6}

The comparison of the results of reactFlow and the literature for dimensionless velocity and temperature profiles are presented in Figure 4.1 and Figure 4.2. The resulting profiles are compared at four different axial points, as shown in the figures. The axial points are z=1D, z=5D, z=10D, z=50D and z=100D, which are the distances from the inlet regarding channel diameter. The continuous lines are the results of reactFlow at different axial points, while the dashed lines are from the literature [21].

According to Figure 4.1, the distribution of dimensionless velocity profiles of reactFlow is in good agreement with the literature profiles for every axial point. At the regions close to the wall, some divergence of the velocity profiles is observed. This divergence disappeared through the regions close to the centerline. Since the non-uniformity factor of the radial distribution of the mesh points is not explicitly specified in the literature, the most fitting stretch factor is used in the analysis, as shown in Table 4.1. The results of reactFlow show great accordance with the results of the literature.
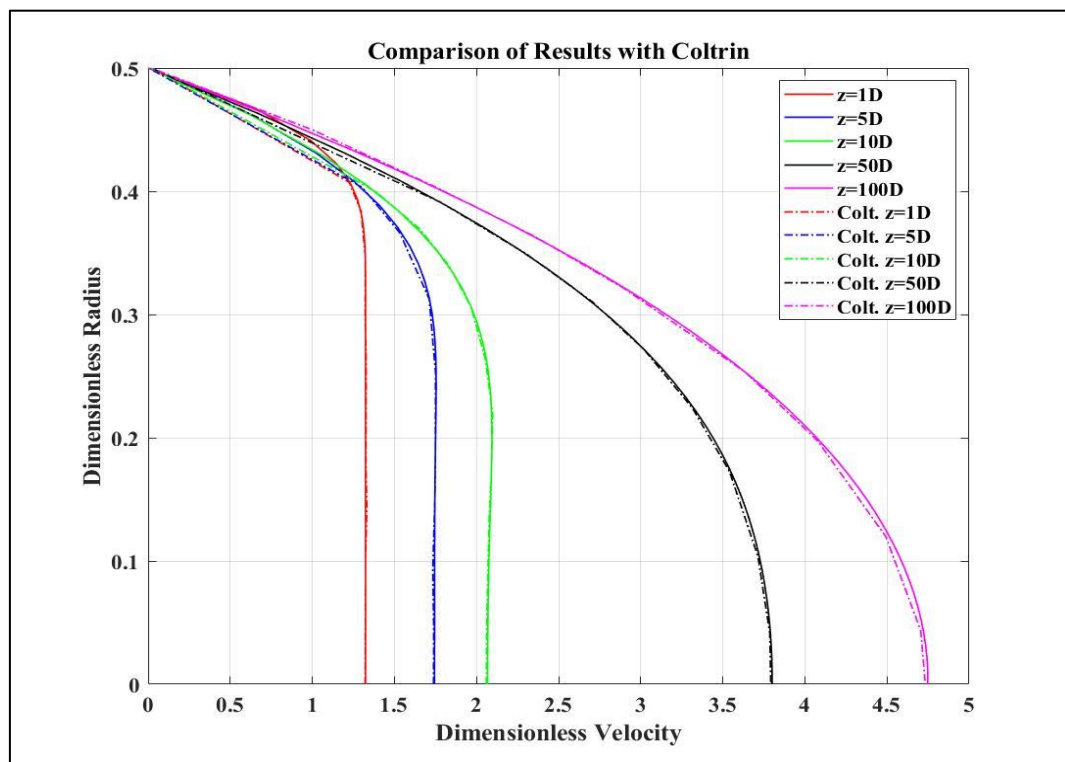
Figure 4.1 The Comparison of Results with Literature for Velocity Profiles

The dimensionless temperature profiles for literature and reactFlow are presented in Figure 4.2. As in the case of dimensionless velocity profiles, the results are in good agreement for every compared axial point. The divergence of temperature profiles on the regions close to the wall can be observed. The source of this difference could be the settings of the mesh domain, which is not given in the literature.
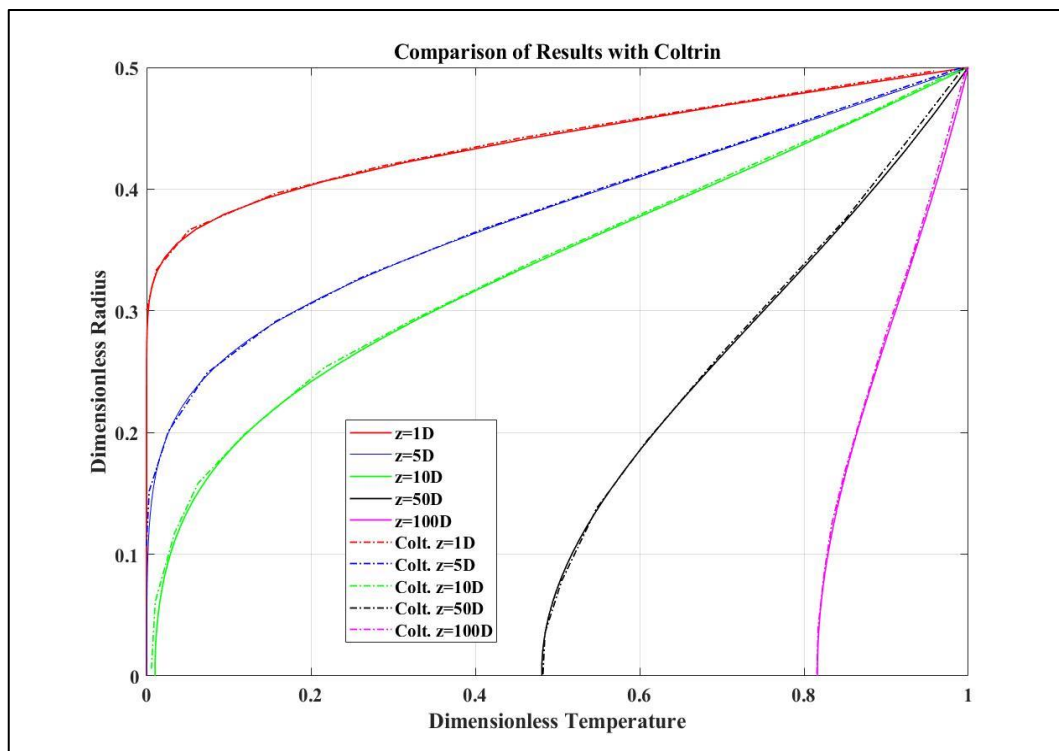
Figure 4.2 The Comparison of Results with Literature for Temperature Profiles
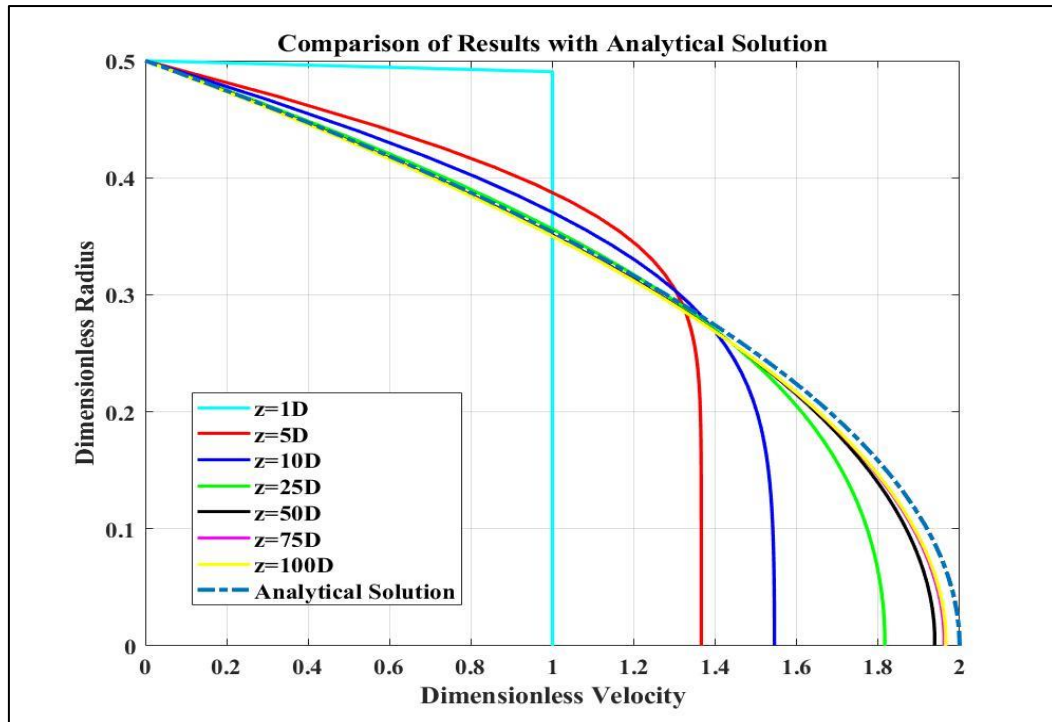
Figure 4.3 The Comparison of Results with Analytical Solution

In addition to literature data, the results of reactFlow are compared with the analytical solution, which is stated in section 2.3 for the channel flow problems. In this case, the inlet and boundary conditions are used, as given in Table 4.1. Moreover, the temperature difference between the inlet and the wall is dissipated and both values are taken as inlet gas temperature, shown in Table 4.1. The results are presented in Figure 4.3. In the figure, solid lines are the results of reactFlow for different axial points. It can be observed from Figure 4.3 that the flow calculated by reactFlow is reached a fully developed condition at axial position x=50D. The value of maximum dimensionless velocity is close to 2, which is also calculated by the analytical solution. The pressure gradient in the axial direction is calculated at inlet flow conditions and assumed to be constant through the pipe for the analytical solution. However, it is calculated for every axial point by reactFlow. The difference between calculation methods can be the reason for the difference between the values of maximum dimensionless velocities of both solutions.

61

4.1.2 Reacting Case Validation

After completing the validation of the non-reacting model of the code reactFlow, a reacting version of it should also be validated using data from the literature. However, the analyses and the experiments found in the literature are generally out of the scope reactFlow. In literature, the cases in which surface chemistry is also considered or flame extinction analyses are studied have widely been investigated. In order to stay within the limits of reactFlow and make the validation case as less complex as possible to see the behavior of reactFlow, two benchmark problems for the validation of the reacting version of the code reactFlow are created. Inputs for benchmark problems are presented in Table 4.2 and Table 4.4. In addition, the same issues are also investigated using CHEMKIN software [33], a verified and well-known program commonly used in literature, to create a benchmark for the studies.

Table 4.2 The Boundary Conditions and Mesh Setup of Benchmark Case-1 for Validation

Name of Parameter	Unit	Value
Channel Diameter	m	0.01
Inlet Velocity	m/s	1.00
Inlet Temperature	K	400
Wall Temperature	K	1600
Inlet Pressure	Pa	101325
Inlet Equivalence Ratio	-	1.0
Inlet Fuel Species	-	CH_4
Inlet Oxidizer	-	Air
Number of Nodes	-	21
Stretch Factor	-	1.1
Absolute Error Tolerance	-	10^{-5}

The thermodynamic, transport and chemical kinetic properties of reacting gases are calculated using Cantera and Chemkin for the same mechanism. The mixture-averaged diffusion properties are used in the analyses. The mechanism is selected as global methane-air combustion developed at CERFACS. This mechanism contains 2 reactions with 6 species and is valid for a wide range of equivalence ratios, pressure and temperature [34], as given below. The axisymmetric channel diameter is selected as 0.01 m. The inlet temperature is 400K, while the wall temperature is 1600K, which is necessary for the ignition of the fuel. The equivalence ratio of methane-air combustion is selected as 1.0 with the inlet conditions for pressure and velocity, as given in Table 4.2.

$$CH_4 + 1.5O_2 \implies CO + 2H_2O$$
$$CO + 0.5O_2 \iff CO_2$$

(4.1)

The distribution of temperature fields along the axial domain for the results of reactFlow and Chemkin are presented in Figure 4.4 and Figure 4.5, respectively. The upper boundary in the figures is the wall, the left boundary is the inlet of the channel and the lower boundary is the symmetry axis. The dimensional quantities are normalized using the diameter of the channel to make the results of the analyses comparable with each other. According to the figures, the temperature distribution in the channel domain is slightly varied for analyses. However, the position of flame is calculated at the same axial location by both reactFlow and Chemkin, which is the most important outcome of this benchmark study.
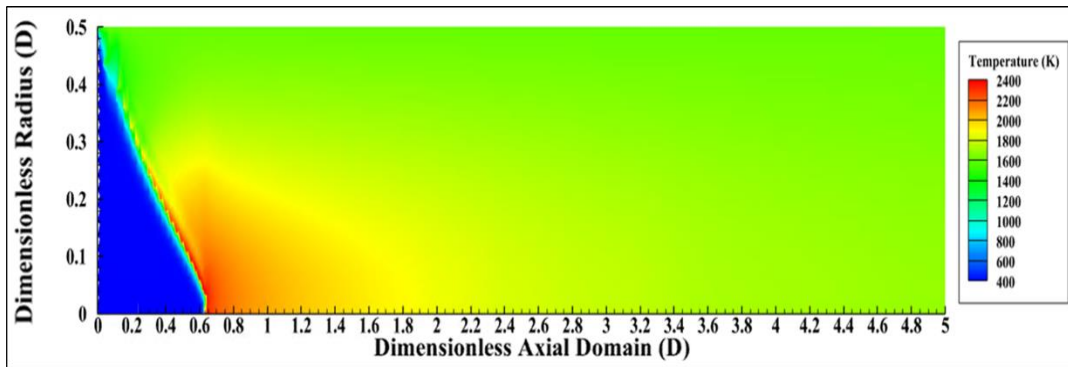
63
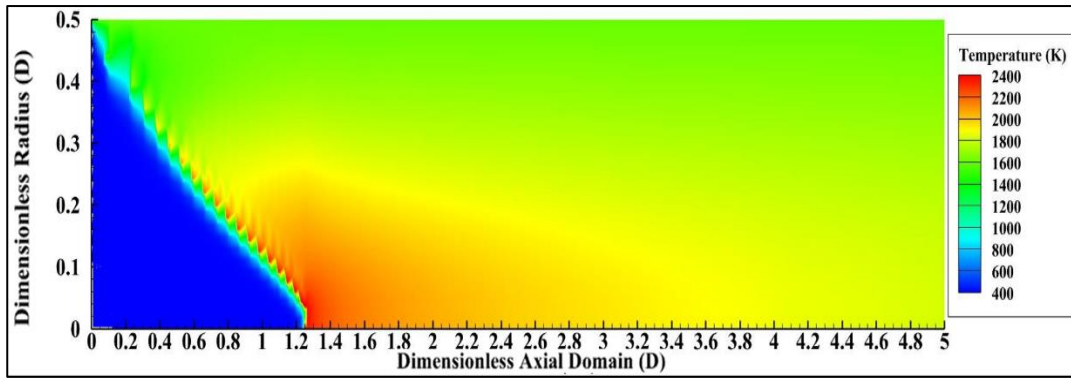
Figure 4.4 reactFlow: Temperature Distribution for Benchmark-1
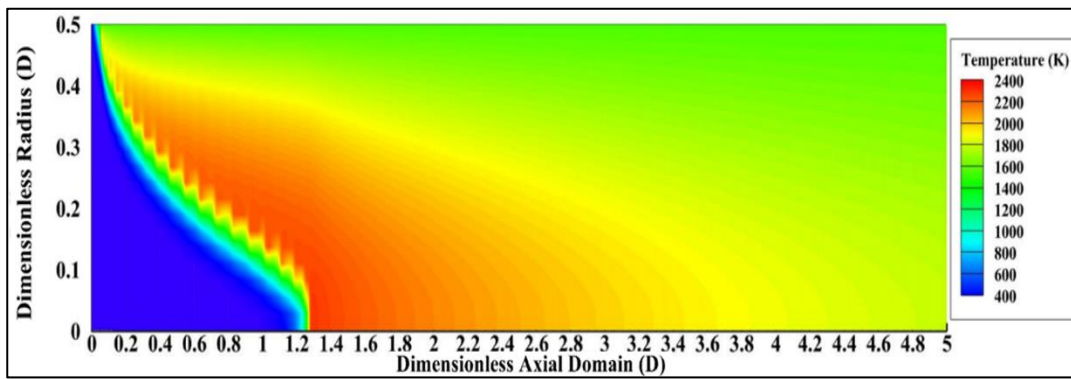
Figure 4.5 Chemkin: Temperature Distribution for Benchmark-1
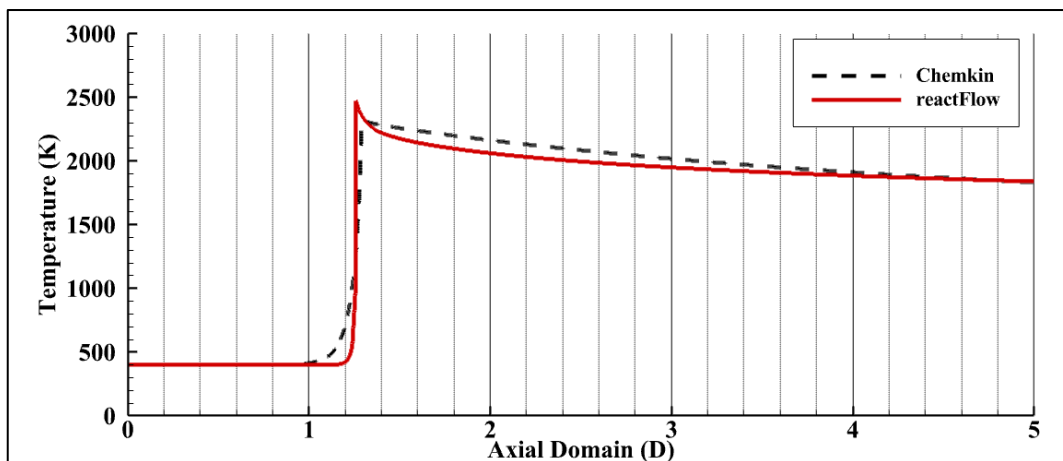
Figure 4.6 The Centerline Temperature Distribution for reactFlow and Chemkin

The temperature distribution lines on the centerline of the channel for both analyses are compared around the position of the anchored flame in Figure 4.6. A jump in the value of temperature on the centerline can be observed between the axial position of 1.25D and 1.30D from Figure 4.6. The analyses show that the flame starts to develop at 1.249D in the axial direction for reactFlow analysis. In addition, the flame initially develops at 1.28D in the axial direction for Chemkin analysis. At that axial location, the estimated flame front by both studies is significantly close to each other, with a difference of 2.42%, which is tabulated in Table 4.3.
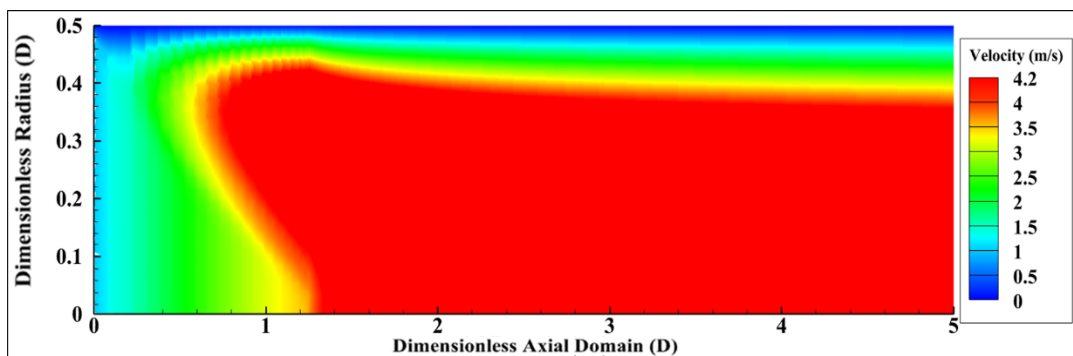
Figure 4.7 reactFlow: Velocity Distribution for Benchmark-1
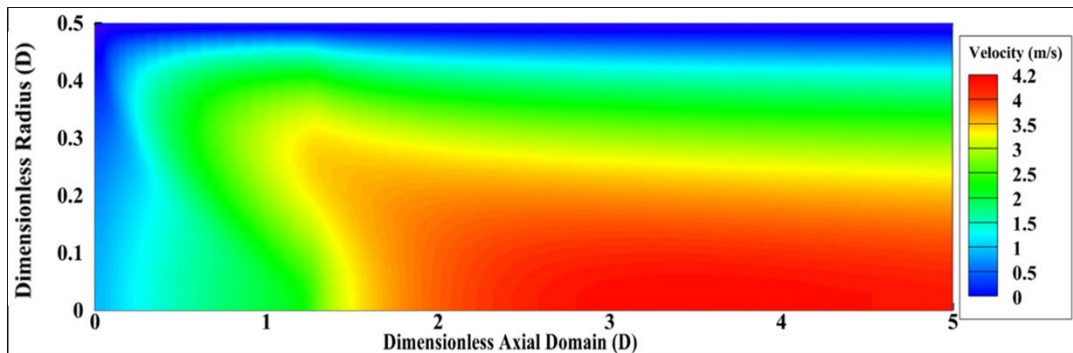
Figure 4.8 Chemkin: Velocity Distribution for Benchmark-1

Table 4.3 Comparison of Axial Flame Position for reactFlow and Chemkin

Case	Axial Flame Position
reactFlow	1.249 D
Chemkin	1.280 D
Difference	2.42%

The velocity distributions of reactFlow and Chemkin for the flow domain are presented in Figure 4.7 and Figure 4.8. The velocity distributions are slightly different, especially in the region where combustion is completed. The velocity lines around the anchored flame position are presented in Figure 4.9 for both analyses. It can be observed that the velocity of the flow fields is estimated significantly close to each other in the regions before and around the flame by both analyses. However, the values of velocities of both studies are separated from each other through the domain after combustion is completed.
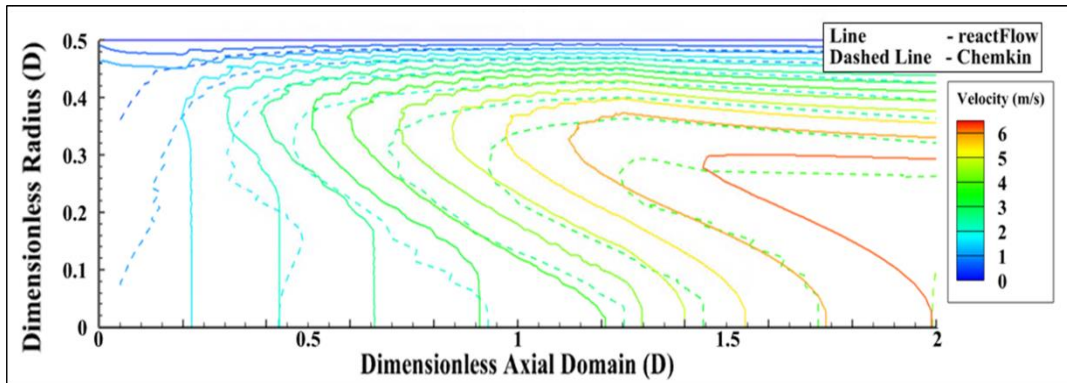
Figure 4.9 Comparison of Velocity Distributions for Benchmark-1

A study of mesh dependency is conducted for benchmark case-1 using reactFlow for different numbers of radial mesh points with the same value of stretch factor and inlet conditions given in Table 4.2. The number of radial mesh in the benchmark case is 21. The number of mesh points in the radial direction is increased to 31 and 41 to observe the effects of mesh on the solution fields. The temperature field for analyses is presented in figures between Figure 4.10 and Figure 4.12. The wiggles of the temperature field are observable around the flame front, while they are diffused with the increase in the number of radial mesh, as presented in Figure 4.11 and Figure 4.12. The wiggles on the flame front are dependent on the mesh number in the radial direction. The wiggles become subtle by increasing the mesh number. In addition, the flame position in the radial channel is observed to be affected by the number of radial mesh. The difference between flame positions is calculated as less than 15%. The molecular diffusion due to the resolution of the numerical problem is decreased with the increase in mesh number. Therefore, the flame in the channel is anchored closer to the channel inlet with the increase in the resolution of the mesh.

.
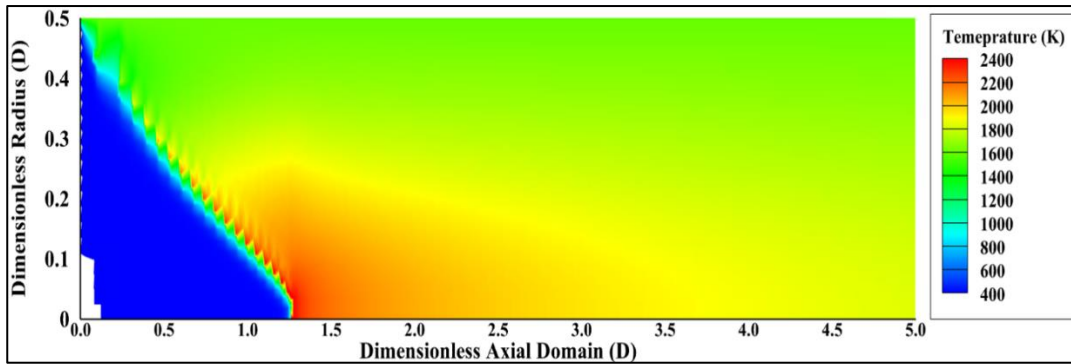
Figure 4.10 Temperature Field for the Case with 21 Radial Mesh Points
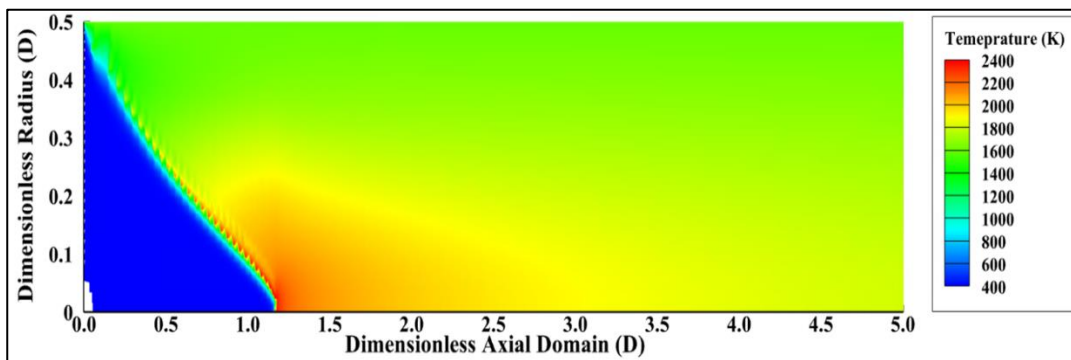
Figure 4.11 Temperature Field for the Case with 31 Radial Mesh Points
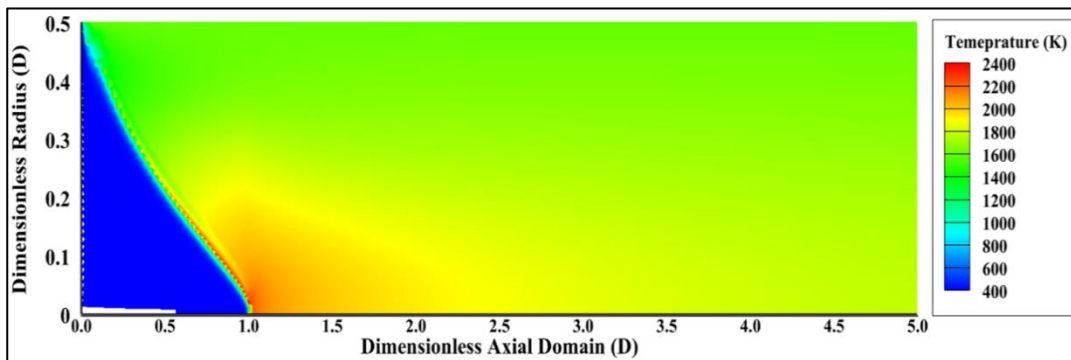
Figure 4.12 Temperature Field for the Case with 41 Radial Mesh Points

In the second benchmark case, the inlet velocity is decreased to 0.5 m/s, as given in Table 4.4 and the analyses are conducted to compare reactFlow and Chemkin solutions. The remaining inlet conditions are kept the same as benchmark case-1. In Figure 4.13 and Figure 4.14, the comparison of temperature fields of solutions of reactFlow and Chemkin are presented. The flame is stabilized at an axial position of 0.6 cm for both reactFlow and Chemkin. However, as in the case of benchmark-1, the temperature field is underestimated by reactFlow after the flame front for the region between the centerline and the channel wall. The temperature for the Chemkin case started to increase earlier and more smoothly than reactFlow, as presented in Figure 4.15. The temperature is determined higher for reactFlow than Chemkin at the flame position. However, temperature distributions on the centerline axis are calculated with similar trends by solvers after the flame region.

Table 4.4 The Boundary Conditions and Mesh Setup of Benchmark Case - 2 for Validation

Name of Parameter	Unit	Value
Channel Diameter	m	0.01
Inlet Velocity	m/s	0.50
Inlet Temperature	K	400
Wall Temperature	K	1600
Inlet Pressure	Pa	101325
Inlet Equivalence Ratio	-	1.0
Inlet Fuel Species	-	CH_4
Inlet Oxidizer	-	Air
Number of Nodes	-	21
Stretch Factor	-	1.1
Absolute Error Tolerance	-	10^{-5}

Figure 4.13 reactFlow: Temperature Distribution for Benchmark-2
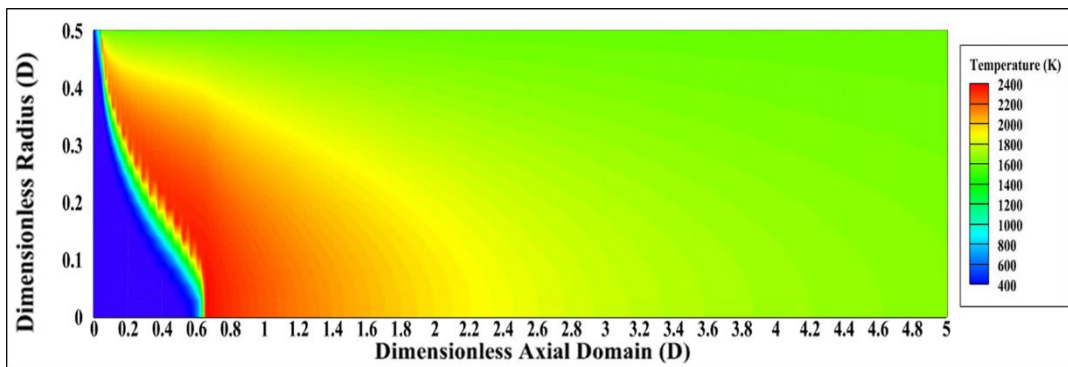
Figure 4.14 Chemkin: Temperature Distribution for Benchmark-2
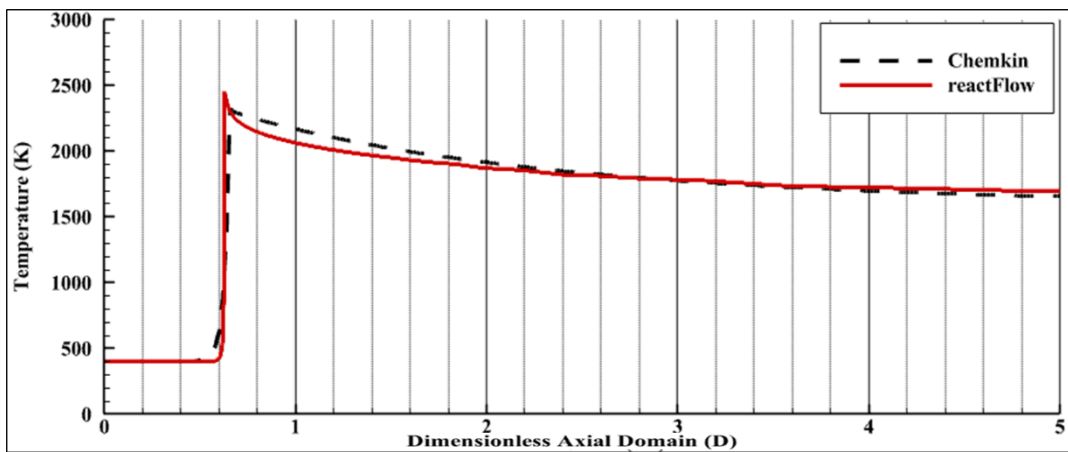
Figure 4.15 Comparison of Flame Positions at Centerline for reactFlow and Chemkin

Table 4.5 Comparison of Axial Flame Positions for reactFlow and Chemkin

Case	Axial Flame Position
reactFlow	0.629 D
Chemkin	0.650 D
Difference	3.23%

The velocity fields for reactFlow and Chemkin are given in Figure 4.16 and Figure 4.17. According to the figures, the velocity after the flame region is overestimated by reactFlow with respect to Chemkin. At the same time, similar velocity fields are observed for the area between the inlet of the channel and flame position, identical to benchmark case-1. The differences between velocity fields and temperature fields for reactFlow and Chemkin for benchmark cases 1 & 2 can be physically related to each other. In solutions of reactFlow, the temperature level is not significantly increased in a region between the centerline and channel wall. However, the velocity is dramatically raised to higher levels on the same area after the flame front, which is not the case in Chemkin solutions. In the solutions of Chemkin, high-temperature levels are observed between the centerline and wall after the flame front. Moreover, the velocity level is lower than reactFlow solutions in the same region.

This behavior can be caused for several reasons. One of them is due to differences in the algorithms of the codes. No relaxation factor or correction term for any coefficient is applied in reactFlow since reactFlow is an immature code with respect to Chemkin. In addition, the reacting flow in a channel is a highly stiff problem and the code reactFlow is very sensible to unphysical behavior of varying properties in a flow field. The unphysical results cannot be filtered during the iterations, affecting the convergence terms in reactFlow.
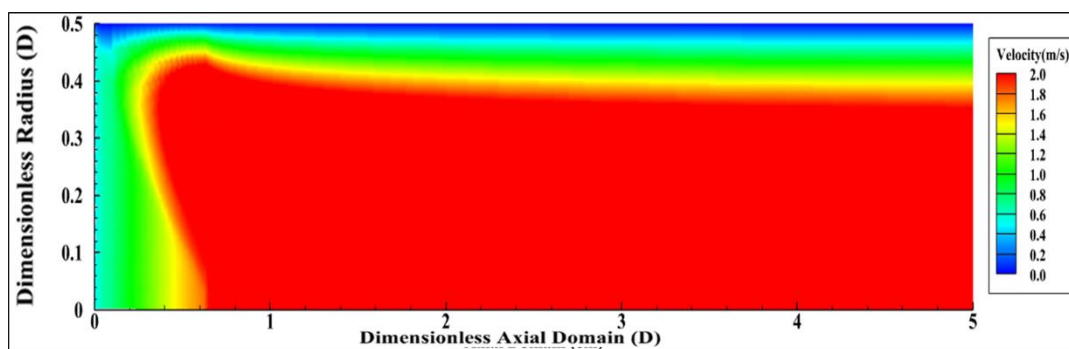
Figure 4.16 reactFlow: Velocity Distribution for Benchmark-2
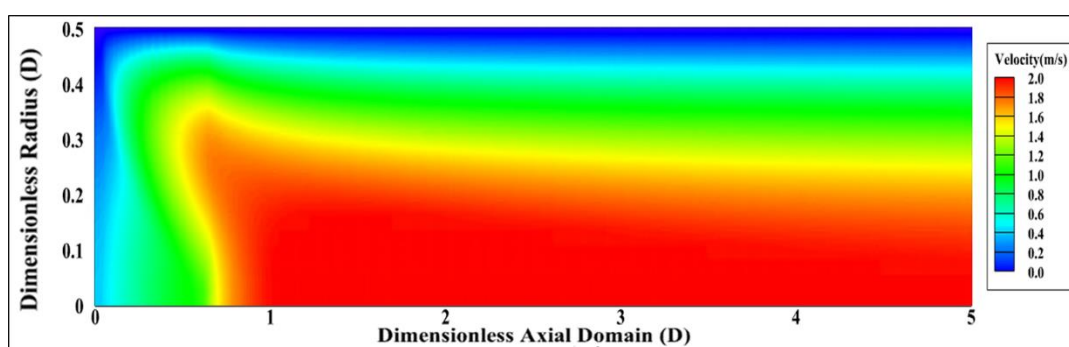
Figure 4.17 Chemkin: Velocity Distribution for Benchmark-2

The conservation of species is also compared for solutions of reactFlow and Chemkin in benchmark case-2 and the results are given in figures between Figure 4.18 and Figure 4.24. In Figure 4.18, the variation of mass fractions of CH_4, O_2 and CO_2 on the centerline of the channel are presented for reactFlow and Chemkin solutions. Since the flame is predicated on the same axial positions for both solvers, the decay and increase of the mass fractions of species have occurred between 0.6 cm and 0.65, which is the flame position on the centerline. The destruction of CH_4 and O_2 on the centerline started around 0.5 cm, following a smooth curve through the flame position for Chemkin, while it sharply started around 0.62 cm for reactFlow. The contours of CH4, O2 and CO2 mass fractions for reactFlow and Chemkin are presented between Figure 4.19 and Figure 4.24. The smoother destruction and construction of species are occurred in Chemkin from wall to centerline than reactFlow.

72
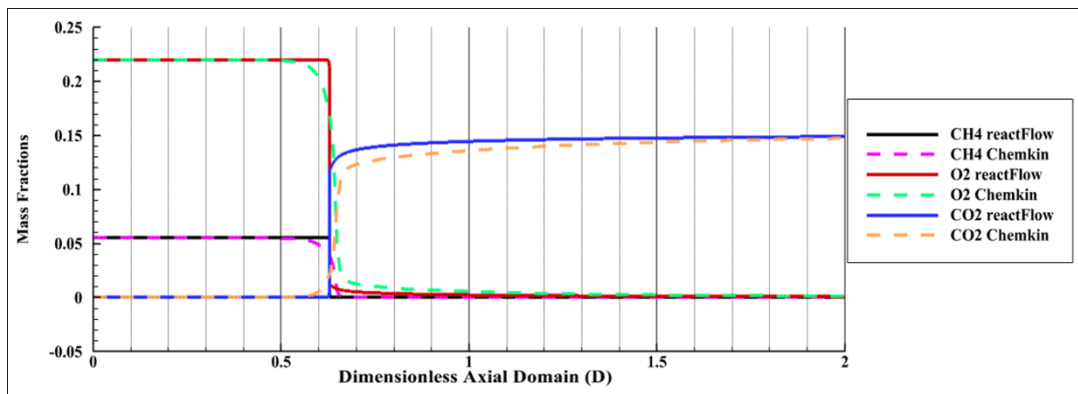
Figure 4.18 Comparison of Mass Fractions of Species on Centerline for reactFlow and Chemkin
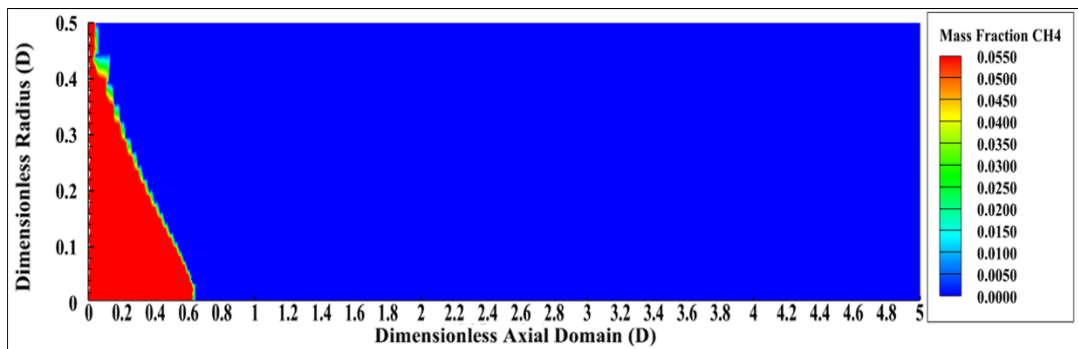
Figure 4.19 reactFlow: Mass Fraction of CH4
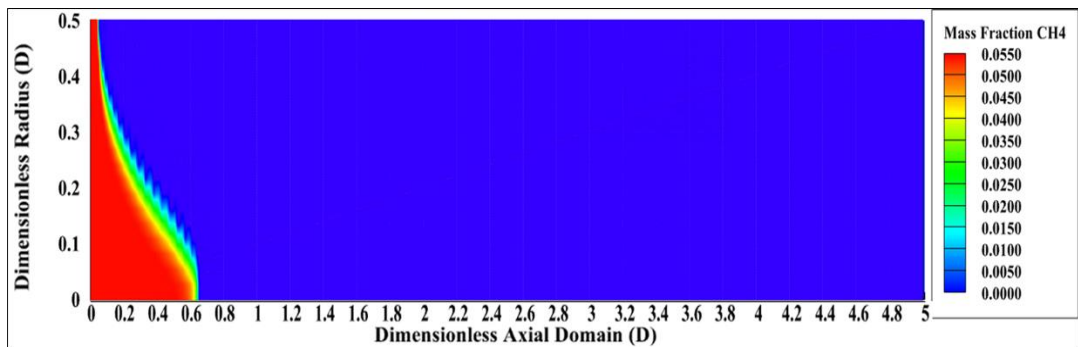
Figure 4.20 Chemkin: Mass Fraction of CH4
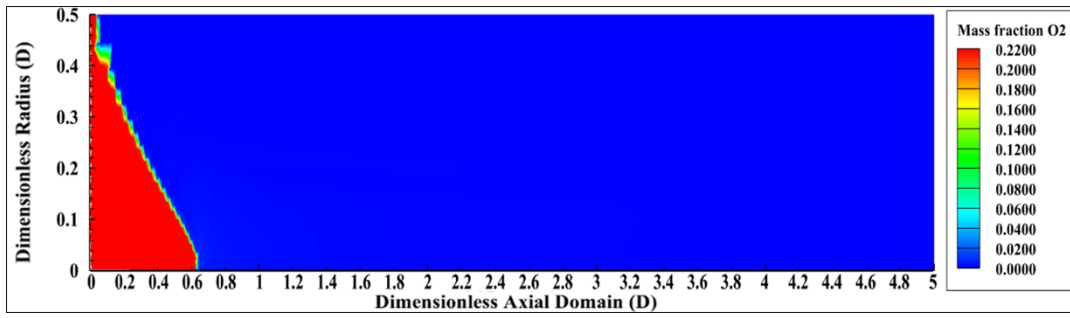
Figure 4.21 reactFlow: Mass Fraction of O2
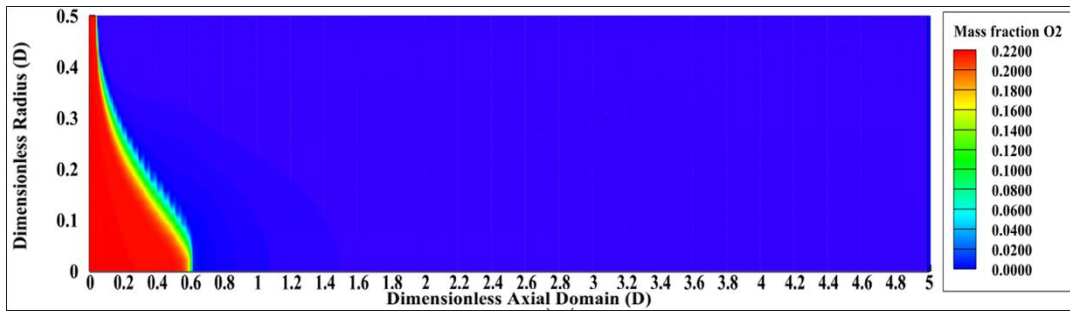
Figure 4.22 Chemkin: Mass Fraction of O2
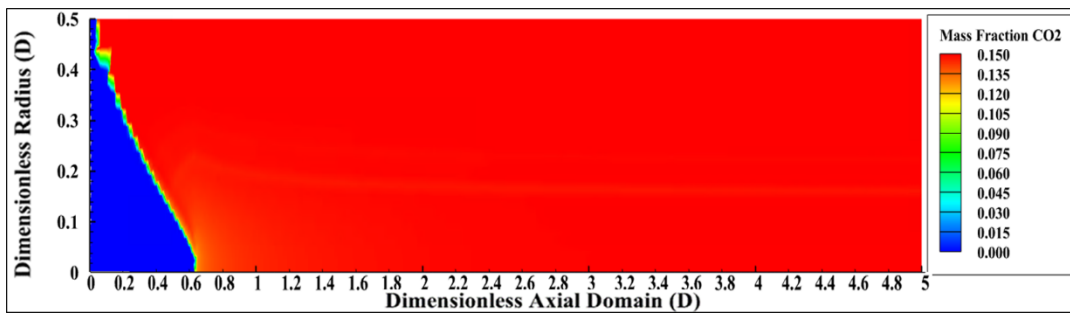
Figure 4.23 reactFlow: Mass Fraction of CO2
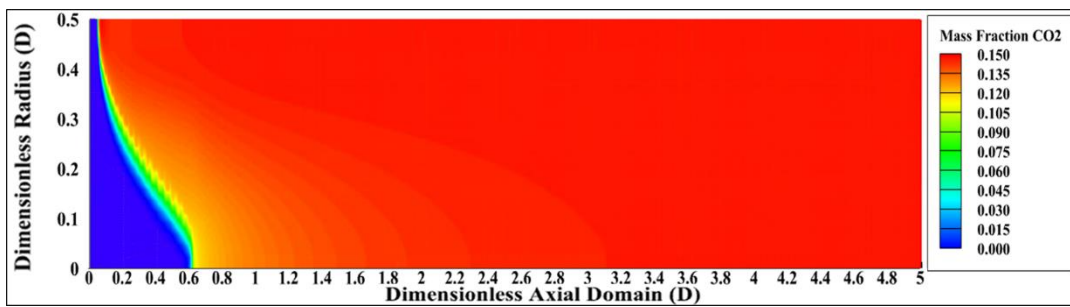
Figure 4.24 Chemkin: Mass Fraction of CO2

74

Although there are slight differences in velocity and temperature fields, the location of flame is calculated well enough by reactFlow with respect to benchmark cases analyzed using Chemkin. The accurate calculation of flame position is essential for reactFlow since its primary goal is to correctly estimate flame position in a channel domain. According to the results presented in section 4.1.2, the developed code reactFlow can be used to analyze flame generation and observe flame location.

4.2   Parametric Study of Sensitivity

A parametric study is conducted using reactFlow to investigate the effect of flow parameters on flame formation and position in a channel. Parameters and their range to be analyzed are tabulated in Table 4.6. The reference analysis for this study is specified as benchmark case-1, of which inlet conditions and mesh setup are presented in Table 4.2. The reacting gas is the mixture of $CH_4 - Air$, as in benchmark cases. Throughout the analyses, only one of the parameters is changed to see its effect on flame position, while other parameters are kept with the values of benchmark case-1. In the analyses, the dimensional quantities are normalized with the inlet diameter of the channel to make them comparable.

Table 4.6 Parameters for Sensitivity Study

Name of Parameter	Unit	Range
Inlet Velocity	m/s	0.5 – 1.0 – 1.5
Equivalence Ratio	-	0.9 – 1.0 – 1.1
Inlet Pressure	atm	0.75 – 1.0 – 1.5
Wall Temperature	K	1200 – 1600 – 1800
Channel Diameter	M	0.005 – 0.010 – 0.0125

4.2.1 Varying Inlet Velocity

The inlet velocity of the channel is changed in a range of 0.5 m/s to 1.5 m/s to observe inlet velocity effects on flame position. The centerline temperature, velocity and species mass fraction distributions for varying inlet velocities are presented in Figure 4.25, Figure 4.26 and Figure 4.27, respectively. The calculated flame positions for different inlet velocities are tabulated in Table 4.7. The temperature and velocity fields for varying inlet velocities are presented between Figure 4.28 and Figure 4.33.
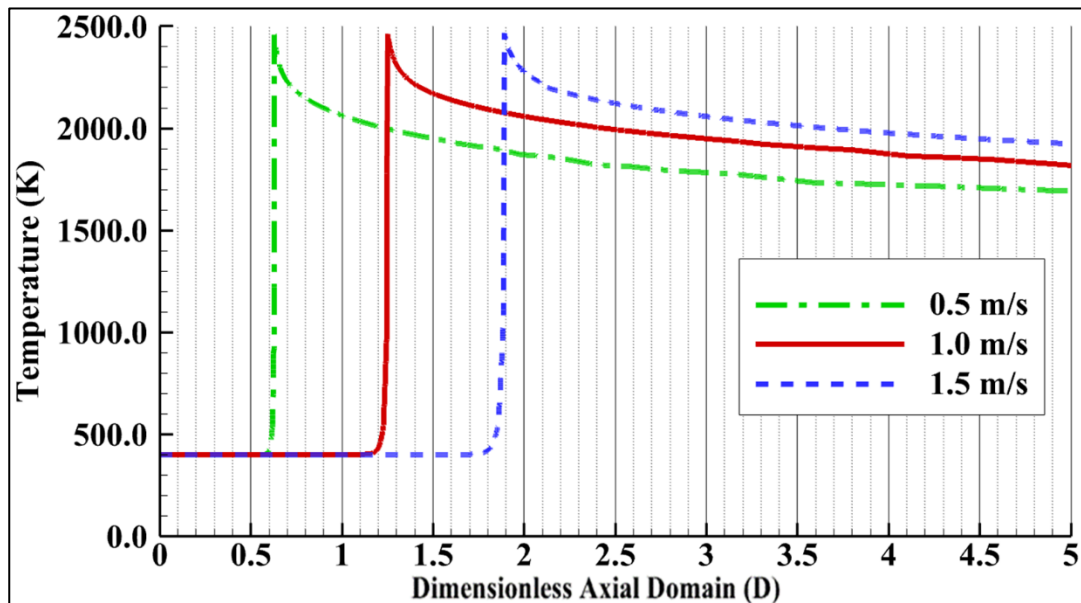
Figure 4.25 Comparison of Centerline Temperatures for Varying Inlet Velocities
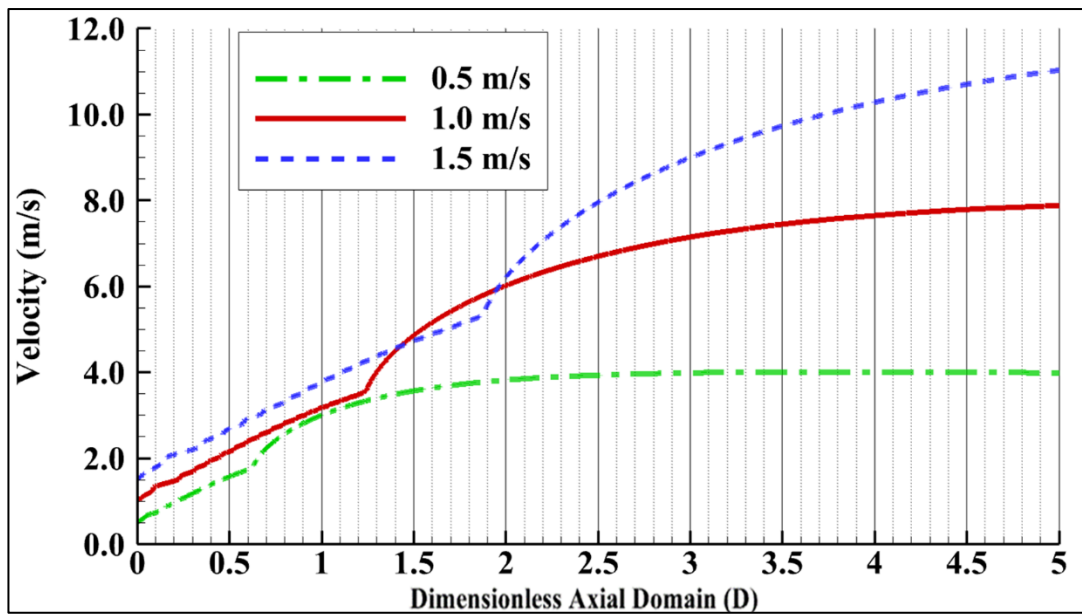
Figure 4.26 Comparison of Centerline Velocities for Varying Inlet Velocities
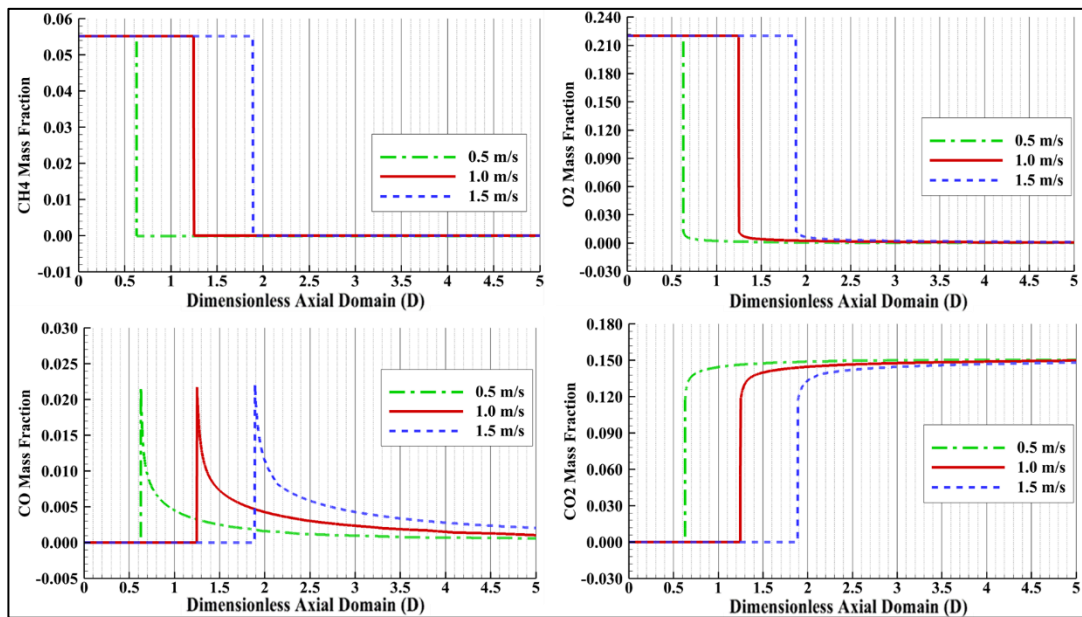
Figure 4.27 Comparison of Centerline Species Mass Fractions for Varying Inlet Velocities
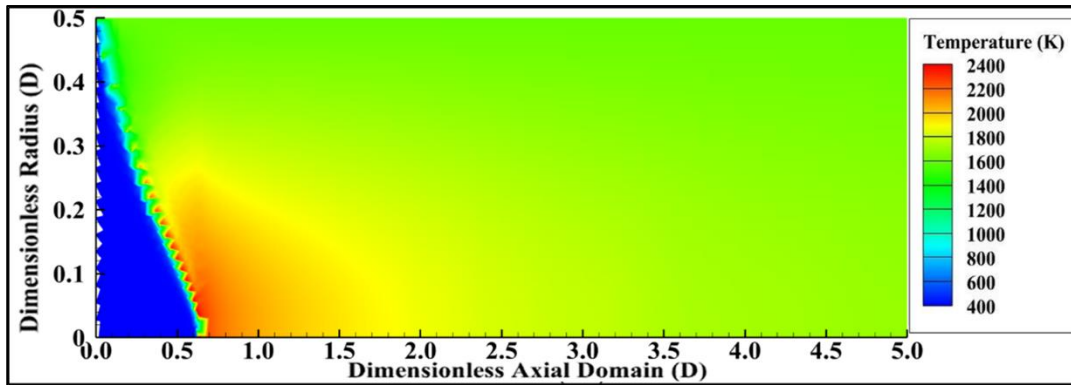
Figure 4.28 Temperature Field for U = 0.5 m/s
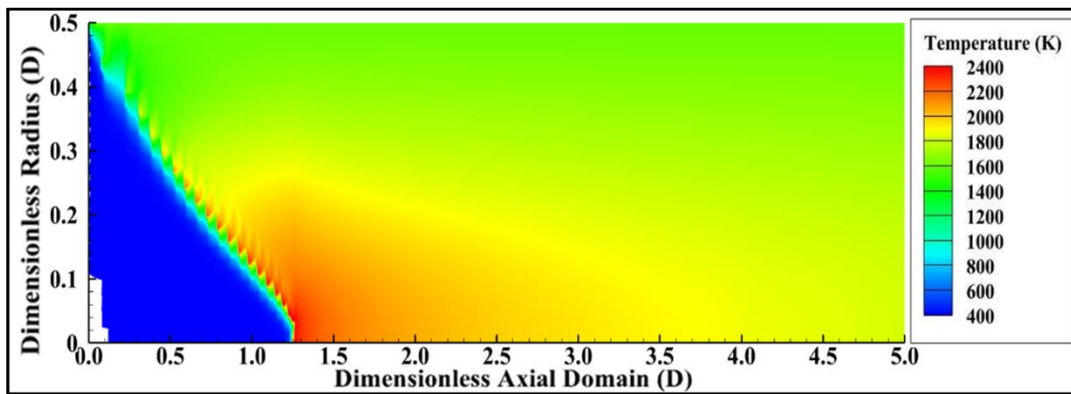
Figure 4.29 Temperature Field for U = 1.0 m/s
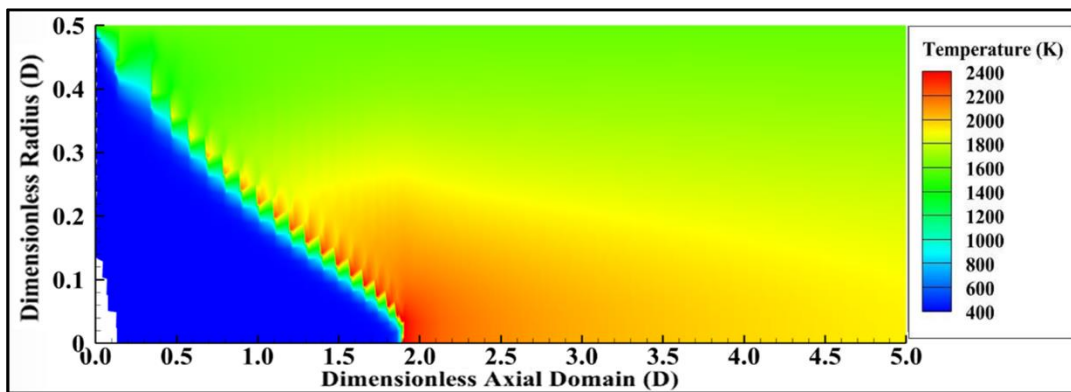
Figure 4.30 Temperature Field for U = 1.5 m/s
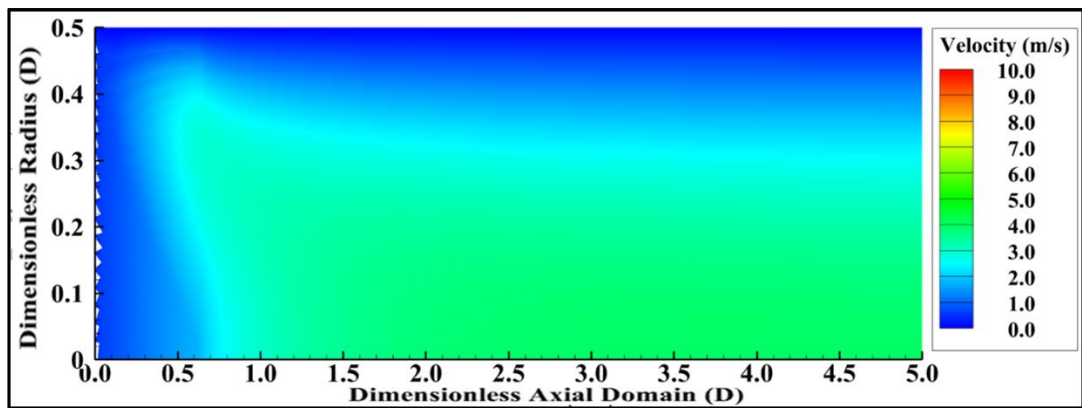
Figure 4.31 Velocity Field for U = 0.5 m/s
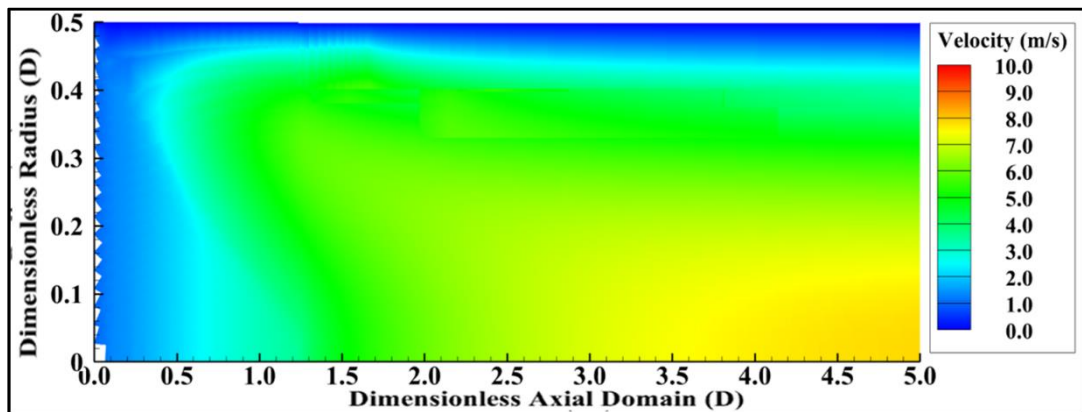
Figure 4.32 Velocity Field for U = 1.0 m/s
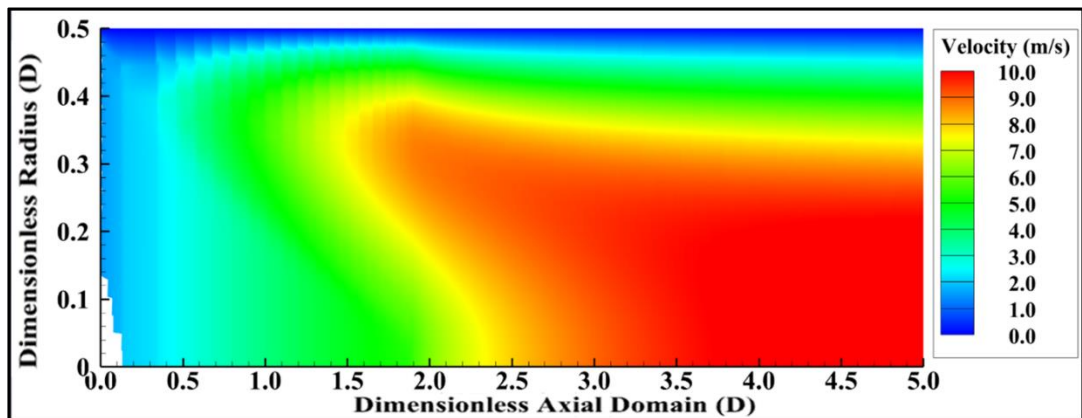
Figure 4.33 Velocity Field for U = 1.5 m/s

The speed of a flame in the channel can be considered as the speed of an unburned mixture of gases for flat flames in one-dimensional cases. When the shape of the flame is flat, the direction of unburned gases corresponds with the normal direction of the channel's cross-section [35]. In this case, the flow velocity becomes equal to the flame speed. However, the flame is not always produced as flat-shaped, as in the case of the Bunsen burner flame [35]. The shape of the flame is formed as a function of flow speed and heat loss. In this condition, the flame speed is proportional to the normal component of the flow velocity. When the flow velocity gets higher, the area of the flame front gets higher and the shape of the flame becomes more conical. This behavior can also be observed by examining the results of temperature fields calculated by reactFlow and presented between Figure 4.28 and Figure 4.30. The anchored flame position gets away from the channel inlet with the increase in inlet velocity. The values of flame position in the axial direction are tabulated in Table 4.7. Moreover, the density of burnt gas gets lower than the density of fresh gases due to the increased temperature of the burnt gas due to combustion. The velocity of burnt gases becomes higher than fresh gases for the same mass flow rate due to mass conservation [35]. The increase in the velocity field through the channel can be observed between Figure 4.31 and Figure 4.33. When the velocity of inlet flow gets higher, the velocity of flow downstream in the channel becomes higher.

Table 4.7 Flame Position in Axial Direction for Varying Inlet Velocities

Inlet Velocity	Axial Flame Position	x/U
U = 0.5 m/s	0.62 D	1.24
U = 1.0 m/s	1.25 D	1.25
U = 1.5 m/s	1.90 D	1.26

The ratio of axial flame position to inlet velocity is presented in Table 4.7. The relation between flame position and inlet velocity is investigated using this ratio. The constant ratio of axial flame position to inlet velocities is calculated and tabulated in Table 4.7. In addition, the temperature fields of each case are plotted as a line plot in Figure 4.34. The temperature lines are overlapped with each other since the ratio of axial flame position to inlet velocity is constant for each case. As a result, inlet velocity can be used as a similarity parameter for problems of reacting channel flows.
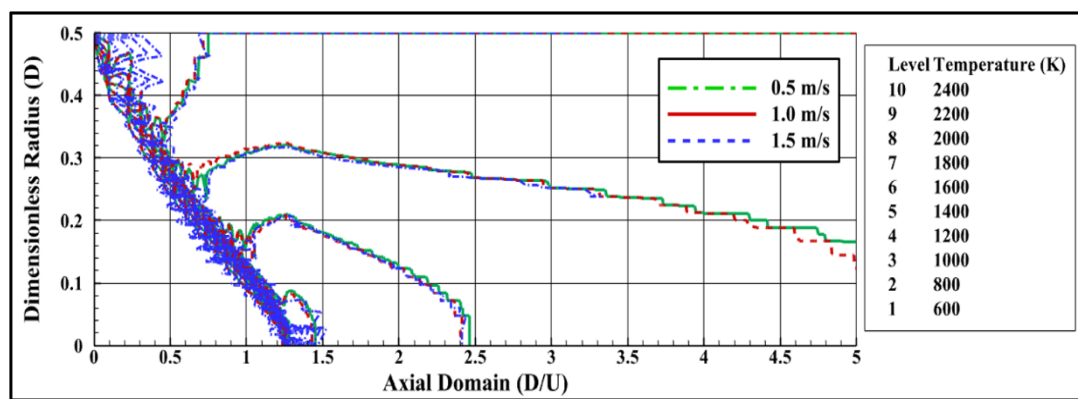
Figure 4.34 Comparison of Flame Shapes for Varying Inlet Velocities

4.2.2   Varying Equivalence Ratio

The equivalence ratio of inlet premixed flow is changed between 0.9 and 1.1 to examine equivalence ratio effects on flame position. The centerline temperature, velocity and species mass fraction distributions for varying equivalence ratios are presented between Figure 4.35 and Figure 4.37. The calculated flame positions are tabulated in Table 4.8.
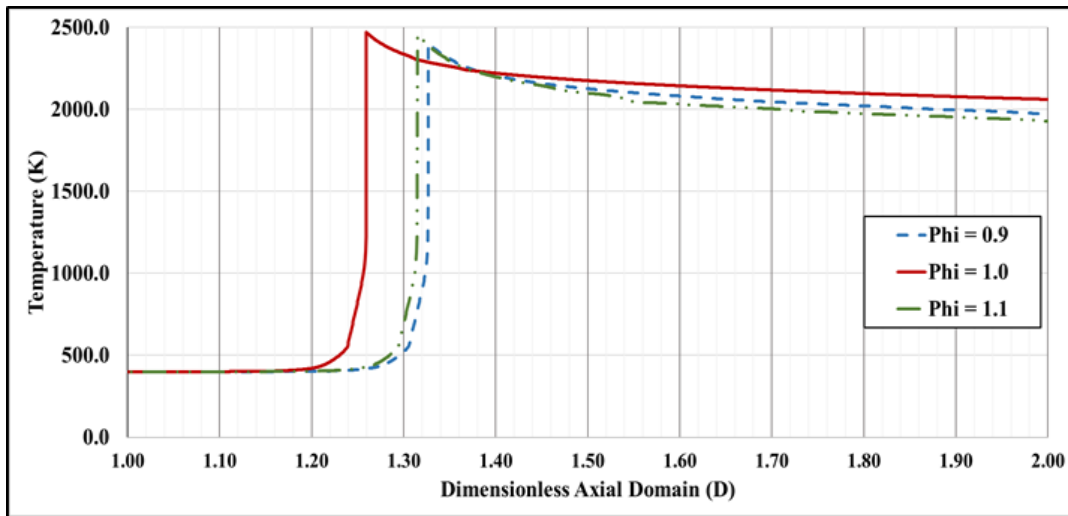
Figure 4.35 Comparison of Centerline Temperatures for Varying Inlet Equivalence Ratios
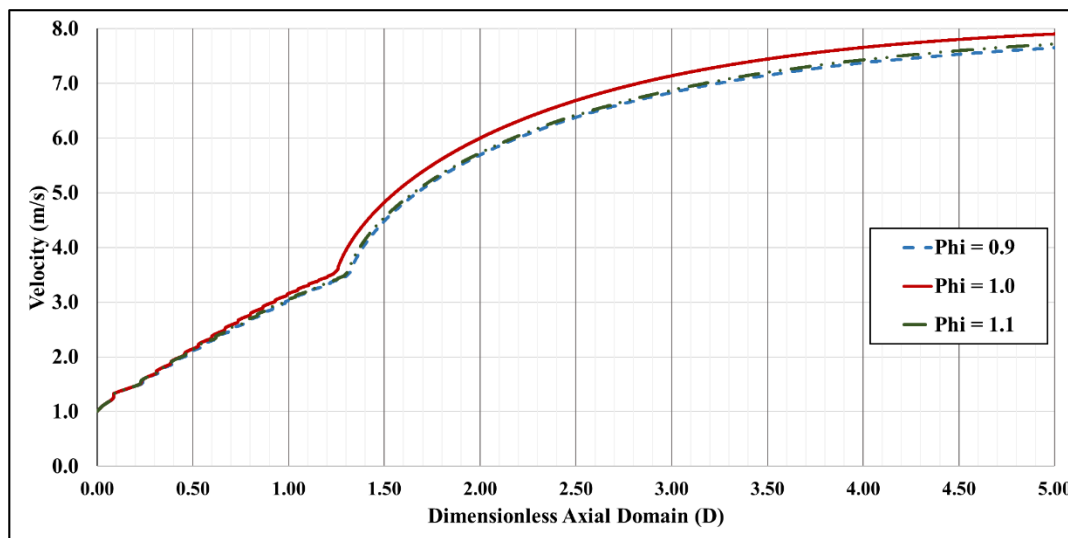
Figure 4.36 Comparison of Centerline Velocities for Varying Inlet Equivalence Ratios
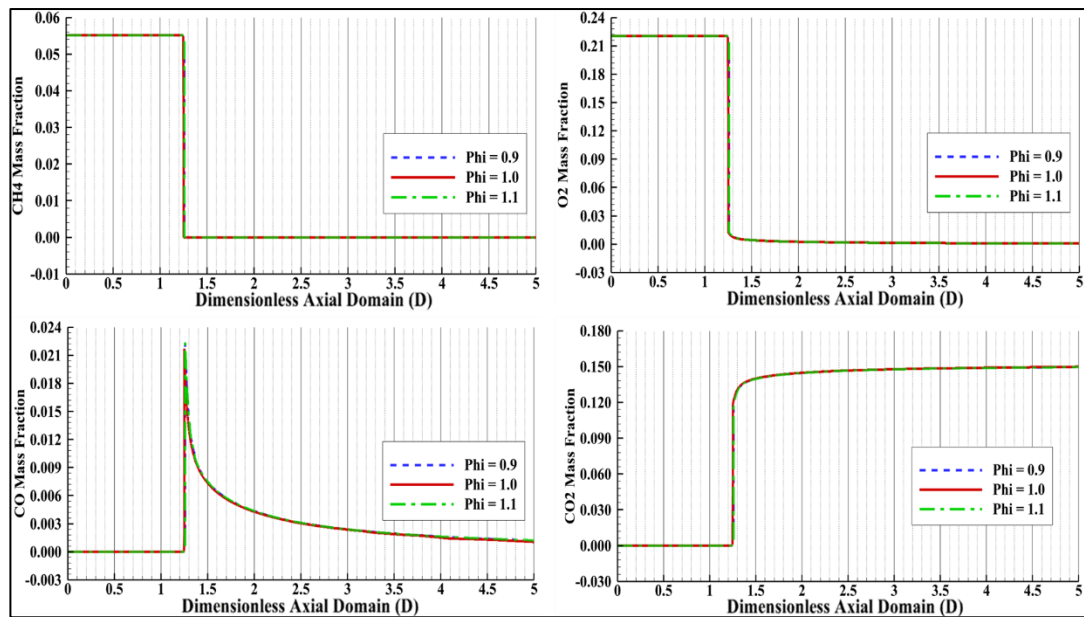
Figure 4.37 Comparison of Centerline Species Mass Fractions for Varying Inlet Equivalence Ratios

The above-presented figures show that the change of equivalence ratio in the given range slightly affects the flame position, as provided in Table 4.8. In addition, minor changes in flame shape can be observed from the contours of temperature and velocity fields presented between Figure 4.39 and Figure 4.44. Since inlet conditions are the same for the three cases except for the equivalence ratio, the properties of the burnt gases are only related to the equivalence ratio and the adiabatic flame temperature of burnt gases [35]. The relation between the burning velocities of the methane-air mixture and varying equivalence ratios can be summarized such that the flame speed becomes the highest for the value of the equivalence ratio, where the adiabatic flame temperature of the mixture is highest [36]. The adiabatic flame temperatures for the range of equivalence ratios for inlet conditions of channel flow given in Table 4.2 are presented in Figure 4.38. The highest temperature value is obtained at the stoichiometric condition, where $\Phi = 1.0$; due to this, the highest flame velocity is expected for $\Phi = 1.0$. As the flame velocity increases, the ratio between inlet flow velocity and flame velocity decreases and this leads flame to be flatter due

to mass continuity. Since the flame is flatter, it stabilized earlier in a channel. As a result, the flame is positioned closer to the channel inlet than in other conditions with different equivalence ratios. For values of equivalence ratios 0.9 and 1.1, the adiabatic flame temperatures are calculated with very little difference from each other, which can be observed in Figure 4.38. Therefore, the flame positions for both cases are estimated at the same point, tabulated in Table 4.8. However, the variations of flow properties are slight for a given range of equivalence ratios, as can be observed from the temperature and velocity fields shown between Figure 4.39 and Figure 4.44.
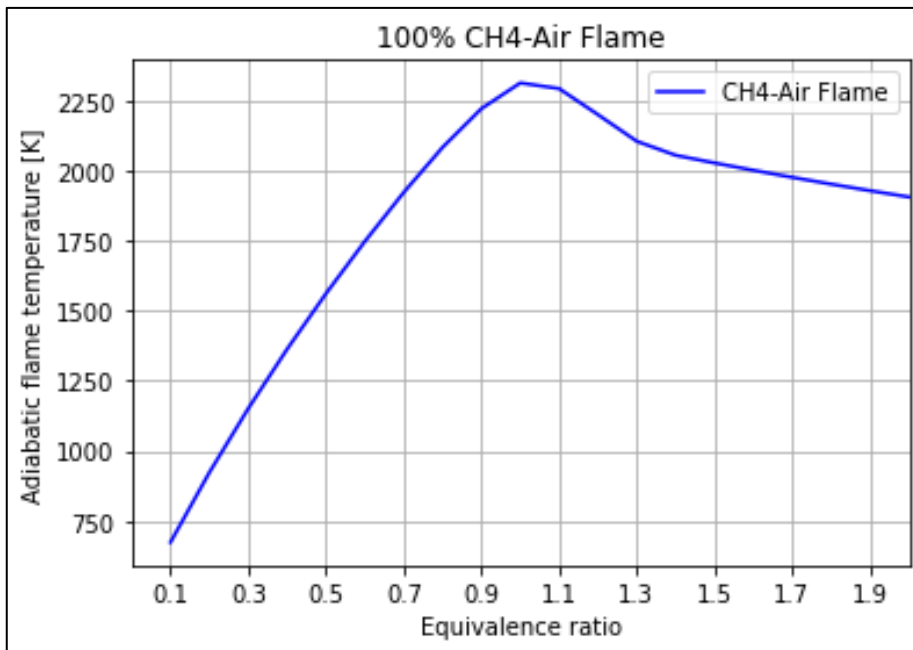
Figure 4.38 Adiabatic Flame Temperature
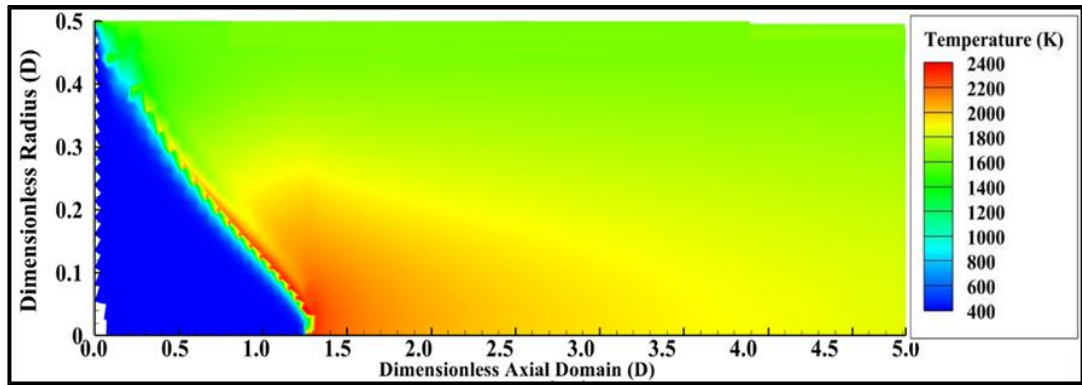
Figure 4.39 Temperature Field for Φ = 0.9
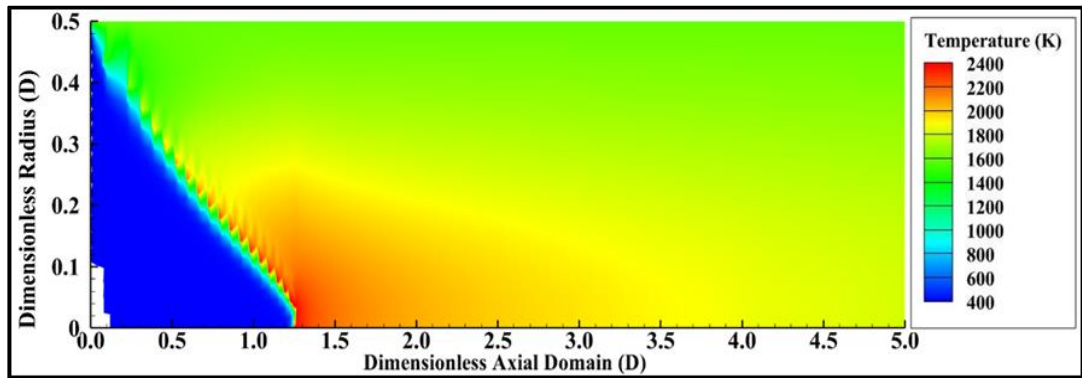
Figure 4.40 Temperature Field for Φ = 1.0
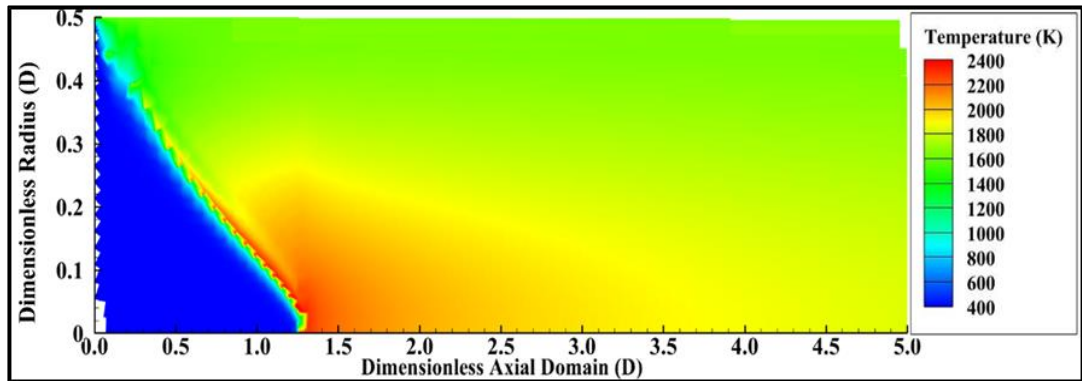
Figure 4.41 Temperature Field for Φ = 1.1
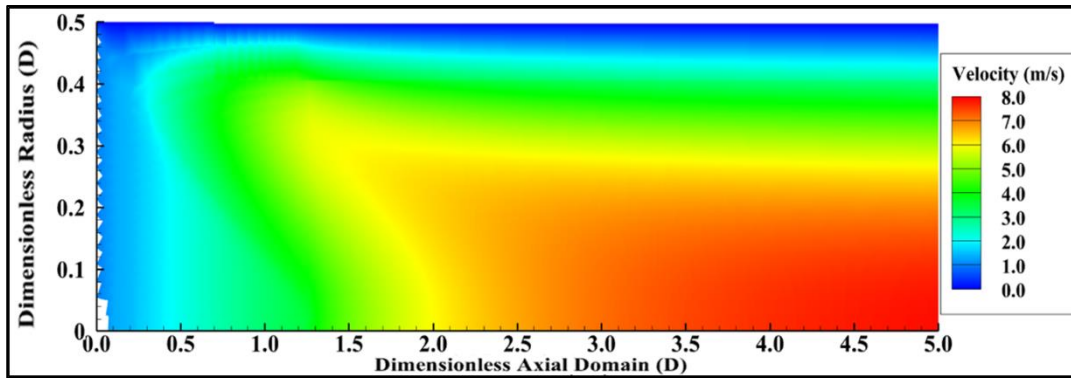
Figure 4.42 Velocity Field for $\Phi = 0.9$
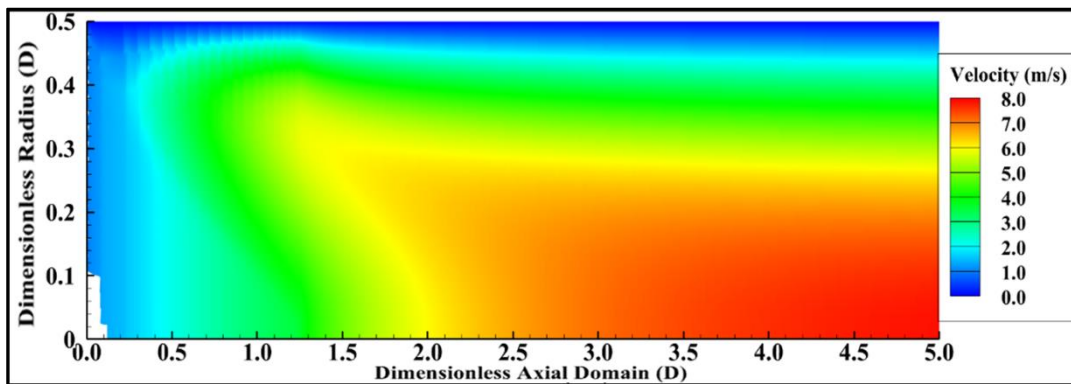
Figure 4.43 Velocity Field for $\Phi = 1.0$
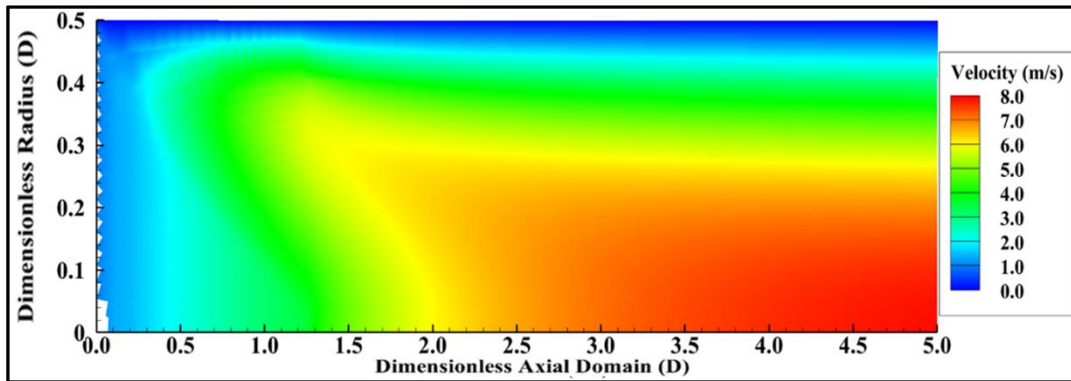
Figure 4.44 Velocity Field for $\Phi = 1.1$

Table 4.8 Flame Position in Axial Direction for Varying Equivalence Ratios

Equivalence Ratio	Axial Flame Position
$\Phi = 0.9$	1.327 D
$\Phi = 1.0$	1.250 D
$\Phi = 1.1$	1.315 D

4.2.3 Varying Inlet Pressure

The flow's inlet pressure is changed from 0.75 atm to 1.5 atm to investigate its effects on flame position. The centerline temperature, velocity and species mass fraction distributions for varying inlet pressures are presented in Figure 4.45, Figure 4.46 and Figure 4.47.
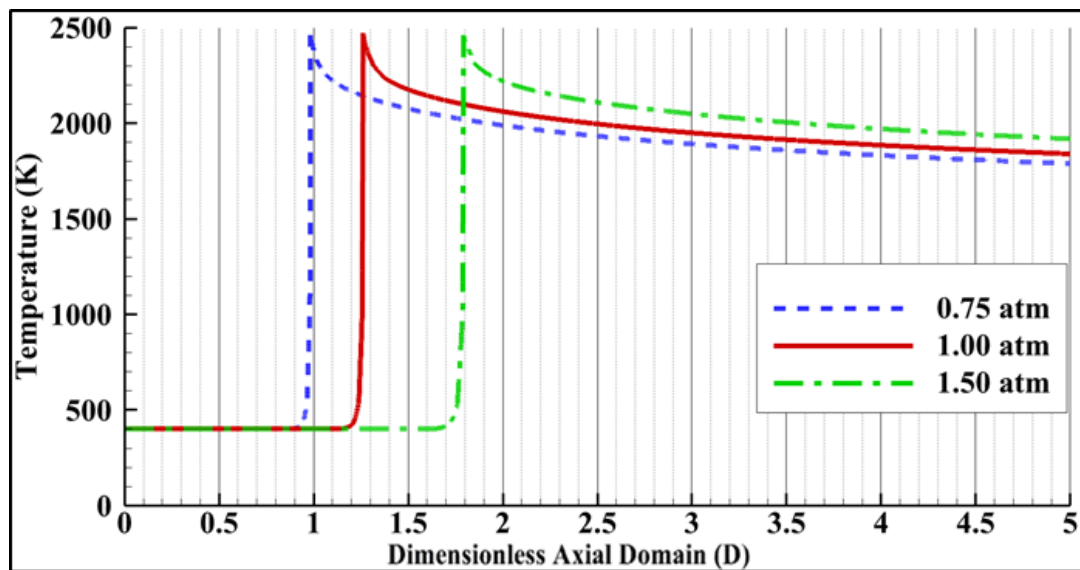
Figure 4.45 Comparison of Centerline Temperatures for Varying Inlet Pressures
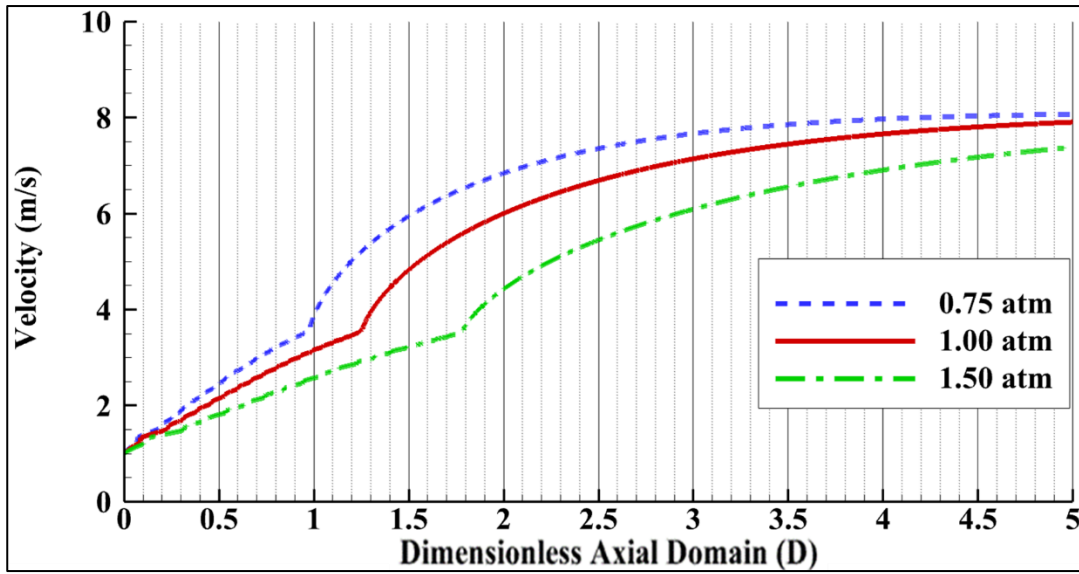
Figure 4.46 Comparison of Centerline Velocities for Varying Inlet Pressures
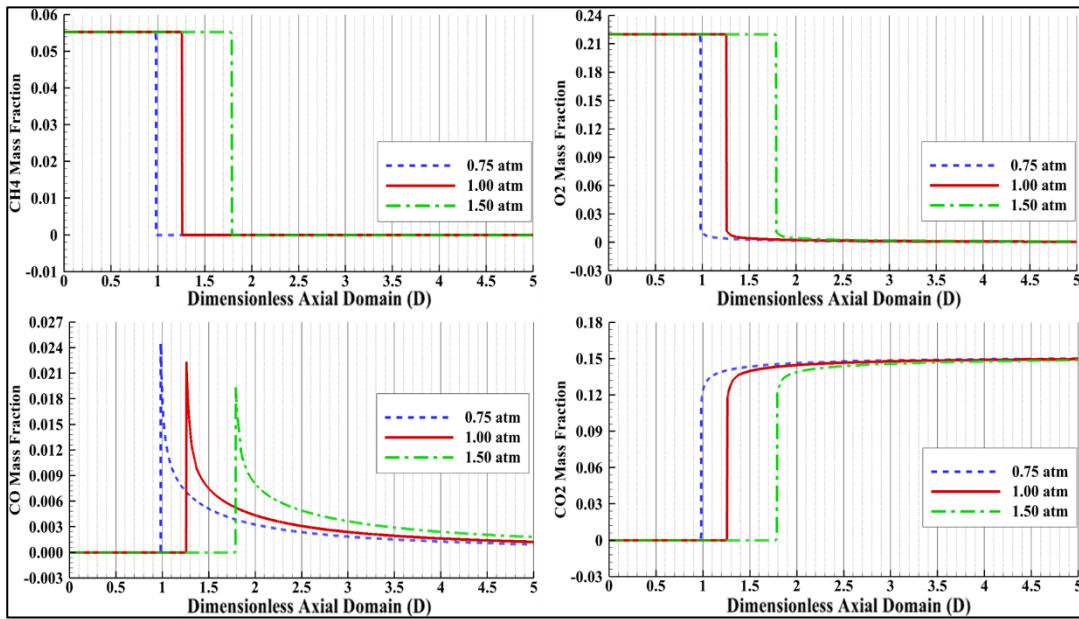
Figure 4.47 Comparison of Centerline Species Mass Fractions for Varying Inlet Pressures

The experimental results for calculating the burning velocity of the methane-air mixture for varying pressure are summarized in [36] and show that the burning velocity, which corresponds to flame velocity, of the methane-air mixture is inversely proportional to the inlet pressure [36]. Thus, flame velocity decreases with increasing inlet pressure. As flame velocity decreases, the velocity ratio between inlet flow and burnt gases increases, which increases the area ratio of fresh and burnt gases to satisfy mass continuity. The shape of the flame gets more conical when the area ratio is increased. The change of flame shape can be observed from the temperature and velocity fields given between Figure 4.48 and Figure 4.53. Therefore, the anchored position of the flame in a channel is delayed proportionally with inlet pressure. The location of temperature shifts, which shows the position of the flame, can be observed in Figure 4.45. The flame speeds for varying inlet pressures are calculated for a two-step methane-air combustion mechanism [34] using Cantera software and tabulated in Table 4.9. According to tabulated results, numerical calculations are in accordance with the experimental results given in [36]. In addition, flame speed is inversely proportional to the root of pressure, and the proportionality constants for each case are presented in Table 4.9. Because of this relation between inlet pressure and flame speed, it can be concluded that pressure can be used as a similarity parameter for the problems of reacting channel flow. Moreover, the velocity change on the centerline is shown in Figure 4.46, where the maximum flow velocity after the flame is examined. Although the flame position is delayed with increasing inlet pressure, the maximum temperature of burnt gases is not changing.
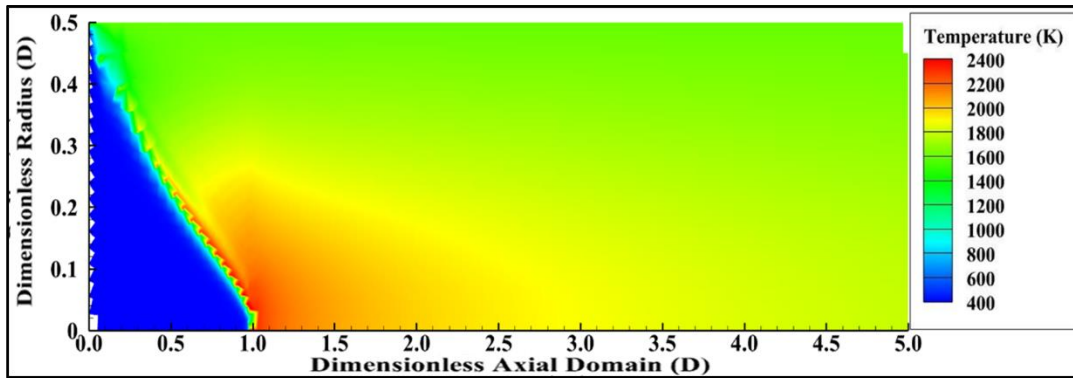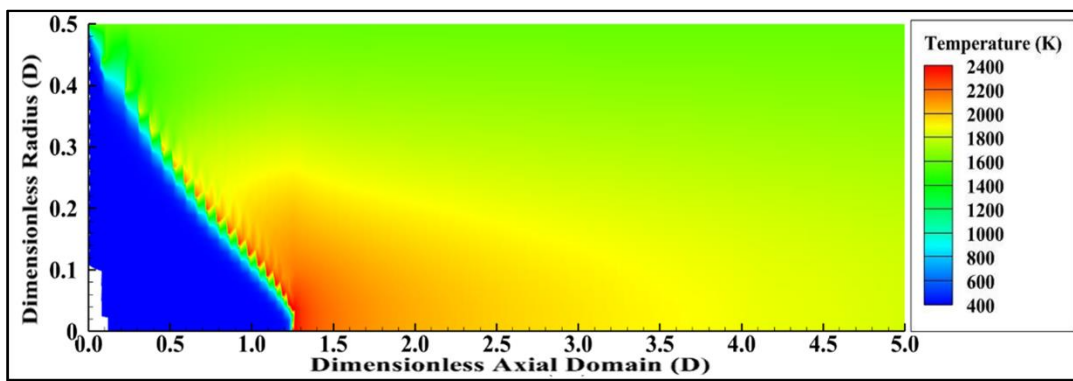
Figure 4.48 Temperature Field for P = 0.75 atm

Figure 4.49 Temperature Field for P = 1.0 atm
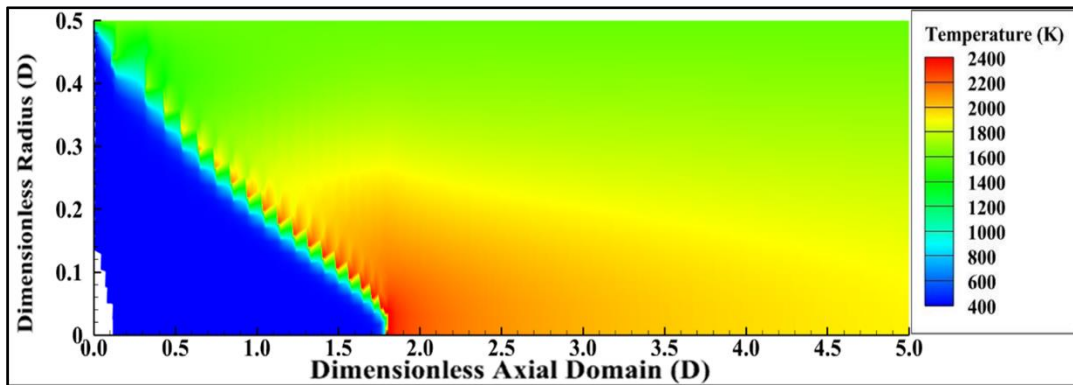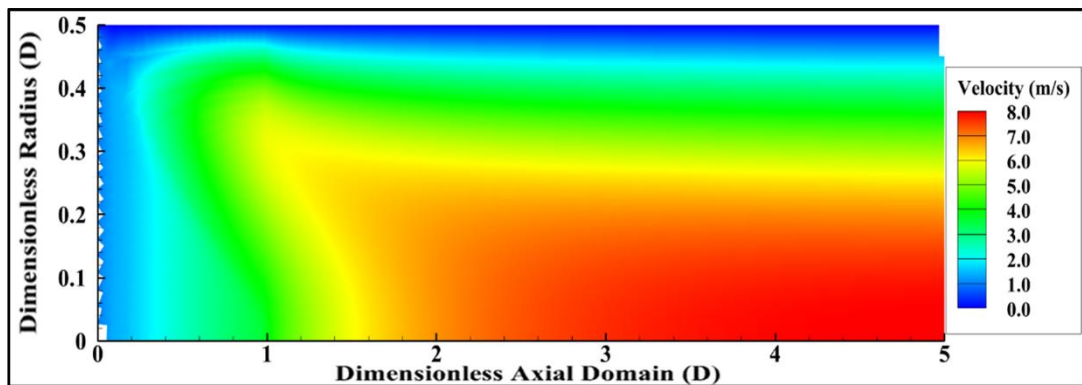

Figure 4.50 Temperature Field for P = 1.5 atm
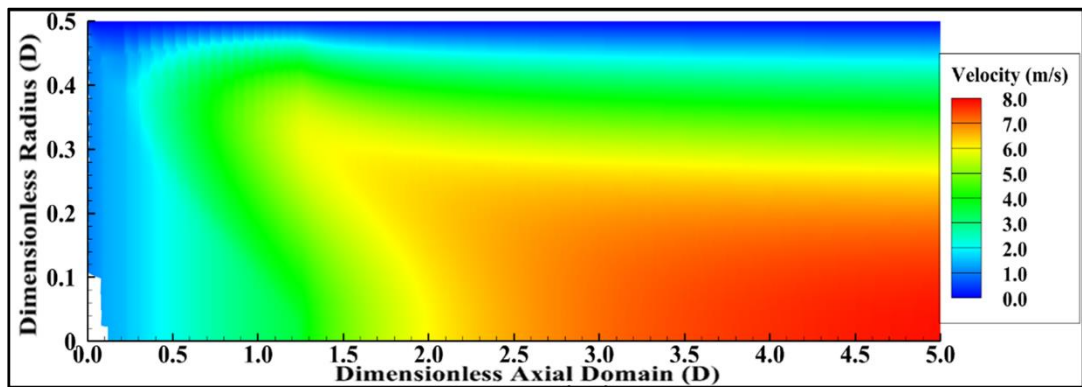
Figure 4.51 Velocity Field for P = 0.75 atm
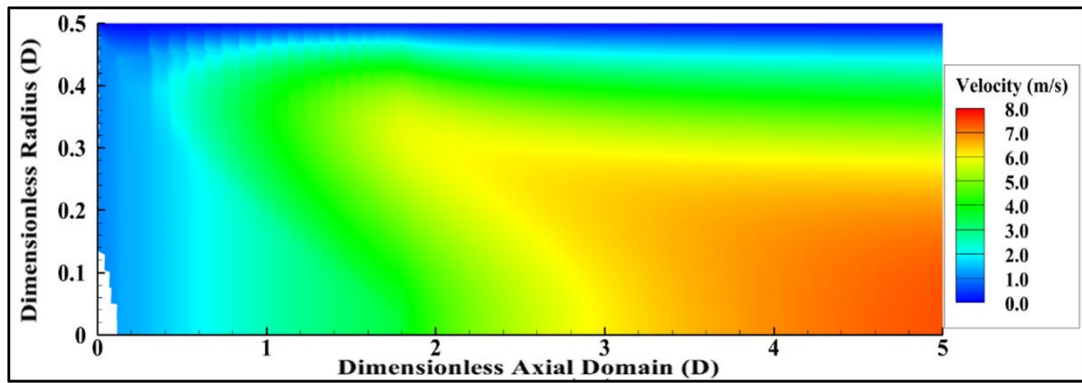

Figure 4.52 Velocity Field for P = 1.0 atm

Figure 4.53 Velocity Field for P = 1.5 atm

Table 4.9 Calculated Flame Speeds for Varying Inlet Pressures

Inlet Pressure	Flame Speed	$S_L/P^{-0.5}$
0.75 atm	74.18 cm/s	64.1
1.00 atm	66.06 cm/s	66.0
1.50 atm	55.74 cm/s	68.3

Table 4.10 Flame Position in Axial Direction for Varying Inlet Pressures

Inlet Pressure	Axial Flame Position
0.75 atm	1.00 D
1.00 atm	1.25 D
1.50 atm	1.80 D

4.2.4 Varying Wall Temperature

The wall temperature of the channel is changed between 1200 K and 1800K in order to investigate its effects on flame position. The centerline temperature, velocity and species mass fraction distributions for varying inlet pressures are presented in Figure 4.54, Figure 4.55 and Figure 4.56.
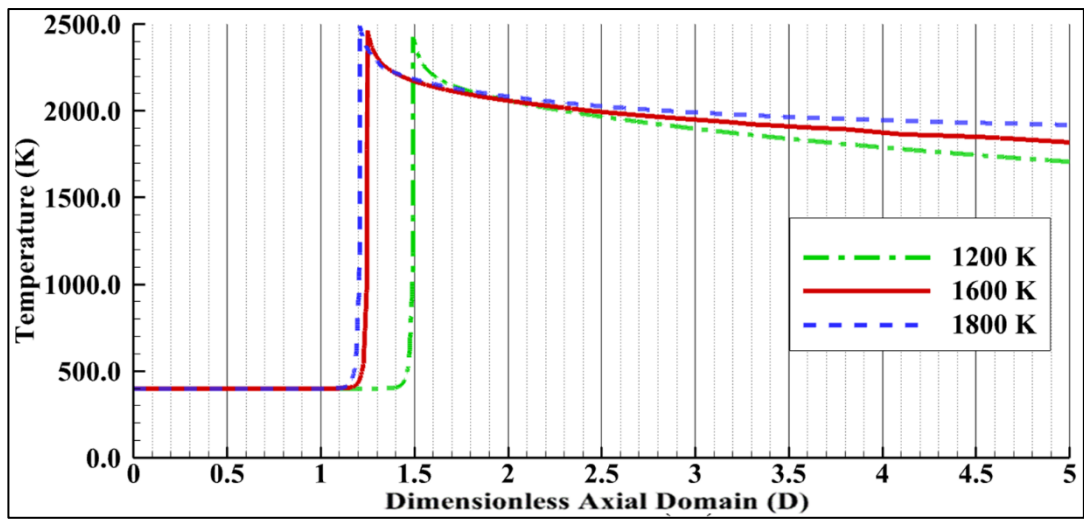
Figure 4.54 Comparison of Centerline Temperatures for Varying Wall
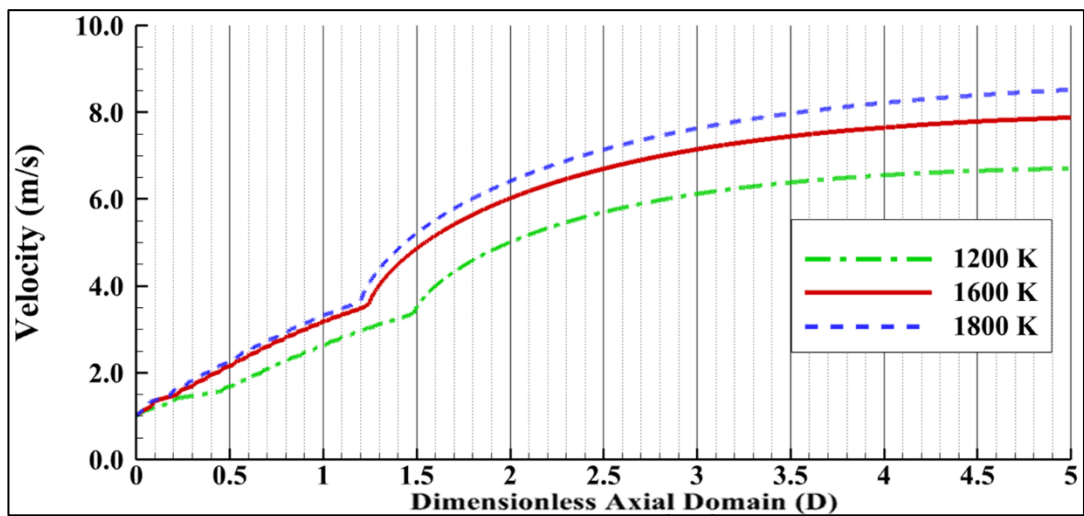Temperatures

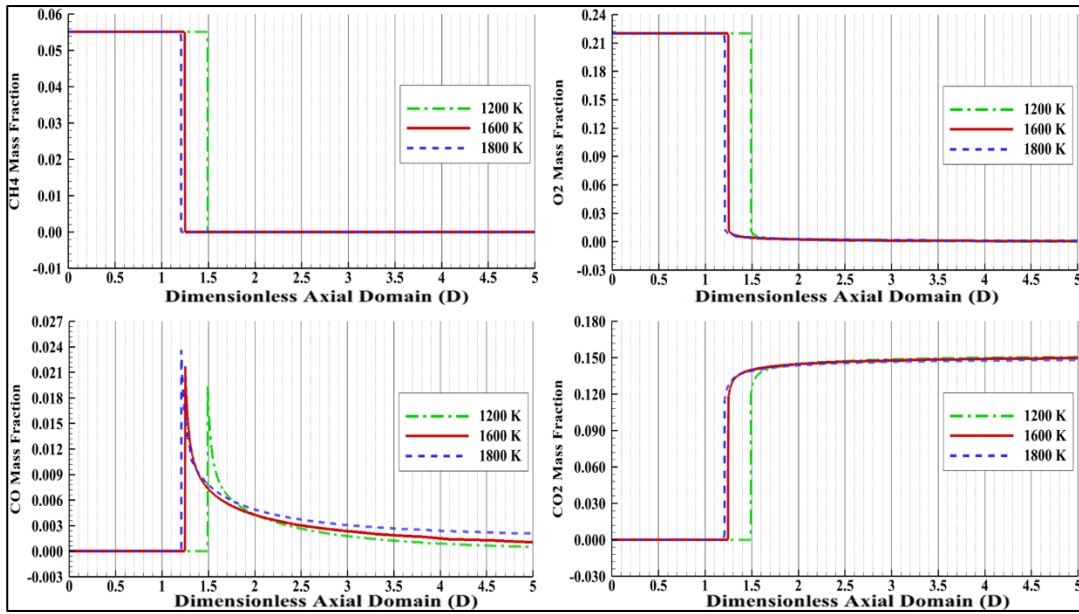Figure 4.55 Comparison of Centerline Velocities for Varying Wall Temperatures

Figure 4.56 Comparison of Centerline Species Mass Fractions for Varying Wall Temperatures

The flame positions can be obtained from Figure 4.54, which shows the centerline temperature distribution for each case. According to the figure, the flame is stabilized closer to the channel's inlet when the wall temperature is higher. In reacting channel flow problems, the wall of the channel is used as an ignition source for the reaction to be started [21]. The ignition is obtained by ensuring a constant or varying temperature profile for the wall or supplying a heat flux. Therefore, heat transfer in a channel is occurred from wall to centerline because of the temperature gradient. The temperature gradient is increased with higher wall temperatures, which enhances heat transfer between the wall and the centerline of the channel. The flow becomes more energetic with improved heat transfer from the wall; consequently, the flow's velocity and temperature tend to be higher. This behavior can be observed for centerline property distributions from Figure 4.54 and Figure 4.55 and the entire channel fields of temperature and velocity between Figure 4.57 and Figure 4.62. The calculated positions of flame are tabulated in Table 4.11.
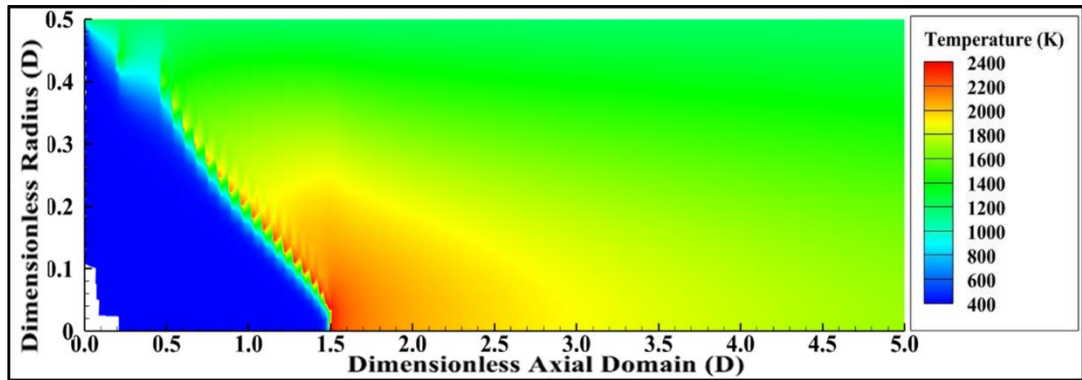
94

Figure 4.57 Temperature Field for $T_{wall} = 1200$ K

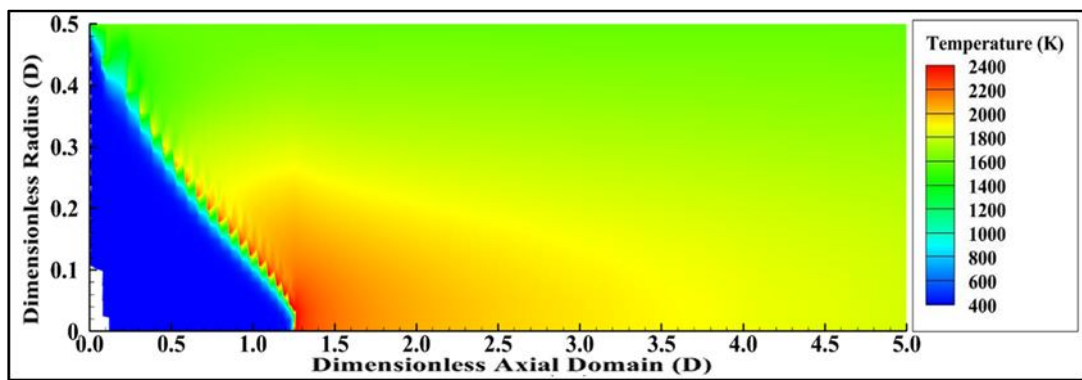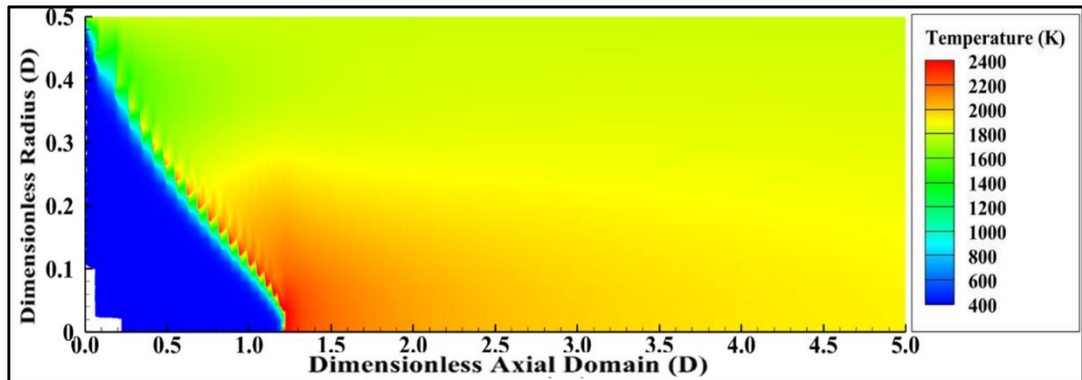Figure 4.58 Temperature Field for $T_{wall} = 1600$ K

Figure 4.59 Temperature Field for $T_{wall} = 1800$ K
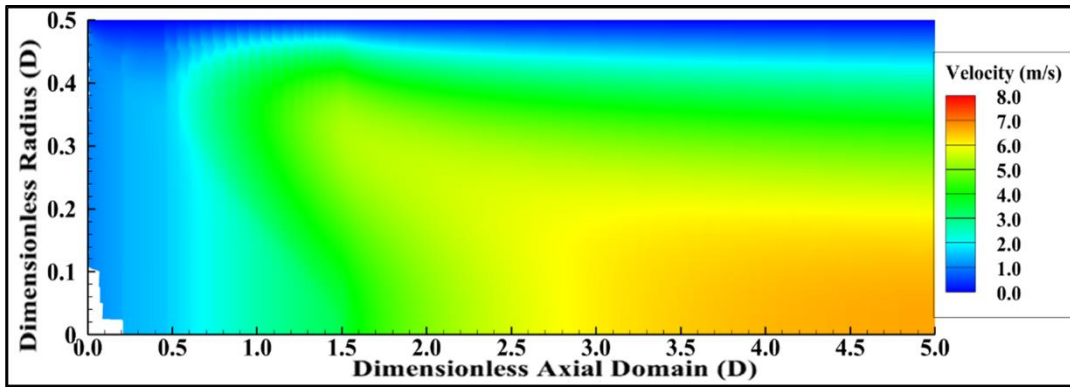
Figure 4.60 Velocity Field for T_{wall} = 1200 K
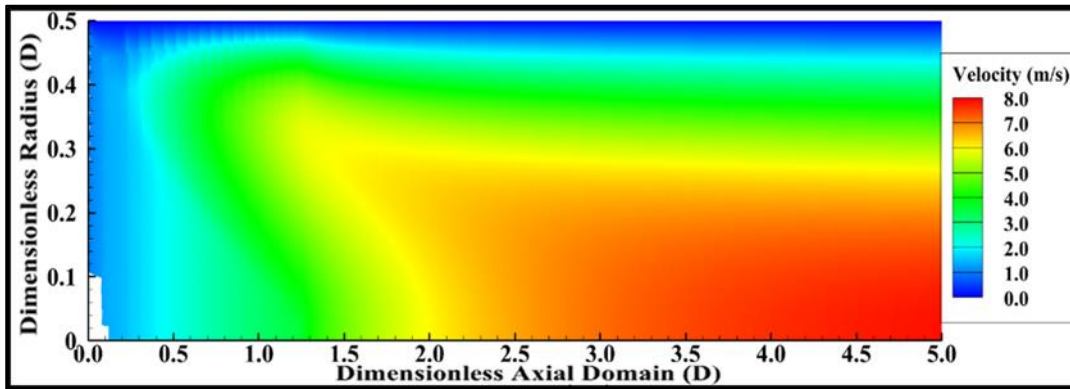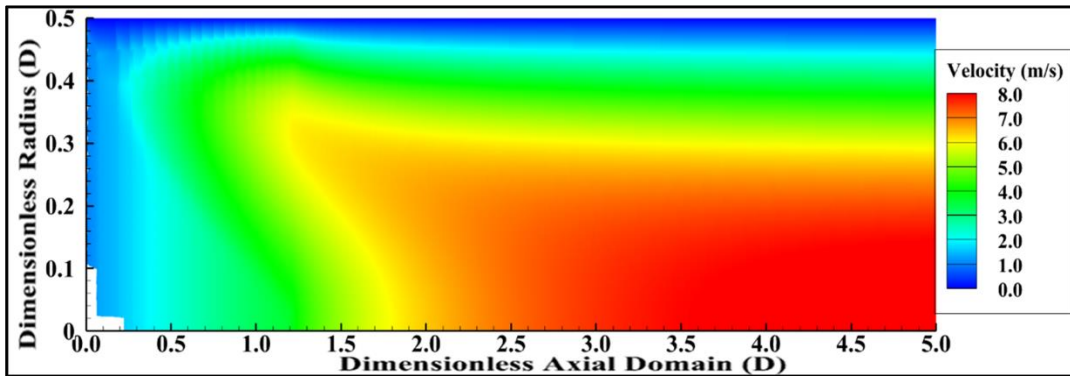

Figure 4.61 Velocity Field for T_{wall} = 1600 K

Figure 4.62 Velocity Field for T_{wall} = 1800 K

Table 4.11 Flame Position in Axial Direction for Varying Wall Temperatures

Wall Temperature	Axial Flame Position
1200 K	1.50 D
1600 K	1.25 D
1800 K	1.20 D

4.2.5 Varying Channel Diameter

The diameter of the channel is changed between 0.005 m to 0.0125 m in order to investigate its effects on flame position. The centerline temperature, velocity and species mass fraction distributions for varying inlet pressures are presented in Figure 4.63, Figure 4.64 and Figure 4.65.
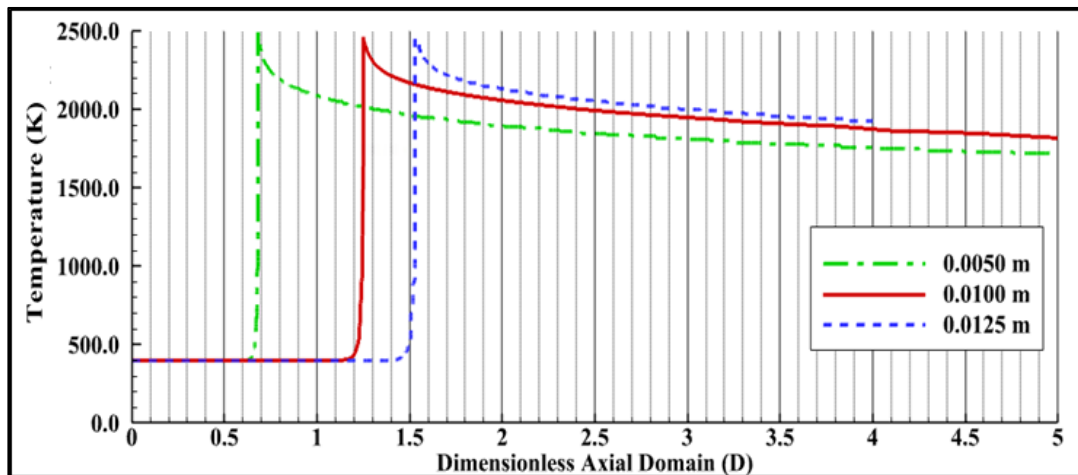

Figure 4.63 Comparison of Centerline Temperatures for Varying Channel Diameter
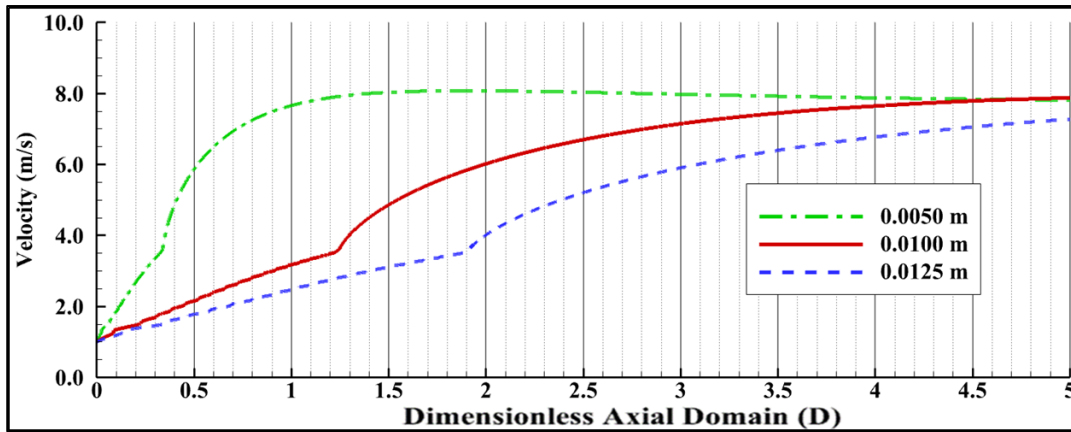
Figure 4.64 Comparison of Centerline Velocities for Varying Channel Diameter

The flame positions can be obtained from Figure 4.63, which shows the centerline temperature distribution for each case. According to the figure, the flame is stabilized closer to the channel's inlet when the channel diameter is decreased. As stated in section 4.2.4, the wall of the channel is used as an ignition source for reacting channel flow cases. When the channel diameter is decreased, the heat transfer between the wall and centerline of the channel becomes more rapid. Due to this, the level of activation energy for reactions to occur is reached earlier in a channel. Therefore, the flame is stabilized closer to the channel inlet for the channels with narrower diameters. However, the flow properties are kept the same for the burnt gases region. The centerline velocity distributions for each case are compared in Figure 4.64. The level of the maximum velocity of the flow is similar for each case since the maximum released chemical energy and the energy difference between the wall and centerline of the channel are the same for each case. The flame shapes for varying channel diameters can be observed from temperature and velocity fields between Figure 4.66 and Figure 4.71. The flame positions for each diameter are tabulated in Table 4.12. Moreover, the relation between channel diameter and axial flame position is investigated. It is concluded that the axial flame position is directly proportional to the cross-sectional area of the channel inlet. The proportionality constants for each case are presented in Table 4.12.
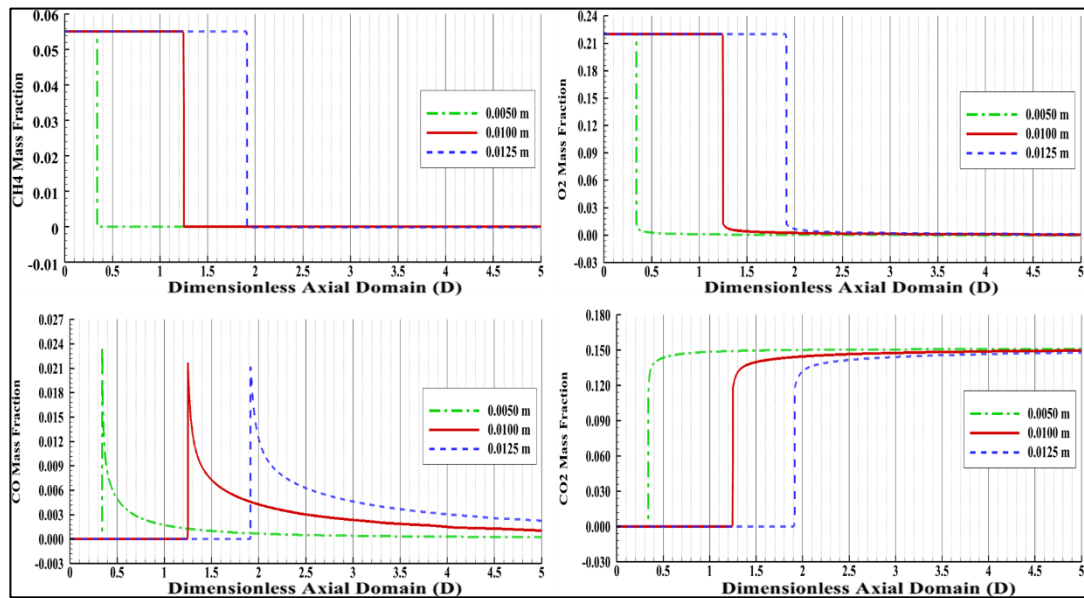
98

Figure 4.65 Comparison of Centerline Species Mass Fractions for Varying Channel Diameter

Table 4.12 Flame Position in Axial Direction for Varying Channel Diameters

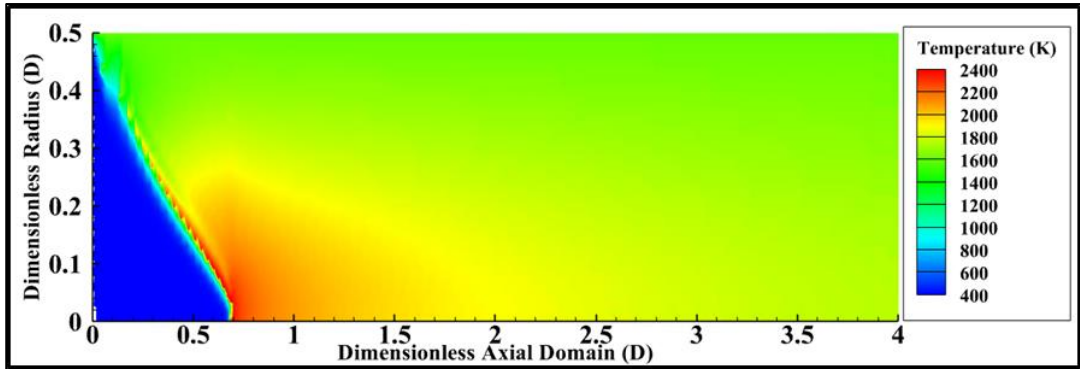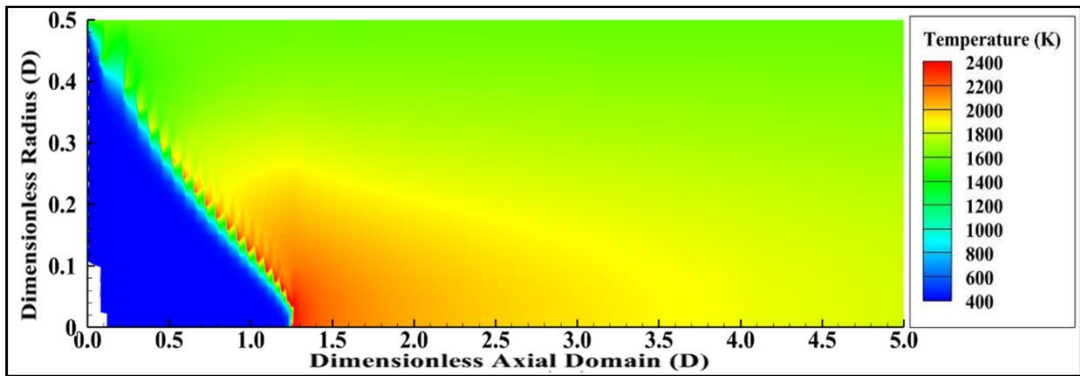| Channel Diameter	Axial Flame Position	$\dfrac{Channel\ Area}{Flame\ Position}$
0.0050 m	0.70 D	$2.24 \cdot 10^{-4}$
0.0100 m	1.25 D	$2.51 \cdot 10^{-4}$
0.0125 m	1.52 D	$2.58 \cdot 10^{-4}$

Figure 4.66 Temperature Field for D = 0.005 m

Figure 4.67 Temperature Field for D = 0.010 m

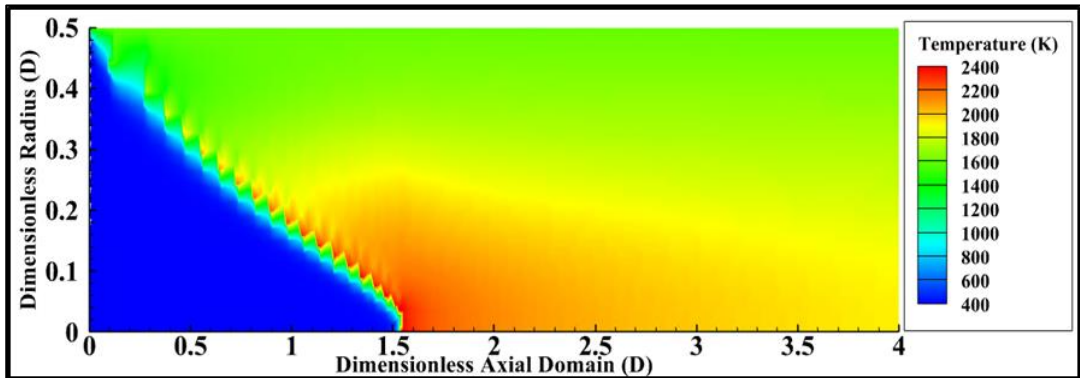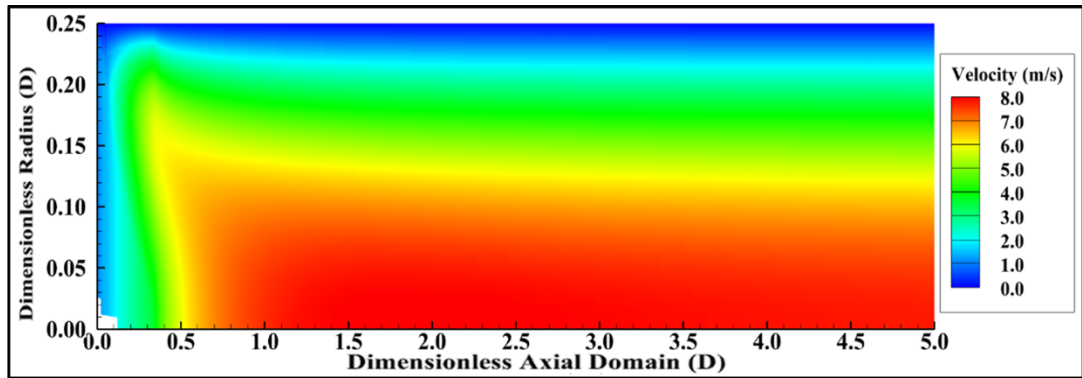Figure 4.68 Temperature Field for D = 0.0125 m
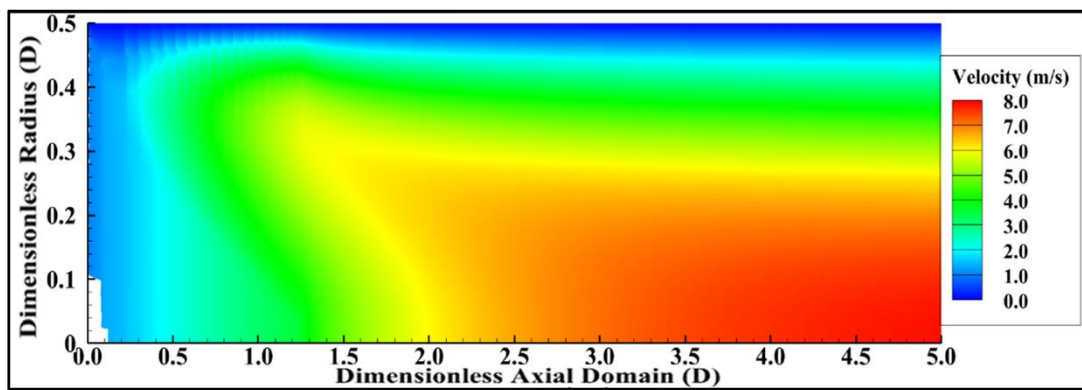
100

Figure 4.69 Velocity Field for D = 0.005 m
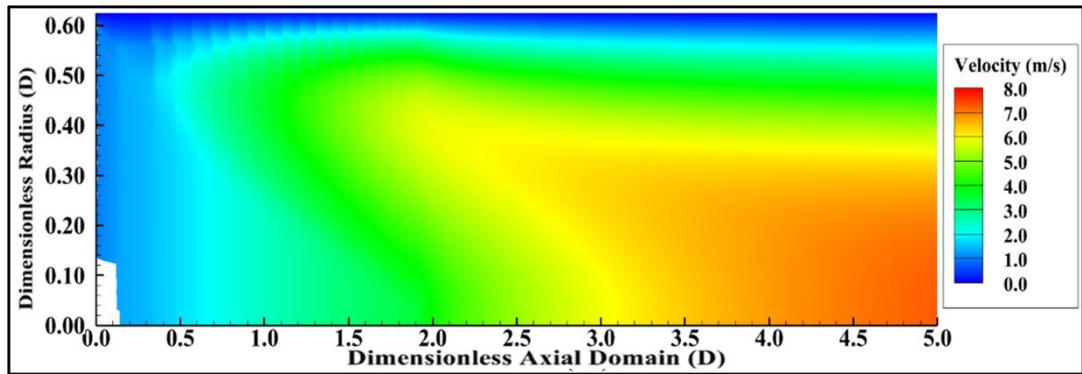

Figure 4.70 Velocity Field for D = 0.010 m

Figure 4.71 Velocity Field for D = 0.0125 m

4.2.6   Comparison of Results

The results of the parametric sensitivity study are summarized in this section. In Figure 4.72, the flame positions are shown for variation of each flow parameter. As stated in the previous section, each flow parameter is varied for three values. It can be observed from the figure that variation of equivalence ratio has a minor effect on the position of flame in a channel. In contrast, the variation of channel diameters is the most influential parameter for the flame position in a channel. The relation between flow parameters and flame position is presented between Figure 4.72 and Figure 4.76. It can be observed from these figures that flame position is linearly proportional to inlet velocity, inlet pressure and channel cross-sectional area. Secondly, the flame is anchored earlier for equivalence ratio with the highest adiabatic flame temperature. In addition, the flame position is inversely proportional to wall temperature.
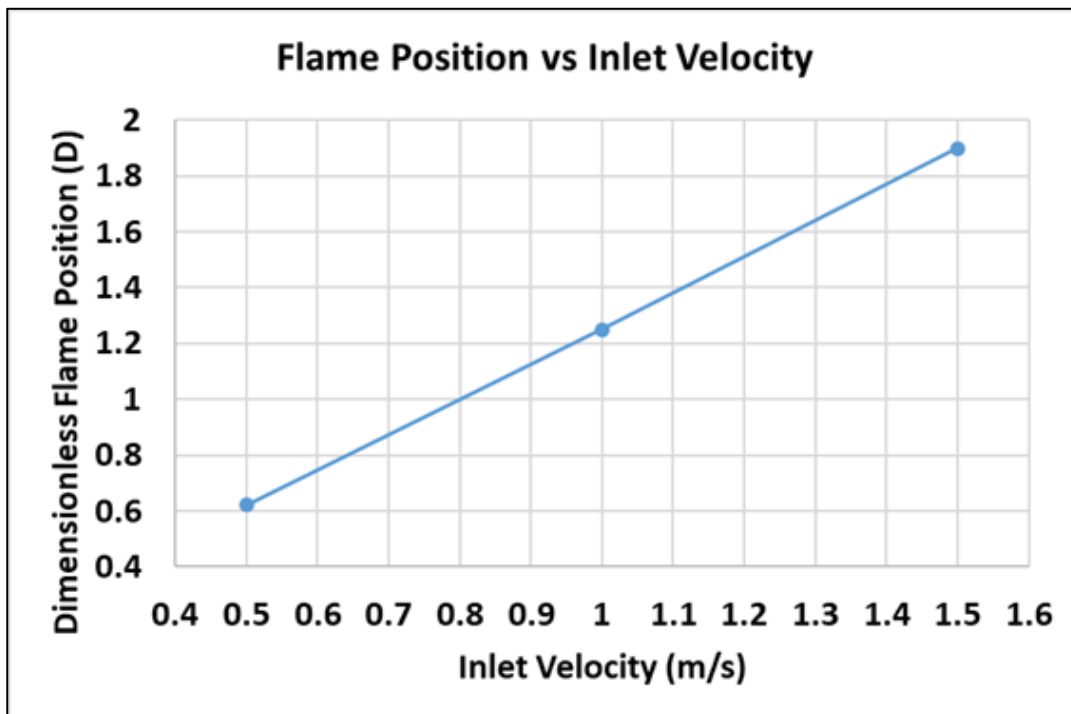

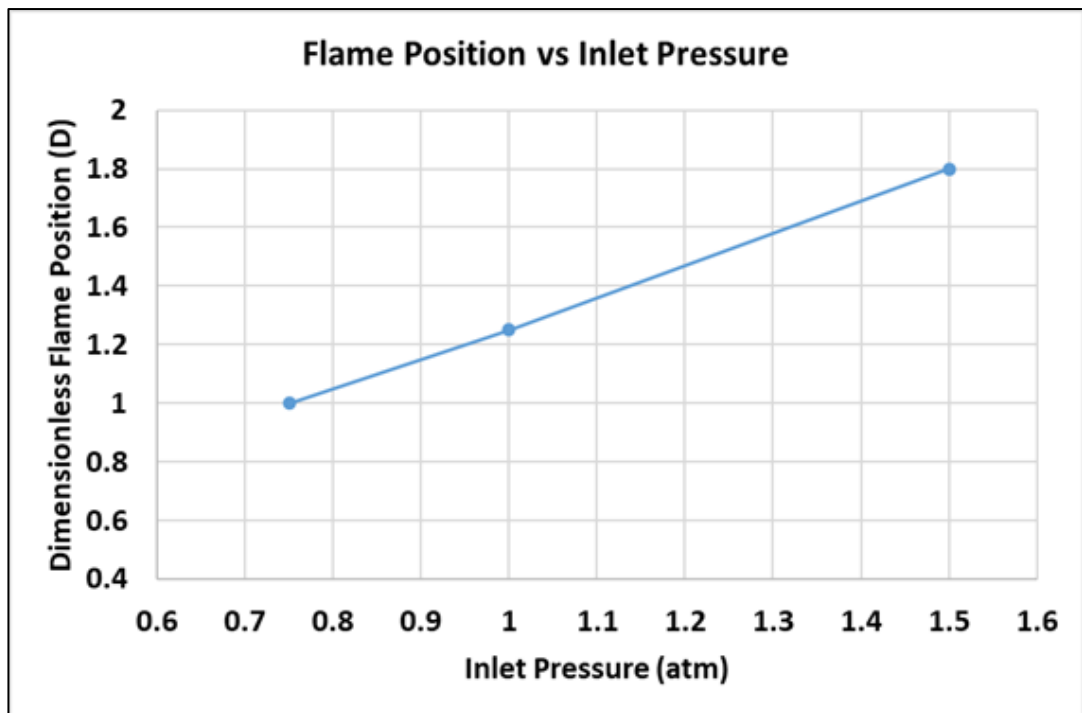Figure 4.72 Variation of Flame Position with Inlet Velocity

Figure 4.73 Variation of Flame Position with Inlet Pressure
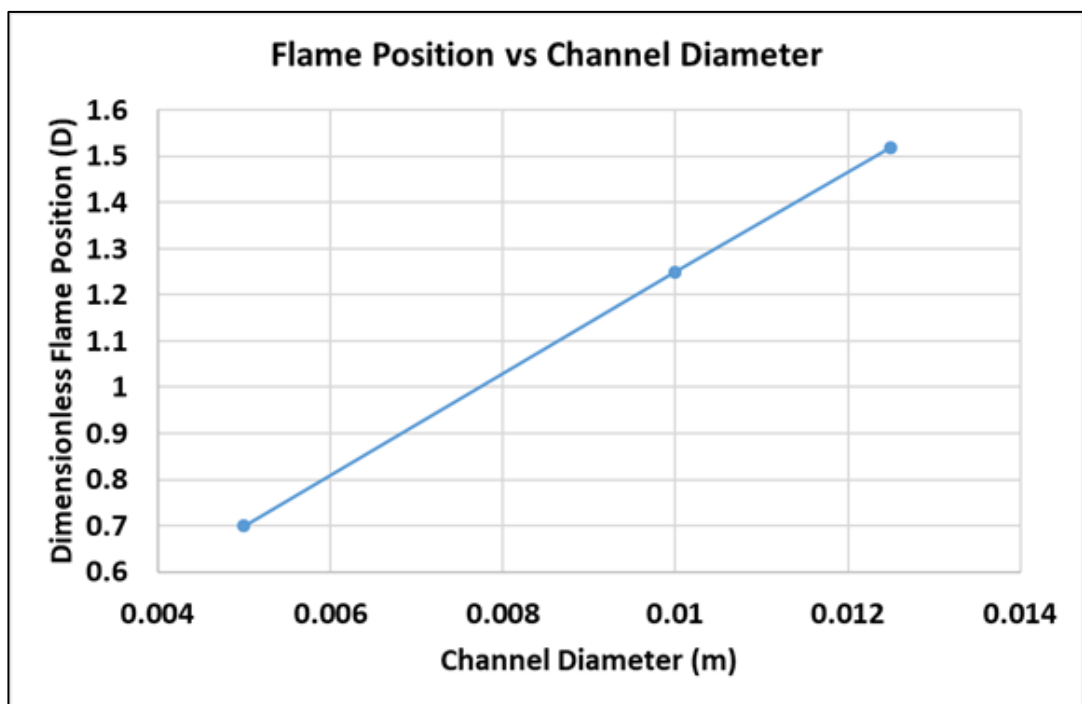

Figure 4.74 Variation of Flame Position with Channel Diameter
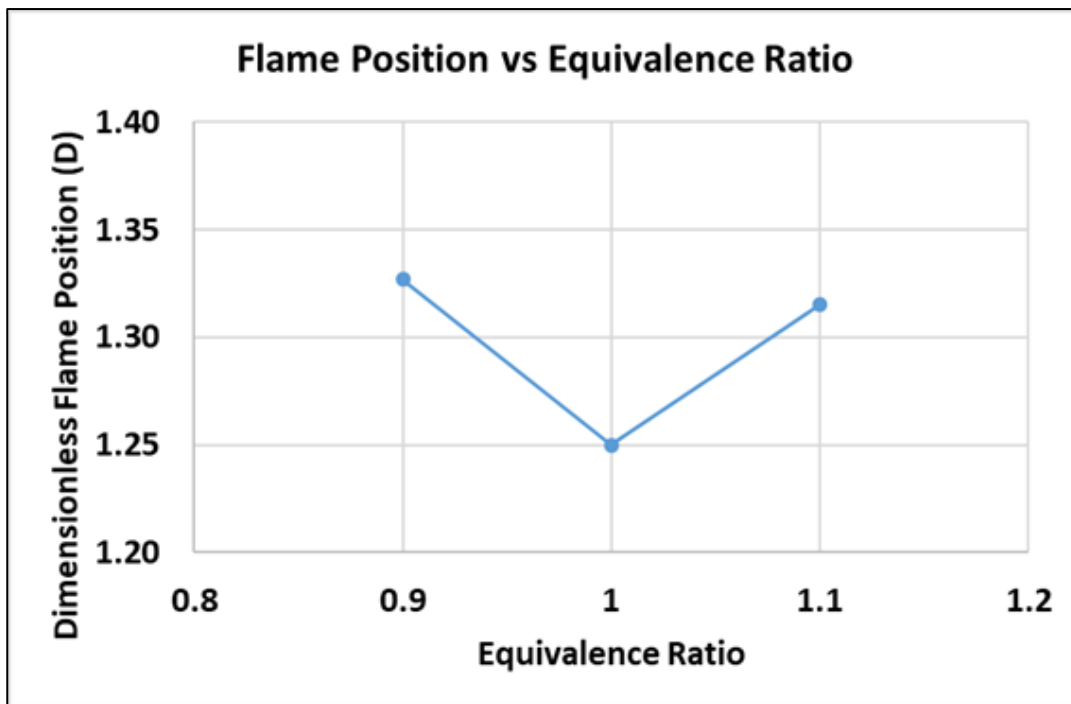
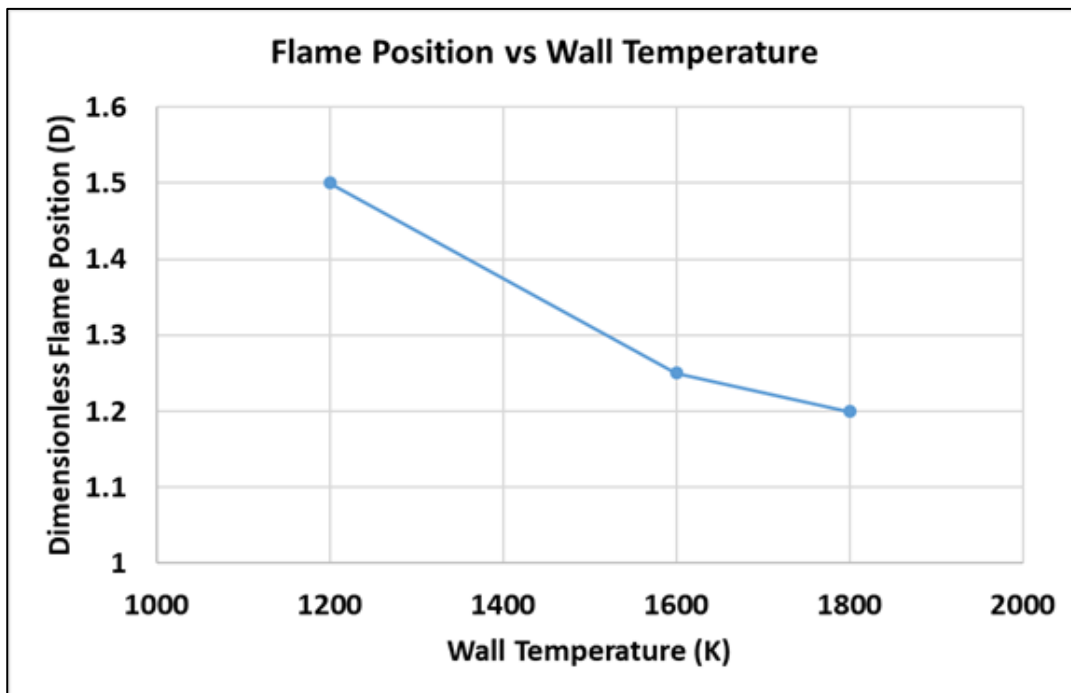Figure 4.75 Variation of Flame Position with Equivalence Ratio

Figure 4.76 Variation of Flame Position with Wall Temperature

In Table 4.13, a summary of flow parameters is tabulated with the specification of the case number, case variable and value of the variable. In Figure 4.77, a graph of flame positions for each case is presented. The flame is stabilized between 1.00D and 1.40D from the channel inlet for 66% of cases. As stated previously, the slightest change of flame position occurs for variation of equivalence ratio, for which the difference between cases is between 5.2% and 6.2%. For the analysis of wall temperatures, 200 K and 400 K are used for temperature differences from the reference temperature value. For case – 10, of which the wall temperature is 1200 K, the flame position is slightly changed with a difference of 4%. However, for case – 12, of which the wall temperature is 1800 K, the flame position is dramatically altered with a value of 20%. For inlet pressure analyses, the increase of inlet pressure of 0.5 atm is stabilized flame 44 % later than the reference flame position value. In addition, when the inlet pressure is decreased to 0.75 atm, the flame is positioned 20% closer to the channel inlet than in the reference case. Inlet velocity is reduced and increased with 0.5 m/s, and the resulting flame positions are differed from the reference flame position for variation of inlet velocity analyses 50.4% and 52% for 0.5 m/s and 1.5 m/s, respectively. The most dramatic changes in flame positions are occurred due to variations in inlet velocity. Finally, when the channel diameter is decreased to 0.005m, the flame is anchored in a channel 44% closer to the inlet with respect to the reference value. In addition, when the channel diameter is increased to 0.0125 m, the flame position is delayed in channel 21.5% to the reference position of flame for channel diameter analyses.

Table 4.13 Summary of Flow Parameters

| Case Number	Case Variable	Value of Variable	Flame Position	Deviation from Reference Value
Case – 1		0.5 m/s	0.62 D	50.4 %
Case – 2	Inlet Velocity	1.0 m/s	1.25 D	-
Case - 3		1.5 m/s	1.90 D	52 %
Case - 4		0.9	1.327 D	6.2 %
Case - 5	Equivalence Ratio	1.0	1.250 D	-
Case - 6		1.1	1.315 D	5.2 %
Case - 7		0.75 atm	1.00 D	20 %
Case - 8	Inlet Pressure	1.00 atm	1.25 D	-
Case - 9		1.50 atm	1.80 D	44 %
Case - 10		1200 K	1.20 D	4 %
Case - 11	Wall Temperature	1600 K	1.25 D	-
Case - 12		1800 K	1.50 D	20 %
Case - 13		0.0050 m	0.70 D	44 %
Case - 14	Channel Diameter	0.0100 m	1.25 D	-
Case - 15		0.0125 m	1.52 D	21.5 %
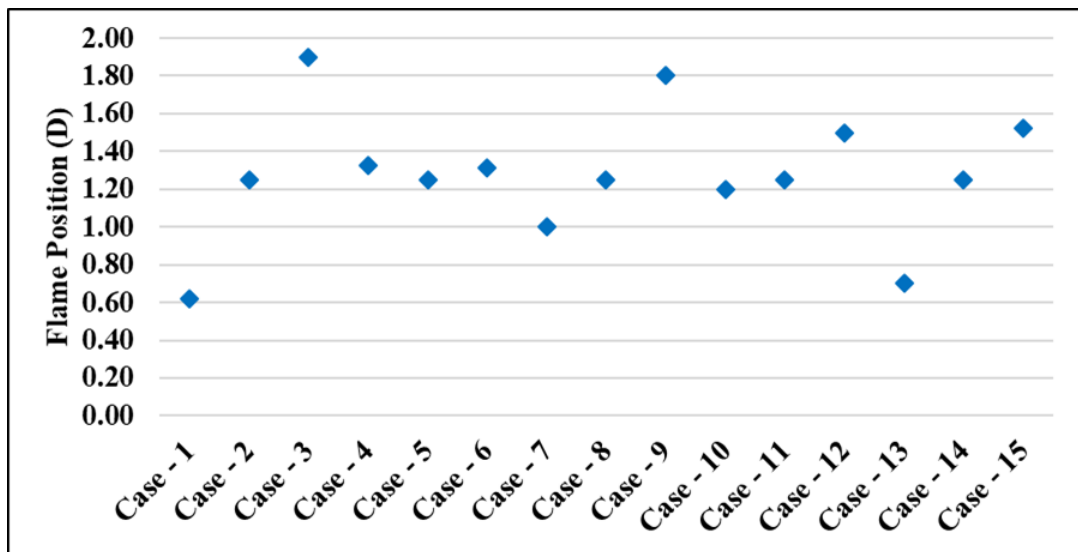
Figure 4.77 Summary of Flame Position for Cases

CHAPTER 5

CONCLUSION

5.1   Results

In this thesis, an algorithm for the solution of chemically reacting flows in a channel reactor is developed by using boundary layer equations. Parabolic PDEs are solved by numerical techniques initially designed for ODE utilizing the method of lines. The finite difference method is used to discretize spatial terms in the set of equations. The resulting set of equations is written in differential algebraic equations and is solved using MATLAB ode15i solver. Using the developed algorithm, the flame position in a channel and the parameters affecting flame development are investigated. As a result, the following results have been obtained:

 a) Algorithm Development
1. An algorithm for chemically reacting channel flows is developed using boundary layer equations via numerical methods and the results are compared with data from the literature. It is found that numerical solutions for the non-reacting case are close to the literature data. In addition, the solutions for the reacting case can be predict the flame position closer to the literature.
2. A numerically insignificant number is defined as an initial condition for non-existing species to avoid singularities. Singularities can arise in numerical solutions due to representing non-existing species as zero.
 b) Sensitivity Analyses for Flow Parameters
3. Parametric flow analyses show that flow parameters affect determining flame position differently.
4. Reynolds number, flame speed and channel cross-sectional diameter can be used as similarity parameters for reacting channel flow calculations.

5. The most negligible effect on flame position is occurred by variation of equivalence ratio, which is around 5%, for the given range of equivalence ratio.

6. The most influential parameter on the flame positions is determined as inlet velocity. Increasing or decreasing the flame position can be changed by around 50% to the reference position.

7. The position of the flame can be altered by changing inlet pressure. The root of inlet pressure is inversely proportional to the flame position.

8. Channel diameter is one of the most influential parameters on flame position and flows field.

9. Wall temperature has a significant effect on both flame position and flow fields.

Experimental studies can be examined in future studies to increase the precision of developed code. In addition, the solver and its environment can be changed to speed up the analyses of the code. Moreover, surface reactions can be added to widen the usage area of code. Finally, a variable temperature profile can be introduced as an input condition on the wall.

REFERENCES

[1] L. L. Raja, R. J. Kee, O. Deutschmann, J. Warnatz, and L. D. Schmidt, "A critical evaluation of Navier-Stokes, boundary-layer, and plug-flow models of the flow and chemistry in a catalytic-combustion monolith," *Catal. Today*, vol. 59, no. 1–2, pp. 47–60, 2000, doi: 10.1016/S0920-5861(00)00271-6.

[2] C. T. Goralski and L. D. Schmidt, "Modeling heterogeneous and homogeneous reactions in the high-temperature catalytic combustion of methane," *Chem. Eng. Sci.*, vol. 54, no. 24, pp. 5791–5807, 1999, doi: 10.1016/S0009-2509(99)00169-4.

[3] A. Güthenke *et al.*, "Current status of modeling lean exhaust gas aftertreatment catalysts," *Adv. Chem. Eng.*, vol. 33, no. 07, 2007, doi: 10.1016/S0065-2377(07)33003-2.

[4] M. E. Coltrin, "A Mathematical Model of the Coupled Fluid Mechanics and Chemical Kinetics in a Chemical Vapor Deposition Reactor," *J. Electrochem. Soc.*, vol. 131, no. 2, p. 425, 1984, doi: 10.1149/1.2115598.

[5] J. C. G. Andrae and P. H. Björnbom, "Wall effect of laminar hydrogen flames over platinum and inert surfaces," *AIChE J.*, vol. 46, no. 7, pp. 1454–1460, 2000, doi: 10.1002/aic.690460718.

[6] M. E. Coltrin, R. J. Kee, and J. A. Miller, "A Mathematical Model of Silicon Chemical Vapor Deposition: Further Refinements and the Effects of Thermal Diffusion," *J. Electrochem. Soc.*, vol. 133, no. 6, pp. 1206–1213, 1986, doi: 10.1149/1.2108820.

[7] J. Andrae, P. Björnbom, L. Edsberg, and L. E. Eriksson, "A numerical study of side wall quenching with propane/air flames," *Proc. Combust. Inst.*, vol. 29, no. 1, pp. 789–795, 2002, doi: 10.1016/S1540-7489(02)80101-8.

[8] J. Andrae, P. Björnbom, and L. Edsberg, "Numerical studies of wall effects with laminar methane flames," *Combust. Flame*, vol. 128, no. 1–2, pp. 165–

180, 2002, doi: 10.1016/S0010-2180(01)00342-X.

[9]   L. R. Petzold, "A Differential/Algebraic System Solver," vol. 94550, 1982.

[10]   U. Dogwiler, P. Benz, and J. Mantzaras, "Two-dimensional modeling for catalytically stabilized combustion of a lean methane-air mixture with elementary homogeneous and heterogeneous chemical reactions," *Combust. Flame*, vol. 116, no. 1–2, pp. 243–258, 1999, doi: 10.1016/S0010-2180(98)00036-4.

[11]   O. Deutschmann and L. D. Schmidt, "Modeling the partial oxidation of methane in a short-contact-time reactor," *AIChE J.*, vol. 44, no. 11, pp. 2465–2477, 1998, doi: 10.1002/aic.690441114.

[12]   C. H. Hwang, C. E. Lee, and K. O. Lee, "Numerical investigation on combustion characteristics of methane in a hybrid catalytic combustor," *Fuel*, vol. 83, no. 7–8, pp. 987–996, 2004, doi: 10.1016/j.fuel.2003.10.024.

[13]   A. Di Stazio, C. Chauveau, G. Dayma, and P. Dagaut, "Combustion in micro-channels with a controlled temperature gradient," *Exp. Therm. Fluid Sci.*, vol. 73, pp. 79–86, 2016, doi: 10.1016/j.expthermflusci.2015.09.020.

[14]   K. Maruta, T. Kataoka, N. Kim, S. Minaev, and R. Fursenko, "Characteristics of combustion in a narrow channel with a temperature gradient," *Proc. Combust. Inst.*, vol. 30 II, no. 2, pp. 2429–2436, 2005, doi: 10.1016/j.proci.2004.08.245.

[15]   R. Schwiedernoch, S. Tischer, O. Deutschmann, and J. Warnatz, "Experimental and numerical investigation of the ignition of methane combustion in a platinum-coated honeycomb monolith," *Proc. Combust. Inst.*, vol. 29, no. 1, pp. 1005–1011, 2002, doi: 10.1016/S1540-7489(02)80127-4.

[16]   O. Deutschmann *et al.*, "DETCHEM Software package." Karlsruhe, 2022, [Online]. Available: www.detchem.com.

[17]   B. R. Munson, T. H. Okiishi, W. W. Huebsch, Rothmayer, and A. P,

Fundamentals of Fluid Mechanics Seventh Edition. 2013.

[18] F. M. White, *Fluid Mechanics 8th Edition*, vol. 11, no. 3. 2017.

[19] H. Schlichting and K. Gersten, *Boundary Layer Theory (9th Edition)*. 2001.

[20] C. Borgnakke and R. Sonntag, *Fundamentals of Thermodynamics*, 8th Editio. Wiley, 2013.

[21] R. Kee, M. E. Coltrin, P. Glarborg, and H. Zhu, *Chemically Reacting Flow Theory, Modelling and Simulation*, Second Edi. Wiley, 2017.

[22] F. P. Incropera and D. P. DeWitt, "Fundamentals of Heat and Mass Transfer." p. 890, 1996, doi: 10.1016/j.applthermaleng.2011.03.022.

[23] J. Hoffman, *Numerical Methods for Engineers and Scientists*, Second Edi., vol. 4, no. 1. Marcel Dekker Inc., 2001.

[24] M. H. Aksel, *Fluid Mechanics Volume-I*, Version 3. 2008.

[25] A. P. For, M. Laminar, C. Reacting, F. In, C. Or, and P. Channels, "CRESLAF - A Program for Modeling Laminar, Chemically Reacting, Boundary-Layer Flow in Cylindrical or Planar Channels," *Chemkin Collect. Release 3.6*, no. September, pp. 1–58, 2000.

[26] J. Mac Hyman, "The method of lines solution of partial differential equations," 1976.

[27] N. K. Madsen, "The method of lines for the numerical solution of partial differential equations," *Proc. 1975 SIGNUM Meet. Softw. Partial Differ. Equations*, pp. 5–7, 1975, doi: 10.1145/800207.806406.

[28] J. Kierzenka and L. F. Shampine, "MATLAB Solver: ode15i." The Mathworks In.

[29] R. J. Kee *et al.*, "CHEMKIN Collection, Release 3.6," *Reaction Design*. San Diego ,CA, 2000.

[30] U. M. Ascher and L. R. Petzold, "Computer methods for ordinary differential equations and differential-algebraic equations," *Comput. Methods Ordinary Differ. Equations Differ. Equations*, pp. 3–305, 1998, doi: 10.1137/1.9781611971392.

[31] I. The MathWorks, "ode15i." https://www.mathworks.com/help/matlab/ref/odeset.html.

[32] D. G. Goodwin, H. K. Moffat, I. Schoegl, R. L. Speth, and B. W. Weber, "Cantera: An object-oriented software toolkit for chemical kinetics, thermodynamics and transport processes." 2022, doi: 10.5281/zenodo.6387882.

[33] Reaction Design, "Chemkin: A software package for the analysis of gas-phase chemical and plasma kinetics," no. September. pp. 1–181, 2000, [Online]. Available: http://www.reactiondesign.com.

[34] B. Franzelli, E. Riber, L. Gicquel, and T. Poinsot, "Large-Eddy Simulation of combustion instabilities in a lean partially premixed swirled flame," *Combust. Flame*, vol. 159, no. 2, pp. 612–637, 2012.

[35] S. R. Turns, *An Introduction to Combustion Concepts and Applications*, Third Edit. 2012.

[36] G. E. Andrews and D. Bradley, "The burning velocity of methane-air mixtures," *Combust. Flame*, vol. 19, no. 2, pp. 275–288, 1972, doi: 10.1016/S0010-2180(72)80218-9.